University of California

San Diego

Diabetes in a dish: Modeling and phenotyping acute and chronic type 2 diabetes mellitus *in vitro* in rodent heart and skeletal muscle cells

Dissertation zum Erwerb des Doktorgrades der Medizin an der Medizinischen Fakultät der Ludwig-Maximilians-Universität zu München

vorgelegt von

Elena Luise Kopp

aus

Freudenstadt

2023

Mit Genehmigung der Medizinischen Fakultät

der Universität München

Berichterstatter:	Prof. Dr. Reinhard Lorenz
Mitberichterstatter:	Prof. Dr. Klaus G. Parhofer
	Prof. Dr. Anette-Gabriele Ziegler
	Prof. Dr. Jörg Schirra
Dekan:	Prof. Dr. med. Thomas Gudermann
Tag der mündlichen Prüfung:	13.07.2023

Content

Abbreviations:

ATP	Adenosine triphosphate
ANOVA	Analysis of variance
BSA	Bovine serum albumin
C2C12	Mouse skeletal muscle myoblast cell line
Cpm	Counts per minute
DMEM	Dulbecco's Modified Eagle's Medium
DAG	Diacylglycerol
ECAR	Extracellular acidification rate
FA	Fatty acid
FBS	Fetal Bovine Serum
FCCP	Carbonyl cyanide 4-(trifluoromethoxy) phenylhydrazone (FCCP)
FFA	Free fatty acids
GLUT	Glucose transporter type
glycoPER	Glycolytic proton efflux rate
HG	High glucose
HGI	High glucose + insulin
HGP	High glucose + palmitate
HGPI	High glucose + palmitate + insulin
HM	High mannitol
HMI	High mannitol + insulin
HMP	High mannitol + palmitate
HMPI	High mannitol + palmitate + insulin
HS	Horse serum
H9C2	Rat embryonic ventricular tissue cell line
H^+	Proton
Ic	Inner circle
IDF	International Diabetes Federation
IR	Insulin resistance
L6	Rat skeletal muscle myoblast cell line

LG	Low glucose
LGI	Low glucose + insulin
LGP	Low glucose + palmitate
LGPI	Low glucose + palmitate + insulin
M	Molar
m	mitochondrion
mM	Millimol
µM	Micromol
nM	Nanomol
n	Number
n.	Nucleus
oc	Outer circle
OCR	Oxygen consumption rate
Cp	Cytoplasm
p	Probability value
pAkt	phosphorylated Akt
Penstrep	Penicillin/Streptomycin
PKC	Protein kinase C
pM	Picomol
PMN	Perinuclear mitochondria
PVM	Perivascular mitochondria
RA	All-trans-retinoic acid
ROS	Reactive oxygen species
Rot/AA	Rotenone and Antimycin A
SD	Standard deviation
sm	Swollen mitochondrion
T1D	Type 1 diabetes
T2D	Type 2 diabetes
TEM	Transmission electron microscopy
3D	Three dimensional

Abstract

Background: Diabetes mellitus is a metabolic disorder, characterized by elevated levels of blood glucose. Type 2 diabetes (T2D) accounts for >90% of cases and is a progressive disease with initially elevated insulin levels and insulin resistance (IR). This study aims to develop a novel method for simulating T2D *in vitro*, including its main aspects: Hyperglycemia, hyperlipidemia and variably elevated insulin levels. Skeletal and heart muscle cells are strongly affected by IR and chronic hyperglycemia.

Methods: We investigated IR, cellular respiration and mitochondrial function under different T2D-mimicking conditions in rodent skeletal (C2C12) and cardiac (H9C2) myotubes. Physiological control conditions included 5mM glucose (LG) with 20mM mannitol as osmotic controls (HM). To mimic hyperglycemia (HG), cells were exposed to 25mM glucose. Further treatment groups included the combination with insulin (I) (1nM, HGI), or palmitate (P) (75 or 150mM, HGP), or both (HGPI). After short-term (24h) or long-term (96h) exposure, we performed radioactive glucose-uptake assays and mitochondrial function assays using the Agilent Seahorse system. Ultrastructural analysis was performed using transmission electron microscopy.

Results: C2C12 and H9C2 cells treated short- or long-term with insulin and/or palmitate and HG became insulin resistant. In mitochondrial respiration assays C2C12 myotubes exposed to T2D-mimicking conditions showed similar maximal respiration rates compared to physiological controls, but significantly lower ATP linked respiration and spare respiratory capacity, implying more uncoupled respiration and mitochondrial dysfunction in skeletal muscle. In contrast, H9C2 myotubes showed elevated ATP linked respiration and maximal respiration upon exposure to T2D mimicking conditions, indicating better adaptation to stress and preferential lipid oxidation in cardiac muscle in a T2D environment. Both cell lines displayed elevated fractions of swollen mitochondria after T2D mimicking treatments.

Conclusions: Our stable, simple, and reproducible *in vitro* model of T2D causes IR, changes in ATP linked respiration, shifts in energetic phenotypes and mitochondrial morphology changes. These changes are consistent with what occurs in muscles of patients suffering from T2D. Our results support the relevance of T2D cell models that will be useful for experimental studies of pathomechanisms and screening for potential targets and therapeutic compounds also in other cell types affected by T2D.

Zusammenfassung

Hintergrund: Diabetes mellitus ist eine Stoffwechselerkrankung, gekennzeichnet durch erhöhte Blutzuckerspiegel. Typ-2-Diabetes (T2D) macht 90% der Fälle aus und ist durch anfangs erhöhte Insulinspiegel und eine progressive Insulinresistenz (IR) charakterisiert. Ziel dieser Studie ist die Entwicklung einer neuartigen Methode zur Simulation von T2D *in vitro*, einschließlich der wichtigsten Aspekte: Hyperglykämie, Hyperlipidämie und variabel erhöhte Insulinspiegel. Skelett- und Herzmuskelzellen sind von IR und chronischer Hyperglykämie betroffen. **Methoden**: Wir haben IR, Zellatmung und Mitochondrienfunktion in verschiedenen T2D-simulierenden Bedingungen in Skelett- (C2C12) und Herzmuskelzellen/Myotuben (H9C2) untersucht. Die physiologischen Kontrollbedingungen umfassten 5mM Glukose (LG) und 20mM Mannitol als osmotische Kontrolle (HM). Um eine Hyperglykämie (HG) zu simulieren, wurden die Zellen mit 25mM Glukose behandelt. Weitere Inkubationen umfassten die Kombination mit Insulin (I) (1nM, HGI) oder Palmitat (P) (75 oder 150mM, HGP) oder beidem (HGPI). Nach kurz- (24h) oder langfristiger (96h) Inkubation führten wir radioaktive Glukose-Aufnahme-Assays und mitochondriale Funktionstests mit dem Agilent Seahorse System durch. Ultrastrukturelle Analysen wurde mit Hilfe der Transmissionselektronenmikroskopie durchgeführt.
Ergebnisse: C2C12- und H9C2-Zellen, die kurz- oder langfristig mit Insulin und/oder Palmitat und HG behandelt wurden, wurden insulinresistent. In Tests zur mitochondrialen Atmung zeigten C2C12 Zellen, die T2D-simulierenden Bedingungen ausgesetzt waren, im Vergleich zu LG Kontrollen ähnliche maximale Atmungsraten, aber eine signifikant niedrigere ATP-Produktion und Reserve-Atmungskapazität, was auf vermehrt entkoppelte Atmung und mitochondriale Dysfunktion im Skelettmuskel hindeutet. H9C2 hingegen zeigten eine erhöhte ATP-Produktion und maximale Atmung, nachdem sie T2D-ähnlichen Bedingungen ausgesetzt waren, was auf eine bessere Stressanpassung und verstärkte Lipidoxidation des Herzmuskels in einer T2D-Umgebung hinweist. Beide Zelllinien zeigten erhöhte Fraktionen geschwollener Mitochondrien nach T2D-simulierenden Behandlungen.
Schlussfolgerungen: Unser stabiles, simples und reproduzierbares *in vitro* Modell von T2D bewirkt Insulinresistenz, Veränderungen in der ATP-Produktion, Verschiebungen in energetischen Phänotypen und eine veränderte Mitochondrienmorphologie. Diese Veränderungen stimmen mit dem überein, was in den Muskeln von Patienten mit T2D auftritt. Unsere Ergebnisse untermauern die Relevanz von T2D-Zellmodellen, die für experimentelle Studien von Pathomechanismen und das Screening nach potenziellen Targets und therapeutischen Wirkstoffen nützlich sein werden, auch in anderen von T2D betroffenen Zelltypen.

1. Introduction

1.1 Background

Diabetes mellitus is a global burden with an obscure prognosis [1]. According to the International Diabetes Federation (IDF), it is predicted that more than 550 million people worldwide will be diabetic by 2030, compared to 108 million in 1980 [2] [3]. In addition, Diabetes is projected to move up to the 7th leading cause of death worldwide by 2030 compared to the 11th in 2002 [4]. In 2017, the medical costs of individuals with diabetes in the United States were $327 billion, which is 2.3 times higher than in non-diabetic patients. The major costs are hospital and outpatient care and increased prescriptions of cost-intensive insulin-analogs [3]. Diabetes is one the most rapidly increasing diseases and improving therapies and prevention methods to reduce diabetes-related premature mortality is of utmost importance.

Diabetes mellitus is a metabolic disorder, characterized by a relative or absolute lack of insulin, resulting in elevated blood glucose levels. In type 1 diabetes (T1D) an autoimmune destruction of the pancreatic β-cells results in little or no insulin production. T1D accounts for 5-10% of diabetic patients and the symptoms include weight loss, polyuria, polydipsia and fatigue. In type 2 diabetes (T2D), symptoms may be similar but are often absent which leads to a high number of undiagnosed cases. T2D accounts for more than 90% of cases and is primarily caused by an inappropriate cellular response to insulin. In response to insulin resistance (IR) or intolerance, pancreatic beta cells hypertrophy and release more insulin, consequently leading to pancreatic exhaustion and failure in later stages of the disease [5]. In contrast to T1D, the physical disease progress of T2D is characterized by obesity in >80% of cases, which is then exacerbated by western diet and physical inactivity leading to IR, hyperglycemia and hyperinsulinemia. Taken together with an older age of onset this results in an extremely robust insulin insensitivity [6]. Subsequently, pathologic changes in metabolism manifest and T2D then often goes along with metabolic syndrome. The IDF defines metabolic syndrome as the combined occurrence of a minimum three of the following symptoms: diabetes and prediabetes, abdominal obesity, dyslipidemia and high blood pressure [7] [8]. The risk of developing T2D rises proportionally with body mass index and can be reduced by diet modulation and increased physical activity [3] [9]. If a change in lifestyle fails, T2D can be treated with a variety of drugs that intervene with glucose and insulin metabolism and can reduce diabetes related complications. Chronic hyperglycemia can lead to microvascular (nephropathy, retinopathy and polyneuropathy) and macrovascular (stroke, cardiovascular disease) complications [3]. In T2D patients, cardiovascular disease is

the major cause of morbidity and mortality accounting for 68% of all diabetes-related deaths [10] [11]. When diagnosed with T2D, the risk of developing heart failure is 2.5 fold in males and double in females [12] [13] and the overall risk of dying prematurely is increased by 5% [3] [14] [15]. By modeling this complex disease *in vitro,* we want to increase and accelerate disease screening and discovery and improve treatment options.

1.2 Modeling diabetes in research

T1D and T2D represent complex endocrine disorders involving different bodily systems. To address the heterogeneousness of the disease *in vivo* animal models are routinely used. In models for T1D the deficiency in insulin production is achieved by mechanisms such as chemical ablation of beta cells (for example high dose streptozotocin) or breeding rodents that spontaneously develop autoimmune diabetes, like the non-obese diabetic mice [16] [17] [18]. Animal models of T2D include beta cell failure and/or IR in both obese and non-obese models and are often induced by high fat diets [19] [20]. To understand the pathophysiology of DM these models are important but limited in aspects such as costs and time and display inter-individual differences. To also address components of aging and male/female differences in disease progression and therapeutical possibilities, animal models or human studies are critical. However, *in vitro* cell models can provide an economically and ethically acceptable research tool and enable the targeting of specific processes linked to a single cell type of interest, without uncontrolled influences of the whole organism. They can be performed in high consistency and reproducibility and can be genetically modified by transfection to investigate specific genes of interest [20]. By developing efficient cell models that can be applied to various cell types of interest, we can draw conclusions to improve *in vivo* studies and save resources.

In general, *in vitro* models of diabetes are derived from the tissues that are mainly involved in the disease pathophysiology, such as muscle, pancreas, adipose tissue and liver [21]. Murine and human pancreatic islet preparations and isolated beta cells have been widely used to test the insulin-releasing activity of drugs for T2D treatment like insulin secretagogues [22] [23]. Well established rodent beta cell lines include cell lines obtained from radiation (RIN cell line) or virally (In-111) induced insulinomas, or the INS-1 cells obtained from rat insulinoma [24] [25]. Human beta cell lines often display genetic defects and grow slowly, nonetheless well characterized cell lines exist (i.e., 1.1 B4 or EndoC-βH1) and are commonly used to screen glucose lowering drugs [26] [27]. Using pancreatic islets for *in vitro* diabetes research is advantageous as all hormone secreting cell types are still contained: α-cells (glucagon), β-cells (insulin), PP-cells (pancreatic polypeptide), δ-cells (somatostatin) and ε-cells (ghrelin).

Human pancreatic islets are used to compare gene expression, β-cell activity etc., between healthy and diabetic donors [28] [29]. Recently, the generation of three-dimensional (3D) cell culture systems has been blooming. Pancreatic organoids are derived from pluripotent stem cells and self-organize into structures that resemble the *in vivo* tissue, with the long-term goal of serving for transplantation in diabetic patients [20].

To cause IR as it is occurring in T2D, most cell models with hepatocytes, adipocytes and myocytes use chronic insulin exposure or fatty acid treatments (mainly palmitate) [30] [31]. IR models have also been produced using treatments with dexamethasone [32] and pro-inflammatory cytokines [33] or exposure to hypoxia [34] **(Table 1)**. Primary adipose cells and the 3T3-L1 adipocyte cell line are frequently used to test and screen drugs for effects on lipolysis, glucose uptake and insulin sensitivity. Adipocytes are mostly obtained from induced diabetic rodents or diabetic patients [21]. Primary rat and human hepatocytes have been used for the development of treatments that reduce glucagon-stimulated glycogenolysis and inhibit gluconeogenesis [35] [36]. The most commonly used immortalized muscle cell lines for *in vitro* diabetes models are L6 and C2C12 myoblasts, whilst human primary muscle cells have been increasingly used recently to explore glucose uptake, glycogen synthesis and glucose metabolism [37] [31] [38] [39].

To simulate the diabetic milieu *in vitro*, not only the cells themselves play a critical role, but also the conditions in which they are cultured. The main reason for metabolic syndrome and T2D is chronic overnutrition consisting mainly of fatty acids and carbohydrates in the developed world [40] [41] [8]. This increased energy supply leads to adipocyte hypertrophy, lipolysis and stress in the endoplasmic reticulum, which results in the release of proinflammatory mediators, creating an inflammatory milieu [42] [43] [44]. Concurrently free fatty acids (FFA) accumulate in non-adipose tissue and can cause fatty degeneration [45]. *In vitro* studies showed that once a cell becomes overwhelmed by the excess supply of FFAs, complete β-oxidation becomes impossible and toxic lipids are generated. These toxic lipids include diacylglycerides (DAG) and ceramide and contribute to mitochondrial dysfunction, generation of reactive oxygen species (ROS), low-grade inflammation, and finally insulin resistance and apoptosis [46] [47] [48] [49] [50] [51] [52] [53] [54]. Correspondingly, symptoms of T2D are caused by both hyperglycemia and hyperlipidemia, whereas hyperglycemia alone would more likely reflect acute or uncontrolled T1D [55] [56]. In cell culture research, it is a common practice to use culture media with supraphysiological glucose concentrations to promote and accelerate cellular growth. Previous studies addressing IR and diabetes in H9C2 and C2C12 muscle cells (details on these cell lines in chapter 1.3.) worked with 22-25 mM glucose as

control and 33-40 mM glucose to mimic hyperglycemia, which is 8 times more than physiological levels [57] [58] [37]. In several studies investigating DM, glucose concentrations of cell culture media are not specified, leaving the reader uninformed **(Table 1)** [38] [59] [60]. The American Diabetes Association and WHO define normoglycemia as a fasting plasma glucose between 3.9 mmol/L and 5.6 mmol/L [61] [62] [63] [64] . Diabetes is defined when the fasting plasma glucose reaches 7.0 mmol/L or higher [65]. We recommend to first grow and differentiate cells in physiological glucose levels of 5 mM [66], as glucose concentrations below 5 mM in myocyte cell culture impair the differentiation process of myoblasts into myotubes [67].

Table 1: Selection of current *in vitro* models of type 2 diabetes and insulin resistance

Cell type and differentiation	Preincubation	Type of treatment, concentration, duration	Read outs	Reference
3T3-L1 adipocytes	DMEM 5mM glucose	Palmitate 0.75mM 17h Hypoxia 16h Dexamethasone 1 µmol/l 24h High glucose 25mM 18h	Inhibition of phosphorylation of insulin receptor and protein kinase B; decrease in insulin dependent glucose uptake Impaired GLUT4 membrane intercalation	31 34 32 68
C2C12 myoblasts	DMEM 25mM glucose	Insulin 60nM 24h Palmitate 0.4mM 24h	Inhibition of insulin stimulated activation of Akt/protein kinase B; Swollen mitochondria	37
	DMEM 5mM glucose	Glucose 15mM 24h Palmitate 0.25mM 24h	Increased apoptosis, increased ROS production	66
C2C12 myotubes	DMEM 5mM glucose	Palmitate 0.75mM 17h	Inhibition of insulin stimulated glycogen synthesis and activation of protein kinase B, diacylglyceride accumulation	31
	DMEM not specified	Palmitate 0.6mM 24h	Reduced Akt phosphorylation, glucose uptake and GLUT4 expression	60
Huh7 differentiated hepatocellular carcinoma	DMEM 25mM glucose	Insulin 60nM 24h Palmitate 0.4mM 24h	Inhibition of insulin stimulated activation of Akt/protein kinase B	37
Primary human myotubes	DMEM not specified	Palmitate 0.5mM 48h	Decrease in insulin stimulated glucose uptake	38
H9C2 myoblasts	DMEM 25mM glucose	Glucose 33mM 36h	Enhanced apoptosis, activation of cardiac hypertrophy proteins	58
		Glucose 40mM 24h	Increased ROS production + apoptosis	57
	DMEM 5mM glucose	Glucose 25mM + insulin 100nM 24h	Decrease in insulin stimulated glucose uptake, Inhibition of insulin stimulated activation of Akt	69
H9C2 myotubes	DMEM not specified	Palmitate 100µM 24h	Decrease in insulin stimulated glucose uptake	59

The simulation of hyperlipidemia requires the treatment with fatty acids (FA). FAs must be conjugated to bovine serum albumin (BSA) to enable transportation into cells. Regarding the toxicity of FAs, concentrations must be chosen carefully [70] [71]. Chavez and Summers showed that the saturated FA palmitate (the most dominant fat in the western fast food diet) causes IR, whereas unsaturated FAs such as oleate or linoleate have little or no effect on insulin signaling and endoplasmic reticulum (ER) stress and even reversed palmitate-induced IR in skeletal muscle [53] [31] [72]. Under palmitate treatment DAG production is increased and activates protein kinase C (PKC). PKC then inhibits the insulin signaling cascade [59]. This suggests using the widely applied FA palmitate for T2D-related hyperlipidemia conditions **(Table 1)**.

Moreover, to imitate metabolic syndrome and T2D, the interplay of hyperglycemia, hyperlipidemia and insulin should be investigated. Given that in most cases of T2D variable amounts of insulin are produced by beta cells, 1 nM insulin was included in the culture media of our *in vitro* model to create a physiologically relevant diabetic environment. Previous studies reported that high glucose treatment alone did not impair insulin-induced glucose uptake in adipocytes, skeletal muscle and cardiomyoblasts, whereas exposure to high glucose (25 mM) plus high insulin (100 nM) for 24 h showed a significant decrease in insulin-stimulated glucose uptake **(Table 1)** [68] [69]. Further, it was reported that different long-acting insulin analogues or insulin are equipotent regarding cardiac glucose uptake and protection from ROS-generated apoptosis in steady-state *in vitro* conditions [73]. Hence varying effects of different insulin preparations are not to be expected. We worked with culture media containing 5 mM glucose as physiological controls. To mimic hyperglycemia, we exposed our cultures to 25 mM glucose and excluded hyperosmolar effects with control cultures exposed to 5mM glucose and 20 mM mannitol. We added 1 nM insulin to respective cultures. High concentrations of palmitate (200-750 µM), which have previously been used in studies investigating IR, cause apoptosis and high myotube loss in skeletal and cardiac muscle cells [60] [74] [75] [76] [77]. We therefore worked with a maximal concentration of 150 µM, which still leads to IR but is less toxic and close to the physiological range (300-410 µM in humans [78] and 100-400 µM in rats [79] [80]). In conclusion, exposure to high glucose, palmitate and insulin together, may be closer to conditions observed in T2D patients compared to previously described cell-based approaches.

1.3 Modeling type 2 diabetes in skeletal and heart muscle cells

Skeletal muscle is the primary recipient for postprandial glucose and T2D patients often show significantly impaired blood glucose clearance [81] [82]. Also the higher flux of FFAs in

patients with T2D leads to an increased FA-uptake into myocytes [83]. To assess the effect of T2D/metabolic syndrome on skeletal muscle we chose to use C2C12 cells, a mouse myoblast cell line, which is well established and has been widely used in diabetes research [84]. To achieve more similarity to human muscle tissue we worked with differentiated myotubes, whilst many research groups work with the undifferentiated myoblasts **(Table 1)** [66 85 86 87]. The insulin dependent glucose transporter 4 (GLUT4) is similarly expressed in C2C12 myotubes compared to human skeletal muscle cells, which suits this cell line for research addressing insulin signaling and diabetes [84]. Insulin stimulates glucose uptake into muscle via translocation of GLUT4 from intracellular to the plasma membrane [88 85]. Furthermore, C2C12 cells showed a similar basal glucose uptake compared to human muscle cells, with similar expression levels of the gradient-driven glucose transporter GLUT1, similar myosin and glycogen content [89]. The differentiation process is fast and easy, taking only 4-6 days and demonstrating best results if Horse serum is added to the culture media instead of serum-free differentiation [90].

In the setting of insulin resistance, the myocardium's ability to utilize glucose as an energy source is reduced [91 92], whereas under physiological conditions energy utilization from FA and carbohydrates is based on metabolic demand and availability [93]. Even though FFAs are the major energy source for heart muscle, an excess of plasma FFAs can cause ischemic damage and high oxidative stress [94]. These metabolic changes and the accumulation of lipids in the heart play a critical role in the development of diabetes related cardiac complications, such as diabetic cardiomyopathy [95 96 97 98]. To further understand these mechanisms in heart muscle, we mimicked diabetic conditions in H9C2 cell cultures. H9C2 are myocytes from embryonic rat ventricular tissue [99]. H9C2 myocytes are widely applied in studies addressing cardiac hypertrophy, metabolism, ischemic stress and IR/diabetes [100 101 102 103]. The differentiation process of H9C2 is time consuming and affords handling in the dark. In previous diabetes studies with H9C2 cells, researchers worked mainly with undifferentiated myoblasts, which express little cardiac specific markers and can still have the ability to differentiate into skeletal muscle instead of cardiac muscle **(Table 1)** [104 69 58 105]. In 2017 Patten *et al.* stated that the combination of serum reduction with retinoic acid (RA) supplementation in the differentiation process did increase the expression of cardiac troponin T, as well as a second cardiac specific marker, Myosin Light Chain 2V [106]. Lopashuk *et al.* identified that only differentiated H9C2 cells switch from glycolysis to oxidative phosphorylation, which is characteristic for heart tissue [107]. Also, insulin-signaling molecules such as insulin receptor substrate-1 and GLUT4 are significantly more expressed by differentiated H9C2 myocytes [108].

In conclusion, both cell lines should be differentiated into myotubes to explore heart and skeletal muscle specific processes related to T2D.

1.4 Simulating type 2 diabetes as a chronic condition

Type 2 diabetes and metabolic syndrome develop over time and are the result of a culmination of gradual changes in metabolism. With a degrading cellular response to insulin, blood glucose levels rise steadily followed by the release of high amounts of insulin by pancreatic beta cells. This results in muscle cells becoming increasingly insensitive to insulin causing a chronic state of hyperglycemia, hyperlipidemia and hyperinsulinemia. If this state is maintained, pancreatic beta cells begin to fail and DM manifests [109 110]. Given that T2D is a chronic condition, we exposed our cell cultures to diabetic conditions for 96 hours. These long-term treatments were compared to 24h short-term treatments.

1.5 Exploring insulin resistance by measuring glucose uptake into cells

Adipocytes and muscle cells express the insulin sensitive GLUT4. It has been shown that its expression and translocation to the plasma membrane is decreased in individuals suffering from diabetes [111 112 113]. By measuring glucose uptake, changes in GLUT4 translocation upon insulin stimulation can be observed and IR can be detected. There are various methods to measure glucose uptake, such as the detection of fluorescently tagged 2-NBDG (2-(N-(7-nitrobenz-2-oxa-1,3-diazol-4-yl)amino)-2-deoxyglucose). However, the much larger 2-NBDG might not be transported into the cell like glucose. 2-deoxyglucose (2DG) is another glucose analogue, which is transported similarly as glucose and accumulates in the cell as 2-deoxyglucose-6-phosphate (2DG6P). To detect 2DG6P, bioluminescent, fluorescent and radioactive assays are available [114 115]. We chose the radioactive ^{3}H-2-deoxy-glucose-uptake assay which is state of the art to assess IR due to its high sensitivity [116].

1.6 Diabetes and mitochondrial dysfunction

Mitochondria are not only the source of energy for living organisms, but also serve for determining the life and death fate of individual cells, whole organs, and ultimately the entire organism. It is known that altered mitochondrial function contributes to aging and disease development, including neurodegenerative diseases, cancer and atherosclerosis [117 118 119-121]. The organs that mostly rely on mitochondrial function are the same ones that are affected in common “complex” diseases, including myopathies, neuropathies, nephropathies and metabolic or endocrine diseases [122]. Controversy exists as to whether mitochondrial damage and ROS production can lead to the development of DM, or the cycle

of hyper-glycemia and –lipidemia lead to mitochondrial dysfunction [95 108 123 124 125]. Various human studies suggested the existence of mitochondrial dysfunction in muscle cells of obese and insulin-resistant patients [126 127 128].

Mitochondria produce adenosine triphosphate (ATP), the energy currency of the cell. Thus, mitochondria play a central role in metabolic processes including substrate oxidation and oxidative phosphorylation and have to adapt rapidly to changing metabolic conditions [129]. If mitochondria are dysfunctional, then the subsequently reduced oxidation of FAs results in lipid accumulation, including diacylglycerols and ceramides, which can cause IR [81]. It is suggested that there is a strong correlation between the development of heart failure and mitochondrial dysfunction, given that ATP-synthesis is reduced and more ROS are generated in cases of heart failure [130]. ROS have a destructive potential because of their high reactivity with biologically important molecules such as lipids, proteins, and DNA [131 132 133 134]. Comprehensive understanding of the mechanisms that relate mitochondrial function and insulin signaling is still lacking. Identifying the factors and mechanisms responsible for changes in mitochondrial energetics could make mitochondria to a potential target for treating diabetes. Therefore, we examined mitochondrial function in rodent skeletal and heart muscle utilizing the Agilent Seahorse XF Analyzer, which is widely accepted as the industry standard for obtaining *in vitro* cellular metabolic parameters. The XF Analyzer measures the major energy-producing pathways of cells: The Oxygen Consumption Rate (OCR) quantifies mitochondrial respiration and the Extracellular Acidification Rate (ECAR) is largely the result of glycolysis [135]. The Seahorse XF Cell Mito Stress Test monitors most aspects of mitochondrial respiration. During the assay, inhibitors of mitochondrial function are injected sequentially to distinguish parameters like basal respiration, ATP linked respiration rates or maximal respiration capacities **(Fig. 1)** [136].

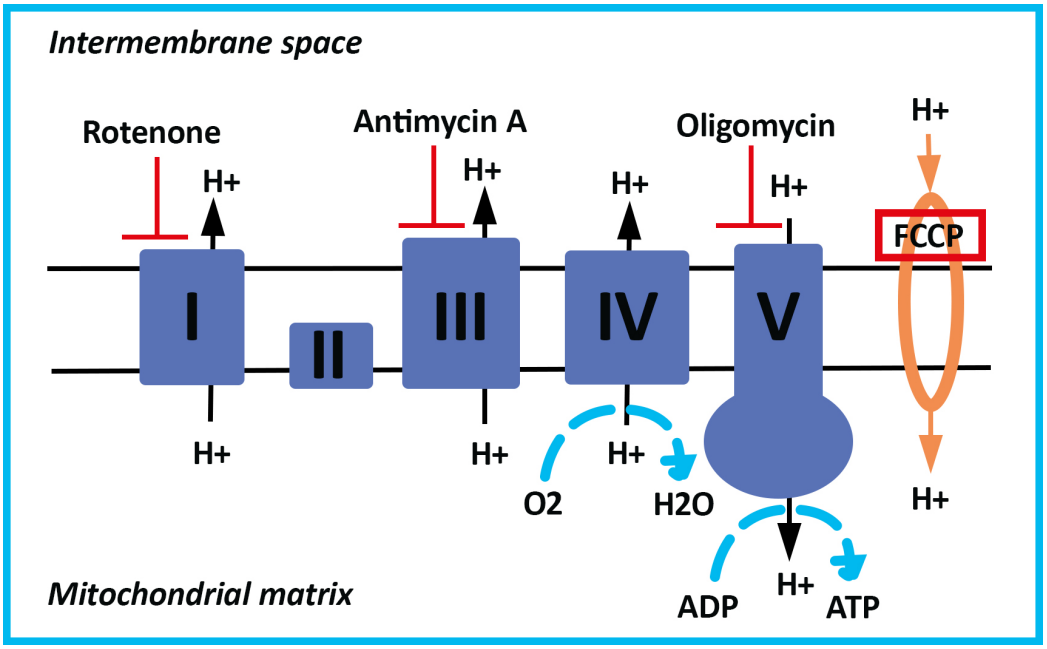

Fig. 1: Inhibition of compartments of the respiratory chain during the Seahorse XF Mito Stress Test. The first injection is oligomycin, inhibiting the ATP synthase (complex V) [137]. The second injection, FCCP, uncouples oxygen consumption from ATP linked respiration. The third injection is a mix of rotenone, a complex I inhibitor, and antimycin A, a complex III inhibitor [138]. Figure by Kopp EL.

To measure glycolytic rates, we performed the Seahorse XF Glycolytic Rate Assay **(Fig. 4)** [139]. Metabolic changes occurring in a diabetic environment can be measured with the OCR/ECAR ratio, which reveals a clear energetic picture of cells. Plotting OCR versus ECAR on an energy map provides a qualitative measurement of the relative utilization of oxidative (OCR) versus glycolytic (ECAR) pathways for energy production **(Fig. 2)**. This technology has been applied for the metabolic phenotyping of cancer cells [140 141 142 143], fibroblasts [144 145] and skeletal muscle cells and fibers [146 147]. We focused on the favored pathway for energy production under baseline conditions in a T2D-mimicking environment.

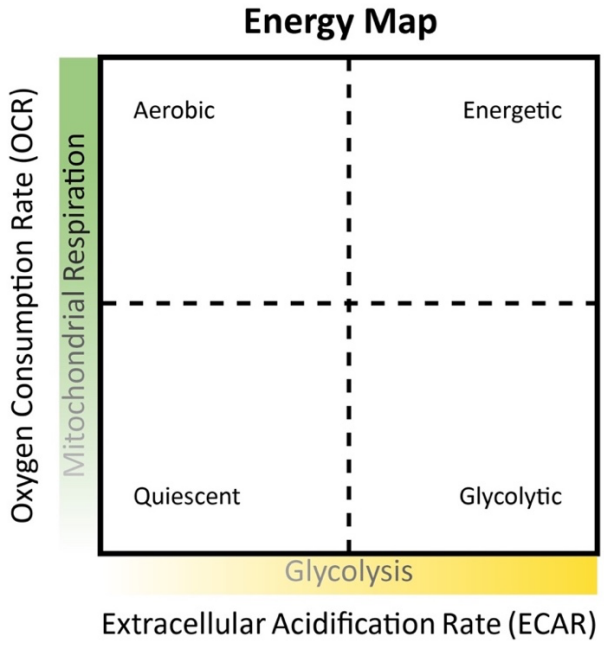

Fig. 2: Energy map using the OCR/ECAR ratio to show the energetic pathways that are utilized for energy production. A higher OCR/ECAR ratio accounts for more oxidative phosphorylation, a lower ratio for more glycolysis [142]. Figure by Kopp EL.

1.7 Morphology and distribution of mitochondria in type 2 diabetes mimicking conditions

Healthy skeletal muscle requires large ATP amounts mostly supplied by mitochondria, to perform its energetically demanding tasks like contraction, ion transport and protein synthesis [148]. A higher mitochondrial content in mammalian muscle cells, correlates with a higher energetic capacity [149] [150] [151] [152]. Energetically active cells are characterized by large mitochondrial networks and mitochondrial fusion, allowing the transport of metabolites and enzymes, while quiescent cells show smaller mitochondria and increased fission [153] [154] [155]. Mitochondrial dysfunction has been reported in muscle of diabetic patients, as well as changes in number, shape and size, such as small, depleted and fragmented mitochondria compared to lean controls [156] [157] [126] [158]. Similar observations were made in hyperglycemia treated rat myoblasts [159] and in muscle from diet-induced diabetic mice [160] [161]. With TEM assessments, Morino *et al.* observed that skeletal muscle mitochondrial density was 38% lower in the insulin resistant offspring of type 2 diabetic parents compared to healthy subjects [162]. It was reported that mitochondria in skeletal muscle from healthy volunteers had more clearly defined internal membrane structure and wider cristae compared to T2D subjects [126]. In addition, Chen *et al.* recently demonstrated that HG treatment induced elevated fragmentation and fission in mitochondria of endothelial cells [163].

Mitochondria are not static organelles; when healthy they are constantly changing in size, location, and shape within the cells. For example, mitochondrial morphology differs depending on where mitochondria are localized in a cell. These differences allow for distinctive responses to various substrates, and interactions with other intracellular structures. Mitochondria of human skeletal and heart muscle are spatially separated into intermyofibrillar and peripherally/subsarcolemmal located mitochondria, which are mostly perinuclear (PNM) and perivascular mitochondria (PVM) [164] [165]. It is thought that intermyofibrillar mitochondria contribute more to contractile function while subsarcolemmal mitochondria provide energy for membrane and transport processes [166]. PNM exhibit dynamic fission/fusion, signal transduction, substrate transport [158] and were shown to be physically closer to protein synthesis/Golgi for perinuclear mitochondrial biogenesis in rabbit cardiac muscle [167]. Consequently, a decrease in PNM can be a sign of decreased protein synthesis and impaired mitochondrial dynamics and ATP production. Ritov *et al.* showed a deficiency of subsarcolemmal mitochondria in type 2 diabetic and obese patients compared to healthy patients, postulating that this deficit contributes to the development of IR [158].

Mitochondrial swelling occurs passively *in vitro* by altering the osmolarity of the medium and actively via electron transport, also known as a mitochondrial permeability transition, by oxidative stress, ROS or by adding agents like phosphorus, calcium, FAs, insulin and more [168] [169] [170] [171]. It can be a natural morphologic part of both oncotic and apoptotic cell death [172] [173]. It occurs with or without rupture of the outer mitochondrial membrane and can be accompanied by the release of proapoptotic proteins like cytochrome *c* [174] [175]. Sun *et al.* observed an increase in swollen mitochondria after 100µM etoposide treatment (12-18h) to induce apoptosis in HeLa cells, in a time and dose dependent manner [176]. Bonnard *et al.* observed mitochondrial swelling in EM pictures of skeletal muscle from mice on a chronic high-fat diet [160].

To understand mitochondrial morphology and appearance after exposing our cultures to T2D mimicking conditions, we utilized transmission electron microscopy (TEM). We expected to see smaller, fragmented mitochondria and possibly changes in distribution and number compared to physiological controls. PNM were quantified, as skeletal muscle can be 2-10% mitochondria by volume and a decrease in mitochondrial number might account for impaired function and contractility [177]. We also compared the appearance of normal versus swollen mitochondria in randomly selected cells of the different conditions.

2. Aims and hypotheses

This study aimed to develop a novel model for simulating T2D *in vitro* in muscle cells, including the main aspects of metabolic syndrome but trying to avoid insulin and metabolite concentrations above the range observed in T2D patients.

Aim 1. Conditions should more closely represent the complexity of T2D

i. Short term exposure to T2D-mimicking conditions alone is not sufficient as T2D is a chronic disease. Longer treatments are required for validating and studying the kinetics of a T2D model

ii. Exposure to high glucose alone is not adequate, as high glucose, high fatty acid and insulin levels combine to the typical pattern of T2D metabolic derangements

iii. Differentiation of muscle cells into myotubes in a physiological environment including normal insulin concentrations to avoid a quasi-diabetic preconditioning of control cells

Aim 2. Characterization of muscle cells under T2D-mimicking conditions

i. Development of impaired insulin-dependent glucose uptake should be studied in response to isolated and combined metabolic derangements present in T2D

ii. and its imprint on mitochondrial function, respiration, number and morphology in myotubes

3. Materials and Methods

3.1 Cell culture

C2C12 (CRL-1772™) and H9C2 (CRL-1446™) cell lines were purchased from American Type Culture Collection (ATCC, Manassas, VA, USA).

C2C12 cells (mouse myoblast) were cultured in Dulbecco's Modified Eagle's Medium (DMEM) (GIBCO/BRL, 11885092) containing 5mM glucose, supplemented with 10% Fetal Bovine Serum (FBS, Thermo Fisher Scientific, 16000044) and 1% Penicillin/Streptomycin

(Penstrep, GIBCO, 15140122). All used culture media were sterile filtered with EMD Millipore Stericup Sterile Vacuum Filter Units (Fisher Scientific, SCGPU05RE). The cells were maintained in vented 75 cm^2 tissue culture flasks (Sarstedt, Germany) and incubated at 37°C under an atmosphere of 95% air and 5% CO2. Seeded at a density of 1,15 x 10^5 cells/ml (determined by: BIO RAD TC20 Automated Cell Counter), the cultures became 50-60% confluent after 48 h. At this time the culture medium was discarded and the cells were routinely split, using trypsin (0.25% Trypsin-EDTA, Gibco, 25200-056) to lift the cells from the culture flask base. To keep the cultures in low passages, stocks were frozen in liquid nitrogen at passage one to three (DMEM with 5% DMSO). Between passage four and five and at a density of 80-90% the cells were counted to determine the seeding densities for each planned experiment. For cell differentiation, the culture medium was discarded and differentiation was initiated. Culture medium was exchanged to DMEM containing 5mM glucose, supplemented with 2% horse serum (HS) (Thermo Fisher, 26050088) and 1% Penstrep was refreshed daily [178]. Cell treatments were started after 5-6 days of differentiation.

H9C2 cells (cardiomyoblasts from embryonic rat hearts) were cultured in DMEM containing 5mM glucose, supplemented with 10% FBS and 1% Penstrep. The cells were maintained in vented 75 cm^2 tissue culture flasks and incubated at 37°C under an atmosphere of 95% air and 5% CO2. Seeded at a density of 1 x 10^5 cells/ml the cultures became 50-60% confluent after 72 h. At this time, the cells were routinely split, as mentioned before. At a density of 85-95%, differentiation was initiated as described by Pereira *et al.* [179]. The culture medium was changed to differentiation medium, consisting of DMEM (5mM glucose), supplemented with 1% FBS, 1% Penstrep and 10nM All-trans-retinoic acid (RA) (Sigma Aldrich, R2625-500MG). RA was diluted in DMSO and stored at -20°C in the dark. Medium change was performed daily in the dark. Morphological changes were assessed using bright field microscopy. Cell treatments for assays were started after 6-8 days of differentiation. To preserve the characteristics of the cell lines, C2C12 and H9C2 cell cultures were used in passage 2-6 in all experiments.

3.2 Treatments

For simplicity, supraphysiologic glucose concentrations in cell culture media will be referred to as “hyperglycemic” in the text. DMEM containing 25mM glucose (GIBCO/BRL, 11995073) was used as a hyperglycemic condition (HG). This hyperglycemic condition was also used in combination with insulin (HGI) (1nM, insulin glargin, Lantus, Sanofi), or palmitate (HGP) (150µM for C2C12, 75µM for H9C2). A further hyperglycemic condition was combined with

both insulin and palmitate (HGPI). Groups treated with low glucose (LG, 5mM) and the same combinations with palmitate and/or insulin served as physiological controls (LGI, LGP, LGPI). To exclude a possible hyperosmolar effect, cells treated with 20mM mannitol plus 5mM glucose served as control cultures (high mannitol, HM). The same treatment combinations were used (HMI, HMP, HMPI) **(Table 2)**. The cells were exposed to the different conditions either short-term (24h) or long-term (96h). Previous to all experiments the culture medium was changed to serum free medium for 4-6 hours.

Table 2: Treatment groups

Group name	**Treatment**
LG *(Low Glucose)*	5mM glucose
LGI *(Low Glucose Insulin)*	5mM glucose + 1nM insulin
LGP *(Low Glucose Palmitate)*	5mM glucose + 150µM or 75µM palmitate
LGPI *(Low Glucose Palmitate Insulin)*	5mM glucose + 150µM or 75µM palmitate + 1nM insulin
HG *(High Glucose)*	25mM glucose
HGI *(High Glucose Insulin)*	25mM glucose + 1nM insulin
HGP *(High Glucose Palmitate)*	25mM glucose + 150µM or 75µM palmitate
HGPI *(High Glucose Palmitate Insulin)*	25mM glucose + 150µM or 75µM palmitate + 1nM insulin
HM *(High Mannitol)*	20mM mannitol + 5mM glucose
HMI *(High Mannitol Insulin)*	20mM mannitol + 5mM glucose + 1nM Insulin
HMP *(High Mannitol Palmitate)*	20mM mannitol + 5mM glucose + 150µM or 75µM palmitate
HMPI *(High Mannitol Palmitate Insulin)*	20mM mannitol + 5mM glucose + 150µM or 75µM palmitate + 1nM Insulin

For long term treatments the concentration of palmitate was escalated every 24 hours to prevent myotube loss **(Table 3)**.

Table 3: Escalation of palmitate concentrations for long term (96h) treatments of C2C12 and H9C2 myotubes. Palmitate concentrations were increased every 24 hours

Treatment duration	Concentration for C2C12	Concentration for H9C2
24h	35µM	5 µM
48h	70µM	25µM
72h	105µM	50µM
96h	150µM	75µM

Before adding sodium palmitate to cell differentiation medium, it was conjugated to fatty acid free bovine serum albumin (BSA). Transportation of palmitate into cells is then enabled and cytotoxicity lowered. Briefly, ultra-fatty acid free BSA (Sigma Aldrich, A8806) was dissolved in the respective differentiation medium for each cell line, heating the solution to approximately 37°C. Sodium palmitate (Sigma Aldrich, P9767) was dissolved in a 150mM NaCl solution, stirring at 70°C. The palmitate solution was added to the BSA solution while stirring at 37°C. After stirring for 1 h, pH was adjusted to 7.4 with NaOH. The conjugated palmitate-BSA solution was aliquoted in glass vials and frozen at -20°C. Stock solutions were made at 75mM.

3.3 ^{3}H-2-deoxy-glucose-uptake

C2C12 Myoblasts (passage four) were seeded into 24-well plates at a density of 1.42-2.72 x 10^4 cells/well. 24h and 96h treatments were started after five to six days of differentiation. 96 h treatment groups were treated on a daily base. Treatments were prepared in respective differentiation medium.

H9C2 Myoblasts (passage four) were seeded into 24-well plates at a density of 1.48- 2.3 x 10^4 cells/well. 24h and 96h treatments were started after six to eight days of differentiation. 96 h treatment groups were treated on a daily base. Treatments were prepared in respective differentiation medium and performed in the dark.

^{3}H-2-deoxy-glucose-uptake assays were performed as follows:

Culture media were discarded 3-4 hours before the assay and changed to serum-free DMEM with 0.25% fatty acid-free BSA. Serum-Starvation was held in respective treatment media (serum-free DMEM with either high or low glucose (5mM vs 25mM) and supplemented with palmitate or 1nM insulin respectively). After starvation cultures were washed twice with Hepes fortified Krebs-Ringer Bicarbonate buffer (HKRB), containing 10 mM Hepes, pH 7.4,

NaH2PO4 (0.83 mM), Na2HPO4 (1.27 mM), NaHCO3 (15 mM), NaCl (120 mM), KCl (4.8 mM), calcium (1 mM), magnesium (1mM), pH 7.35 and 0.25% fatty acid-free BSA. Cultures were incubated in HKRB for 60 minutes at 37°C. To compare basal glucose uptake to insulin dependent glucose uptake, half of the cultures were pre-assigned for acute insulin treatment. These cultures were treated with 100nM insulin from a 100x stock and incubated for 20 minutes at 37°C. After this incubation period ^{3}H-2-deoxy-glucose (^{3}H-2DOG, 2-[1,2-3H(N)]-, 250µCi (9.25MBq), Perkin Elmer, NET549A250UC) was added to each well for further 10 minutes incubation. ^{3}H-2DOG-treatment was terminated by quick aspiration, followed by cold wash (2x) with ice-cold PBS. Next, we added 1N NaOH and swirled the plates slowly for 30 minutes to dissolve the cells. Aliquots of 20µl were taken out of each well for protein measurements. Then the whole lysate of each well was transferred into a scintillation vial. After neutralizing NaOH with 1N HCl, scintillation cocktail (Ecoscint original, National Diagnostics, LS-271) was added. The radioactivity was measured in a scintillation counter.

Results were normalized with protein concentrations and presented as counts per minute (cpm) per mg protein. Alternately, the results were presented as cpm per million cells.

3.4 Mitochondrial function measurements with the Agilent Seahorse XFe 96 Extracellular Flux Analyzer

Glycolytic rate assays and mitochondrial stress tests were performed with an Agilent Seahorse XFe 96 Extracellular Flux Analyzer (Agilent Technologies, La Jolla, California). The analyzer measures real time extracellular acidification rate (ECAR) and oxygen consumption rate (OCR) of cells. For the assay C2C12 and H9C2 cells were seeded in a density of 1.2 x10^{4} cells per well, as previously performed in an Agilent application note [180]. Cells where then differentiated in Seahorse XF 96 microplates and incubated at 37°C, 95% air and 5% CO2. Differentiation and 24h/96h-treatments were carried out as described above. One night before the assay, a sensor cartridge was hydrated in Seahorse XF Calibrant at 37°C in a non-CO2 incubator.

3.4.1 Mitochondrial Stress Test

On the day of the assay the differentiation medium was changed to sterile filtered warmed assay medium (XF base medium + 1mM pyruvate + 2mM glutamine + 10mM glucose, pH 7.4 at 37°C). The cells were then incubated for 1 hour at 37°C and 100% air, to minimize CO2 influence on the assay. Meanwhile the calibration plate was placed in the Seahorse

XFe96 Flux analyzer for a 15–30-minute calibration. When prompted, the calibration plate was exchanged with the cell culture microplate to start the assay. Basal respiration was measured in three cycles (15 min total). Oligomycin (1.0µM), Carbonyl cyanide 4-(trifluoromethoxy) phenylhydrazone (FCCP) (1.0µM), and a mixture of Rotenone and Antimycin A (Rot/AA) (0,5µM) were then added in sequences of 15 min per drug (3 measurement cycles each) **(Fig. 3)**. Each experiment was repeated 3-5 times with 6-15 wells per treatment condition per plate.

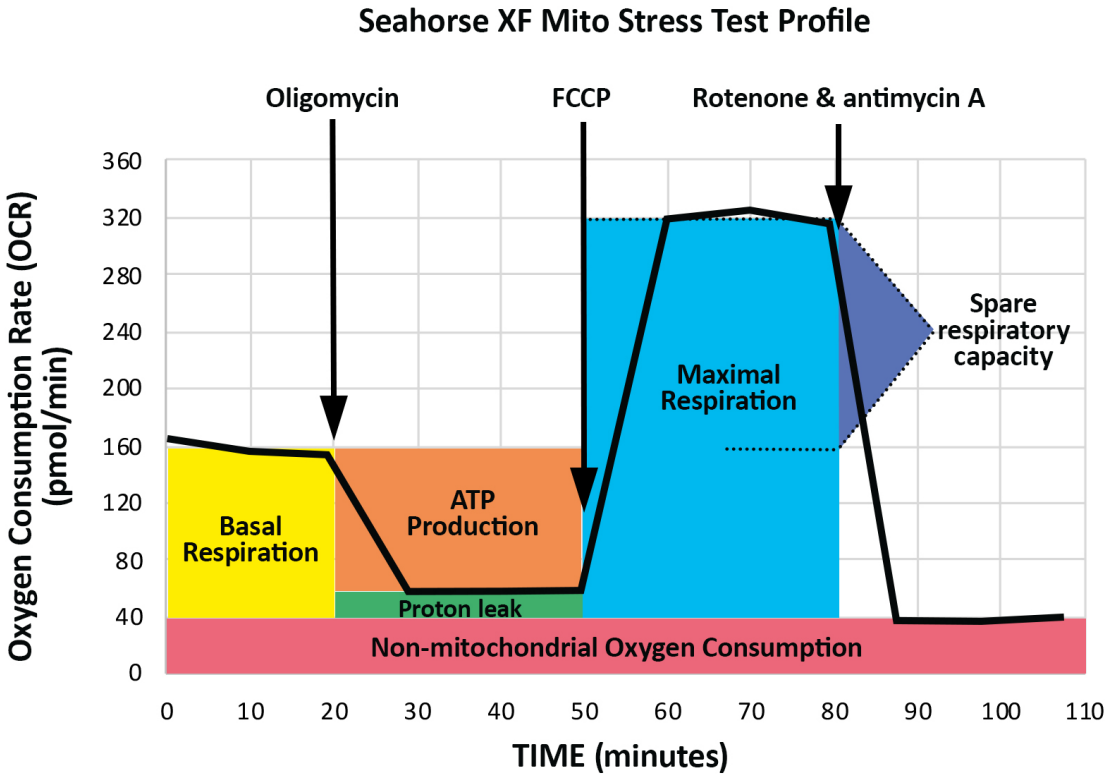

Fig. 3: Seahorse XF Mito Stress Test profile, presented as by Agilent Seahorse Biosciences (https://www.agilent.com/en/products/cell-analysis/seahorse-xf-consumables/kits-reagents-media/seahorse-xf-cell-mito-stress-test-kit, accessed February 16, 2021). Basal respiration meets the baseline cellular energy demand. Upon inhibition of the ATP synthase with oligomycin, the respiration accounting for ATP linked respiration can be calculated. The remaining basal respiration that is not coupled to ATP linked respiration is proton (H+) leak, which can be a physiological mechanism to regulate ATP production. FCCP mimics an energy demand leading to maximal respiration. Spare respiratory capacity indicates the cell's capability to respond to an energetic demand and can be an indicator of cellular fitness or flexibility [136] [181]. Figure by Kopp EL.

The following respiration rates were measured:

- Basal respiration: Oxygen consumption used to meet cellular ATP demand under baseline conditions. It can be set by the rate of ATP utilization and substrate availability and oxidation.

- ATP-linked respiration: Upon injection of the ATP synthase inhibitor oligomycin a decrease in OCR represents the part of basal respiration that accounts for ATP production, meeting the energetic needs of the cell. It is largely set by the ATP demand of the cell and substrate oxidation, which can be decreased if there is a mitochondrial dysfunction.

- Maximal respiration: By adding the uncoupler carbonyl cyanide p-(trifluoromethoxy) phenylhydrazone (FCCP) the maximal OCR can be attained. FCCP mimics an "energy demand" and stimulates the respiratory chain to operate at maximum capacity thus substrates are rapidly oxidized. It is also influenced by substrate supply and oxidation including the functional substrate transport across the plasma and mitochondrial membranes. Changes may reflect membrane defects, altered mitochondrial biogenesis and function and decreased oxidation abilities.

- Spare respiratory capacity: This value can be calculated with basal and maximal respiration values. It indicates the cell's capability to respond to an energetic demand and can be an indicator of cell fitness or flexibility. A decreased capacity can be linked to mitochondrial dysfunction but can also reflect an increased ATP demand/increased basal respiration (i.e., in highly proliferative cells). Increases may reflect high substrate provision or enhanced oxidative capacity [182].

The respiration parameters were calculated as follows:

Table 4: Equations for the analysis of XF Mito Stress Test. Adapted from Agilent Seahorse, by Kopp EL.

Basal Respiration	Equation
Basal respiration	**(Last rate measurement before first injection) – (non-mitochondrial respiration rate)**
Maximal respiration	**(Maximum rate measurement after FCCP injection) – (non-mitochondrial respiration)**
ATP linked respiration	**(Last rate measurement before Oligomycin injection) – (minimum rate measurement after Oligomycin injection)**

3.4.2 Glycolytic Rate Assay

The assay utilizes both ECAR and OCR measurements to determine the glycolytic proton efflux rate (glycoPER) of the cells. On the day of the assay the differentiation medium was changed to sterile filtered warmed assay medium (see above), substituted with 5.0mM HEPES buffer. Basal respiration rates were recorded over three measurement periods, followed by an injection of Rot/AA to inhibit mitochondrial-derived acidification. The second injection was 2-deoxy-D-glucose (2-DG), a glucose analog which inhibits glycolysis through competitive binding of glucose hexokinase, the first enzyme in the glycolytic pathway.

The following values were measured or calculated **(Fig. 4)**:

- Proton efflux rate (PER): Protons exported by cells into the extracellular assay medium during the assay, expressed as pmol/min.

- Glycolytic proton efflux rate (glycoPER): PER derived from basal glycolytic activity of the cell (CO2-dependent acidification is subtracted).

- Compensatory glycolysis: The glycolytic rate in cells upon the addition of mitochondrial inhibitors. Oxidative phosphorylation is inhibited and compensated by increased glycolysis, to meet the cellular energy demand.

- Post-2DG acidification: This value is measured after the addition of 2-DG and accounts for any other sources of acidification that are not attributed to glycolysis or mitochondrial activity.

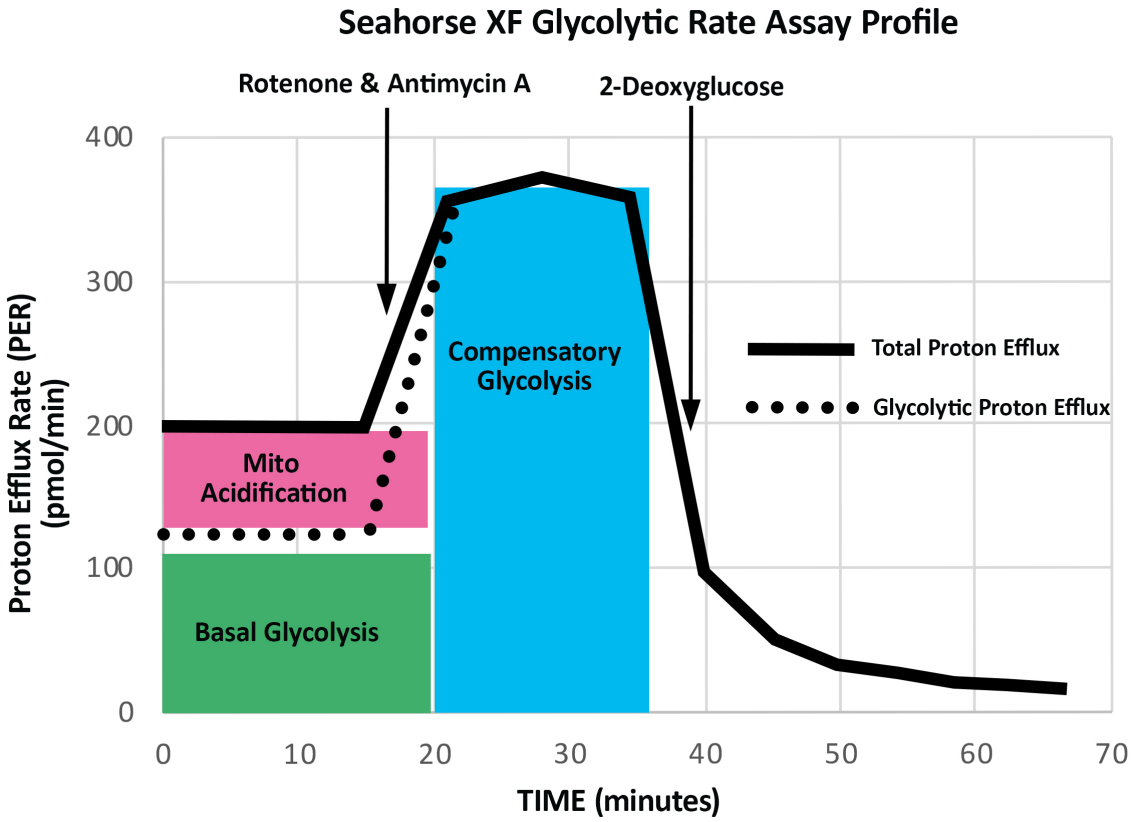

Fig. 4: Glycolytic Rate Assay profile. Adapted from Agilent Seahorse Manuals. Total proton efflux accounts for acidification caused by both glycolysis and mitochondrial oxidation. Rotenone & Antimycin A shut down the respiratory chain and energy production is compensated by increased glycolysis. Proton efflux after inhibition of glycolysis with 2-deoxyglucose accounts for other sources of acidification. By Kopp EL.

3.5 Electron microscopy

C2C12 and H9C2 myotubes maintained short term (24h) and long term (96h) in different T2D-mimicking and control conditions (3.2 Treatments) were fixed and embedded for electron microscopy (EM) as follows: Cell pellets were fixed with 2% glutamate in 0.1 M cacodylate buffer and further postfixed in 1% OsO4 in 0.1 M cacodylate buffer for one hour on ice. The cells were stained all at once with 2% uranyl acetate for one hour on ice, followed by dehydration in graded series of ethanol (50-100%) while remaining on ice. The cells were then washed 1x with 100% ethanol and 2x with acetone (10 min each) and embedded with Durcupan. Sections were cut at 60nM on a Leica UCT ultramicrotome and

picked up on 300 mesh copper grids. Sections were post-stained with 2% uranyl acetate for 5 minutes and Sato's lead stain for 1 minute. Grids were viewed using a Jeol 1400 plus Transmission Electron Microscope and photographed with a Gatan digital camera (Hillsboro, OR). Pictures of whole cells, mitochondria, nuclei and membrane were taken in magnifications between 890x and 9200x. The images were analyzed using Image G. Mitochondrial distribution analysis of perinuclear mitochondria was made in 2000x magnifications. The inner perinuclear circle was defined with a 200-pixel distance to the nucleus membrane, the outer perinuclear circle was defined with a 400-pixel distance to the nucleus membrane. Cell organelles were confirmed to be mitochondria before counting, with pictures of the same cells in 5000x and 15kx magnifications. For mitochondrial size analysis mitochondrial area was measured in square pixels in 15kx magnifications of randomly and blinded taken pictures of mitochondria.

3.6 Light microscopy

Pictures of C2C12 and H9C2 cells were taken with a Keyence light microscope in magnifications of 20x.

3.7 Statistical analysis

All Data analyses were performed using GraphPad Prism 9.0 (GraphPad Software, La Jolla, CA). For glucose uptake assays the results are expressed as mean ± SD of 6 biological replicates for all LG and HG groups and 3 replicates for all HM groups.

For Agilent Seahorse Mito Stress Tests all data shown are the means ± SD of 3-4 replicate assays with 8-15 wells per treatment group per plate. Data of Glycolytic Rate Assays represent the means ± SD of 1-2 replicate assays with 6-11 wells per treatment group per plate. Seahorse data were generated using Wave 2.4 and the Seahorse XF Report Generators from Agilent.

EM pictures were analyzed using ImageJ and Graphpad Prism 9.5.

For statistical analyses we used analysis of variance (one-way ANOVA or two-way ANOVA) followed by Tukey's test for multiple pairwise comparisons, as specified in figure legends. A p value <0.05 was considered as a statistically significant difference.

4. Results

4.1 Cell differentiation and treatments

C2C12 and H9C2 myotubes cultured in LG (5mM glucose) showed healthy growth according to the cell line. Differentiation was effective. The myotubes appeared healthy in shape and size. Before differentiation, C2C12 cells appeared spindle-shaped **(Fig. 5 A)** and fused into muscle fiber and contraction was visible after 5 days **(Fig. 5 B)**. Undifferentiated H9C2 myoblasts appeared spindle-shaped and mononucleated **(Fig. 6 A)**. After 6-8 days H9C2 cells appeared as long and thin- branched cardiomyotubes, analogical to a report by Kimes and Brandt in 1976 **(Fig. 6 B)** [99]. Both H9C2 **(Fig. 6 D)** and C2C12 myoblasts and myotubes cultured in HM grew slower compared to LG control cultures (number per visual field). Culturing C2C12 cells 96h in HM, resulted in an intracellular accumulation of paranuclear droplets in some cells **(Fig. 5 C)**. Both C2C12 **(Fig. 5 D)** and H9C2 **(Fig. 6 D)** myoblasts- and tubes cultured in HG showed healthy growth. Under long term insulin treatment (LGI) we didn't observe changes in growth or morphology in both C2C12 **(Fig. 5 E)** and H9C2 **(Fig. 6 E)** myotubes compared to LG controls.

In first palmitate treatments according to previous publications we observed a high cell loss (decrease in number per visual field, many detached and floating cells) in both C2C12 **(Fig. 5 F)** and H9C2 **(Fig. 6 F)** myotubes cultured in media containing a 750µM palmitate concentration [60 74 75]. After 24h treatment with 750µM palmitate only ~20% of H9C2 and ~30% of C2C12 myotubes were still attached. Due to the planned long exposure of 24h and 96h, we adjusted the concentrations as indicated in Table 3 and observed less cell loss **(Fig. 5 G, H, Fig. 6 G, H)**.

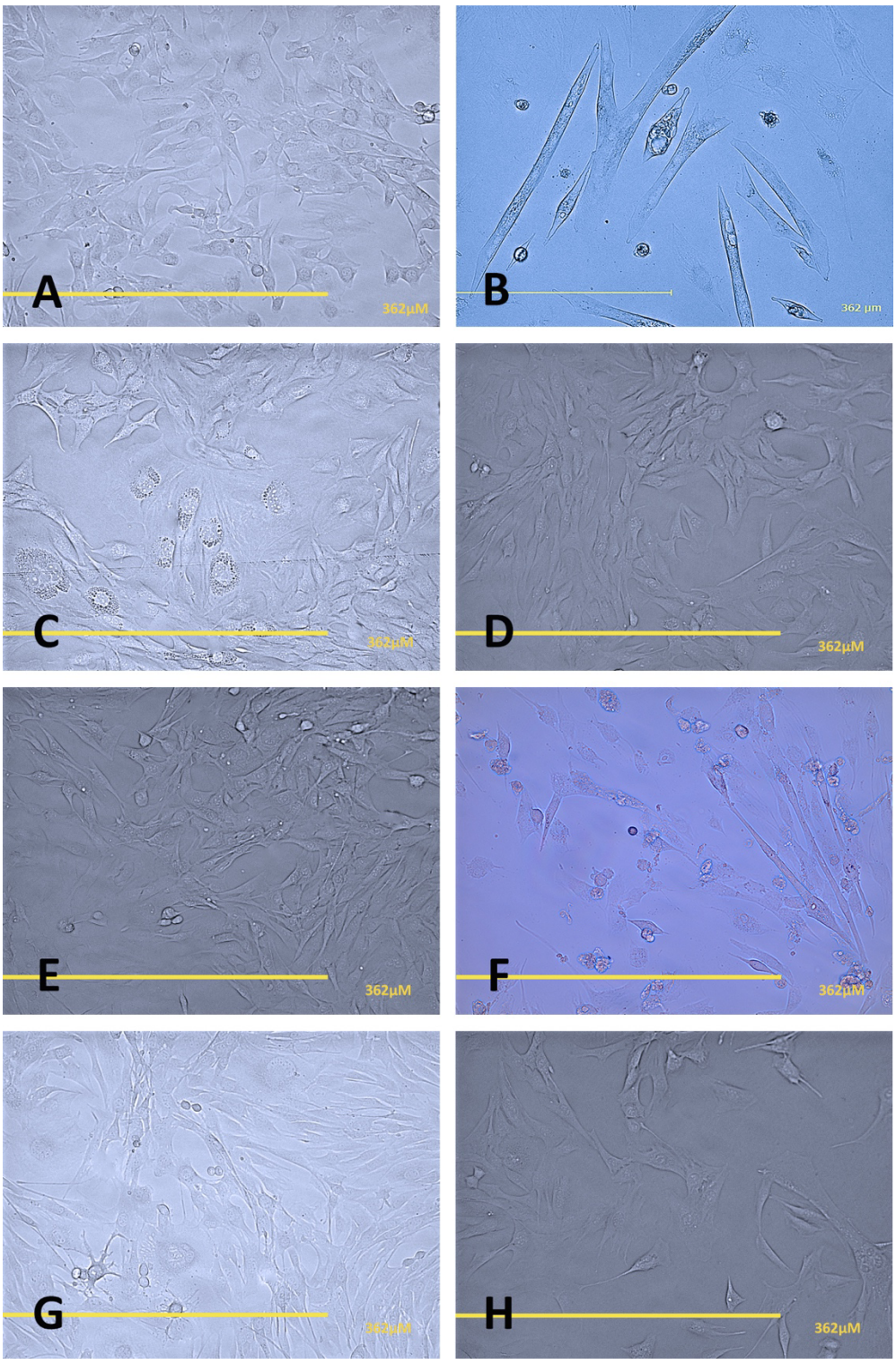

Fig. 5: C2C12 myoblasts and -tubes in different treatment conditions. A: Myoblasts in LG control growth medium. B: Myotubes in LG differentiation medium after 5 days of differentiation. C, D, E: Myoblasts after 96h HM (C), HG (D) and HGI (E) treatment. F: Myoblasts after 24h treatment in 750µM palmitate. G, H: Myoblasts after 96h LGP (G) and HGP (H) treatment, photographed at final concentrations of 150µM palmitate. Pictures were taken in a 20x magnification.

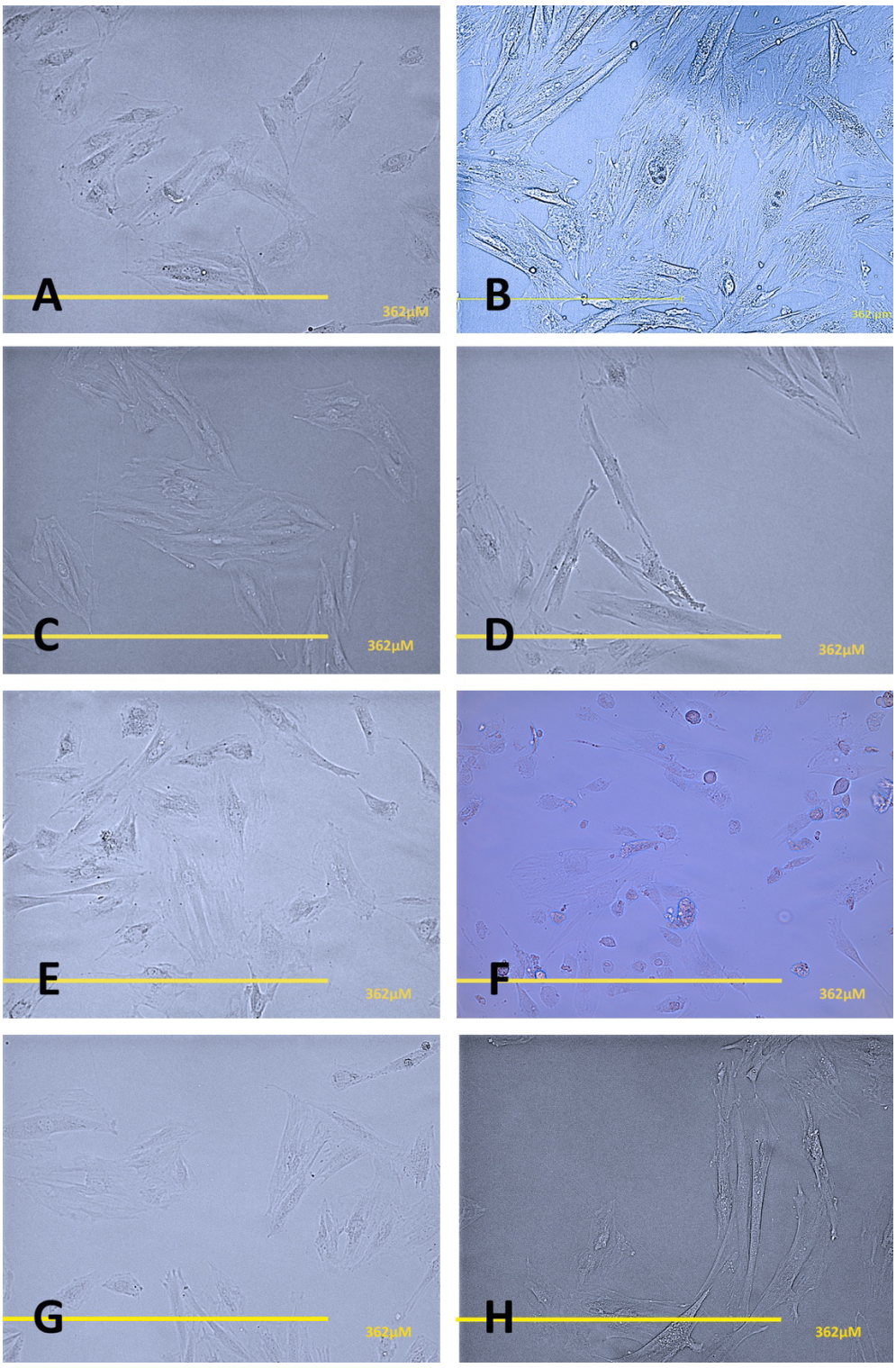

Fig. 6: H9C2 myoblasts and -tubes in different treatment conditions. A: Myoblasts in LG control growth medium. B: Myotubes in LG differentiation medium after 5 days of differentiation. C, D, E: Myoblasts after 96h HM (C), HG (D) and HGI (E) treatment. F: Myoblasts after 24h treatment in 750µM palmitate. G, H: Myoblasts after 96h LGP (G) and HGP (H) treatment, photographed at final concentrations of 150µM palmitate. Pictures were taken in a 20x magnification.

4.2 ^{3}H-2-deoxy-glucose-uptake

Effects of high glucose, high palmitate and insulin on 2-deoxy[^{3}H]glucose uptake in C2C12 and H9C2 myotubes.

To determine basal and insulin dependent glucose uptake of C2C12 and H9C2 myotubes, ^{3}H-2-deoxy-glucose-uptake assays were carried out as described above (see Methods 3.3).

4.2.1 C2C12 myotubes

All cultures treated with T2D-mimicking conditions and controls including insulin and palmitate treatments showed IR. Low glucose control cultures showed a physiological increase in glucose uptake upon 100nM insulin stimulation in short term (24h) treatment **(Fig. 7 A)** (p=0.0055 LG +/- insulin). Short term treatments of 1nM insulin and/or 150µM palmitate in LG cultures impeded the stimulatory effect of insulin (p>0.1 vs basal in each group), leading to IR. Similar effects were seen after 96h treatments **(Fig. 7 D)**. Both after short- and long-term treatment basal glucose uptake was increased in LGI treated groups compared to LG **(Fig. 7 A, D)** (24h LG vs LGI p=0.0091, 96h LG vs LGI p=0.0001). LGP and LGPI treated myotubes displayed decreased glucose uptake rates compared to LG and LGI treatments. Cultures treated short or long term in a HG condition could not increase glucose uptake upon insulin stimulus **(Fig. 7 B, E)** but showed elevated basal rates compared to LG control (HG vs LG p=0.0184 after 24h, HG vs LG p<0.0001 after 96h, graph available in attachments **Fig. 16 A**). In long term HG treatment, basal glucose uptake was increased significantly over time compared to short term treatment (HG 24h vs 96h p<0.0001). We observed no significant increase in insulin dependent vs basal glucose uptake in all HG treatment groups (HG, HGI, HGP, HGPI). Myotubes treated with HGP or HGPI showed significantly lower basal and insulin dependent glucose uptake rates compared to HG and HGI groups **(Fig. 7 B, E, H)**. Myotubes treated with HM or HMI for 24h showed a significant decrease in basal glucose uptake compared to LG or HG (LG vs HM, HG vs HM p<0.0001) and no significant up-regulation of glucose uptake upon insulin stimulation. Interestingly, C2C12 myotubes treated with HM and palmitate (HMP and HMPI) showed a remarkable increase in both basal and insulin dependent glucose uptake, compared to glucose uptake in all other treatment groups **(Fig. 7 C)**. Looking at the half-violin plots with combined data of 24h and 96h treatments, it appears that treatments including mannitol show the widest spread in values due to the stimulatory effect on glucose uptake of palmitate **(Fig. 7 F)**, whereas in cells exposed to HG and palmitate an inhibitory effect of palmitate is apparent **(Fig. 7 H)**.

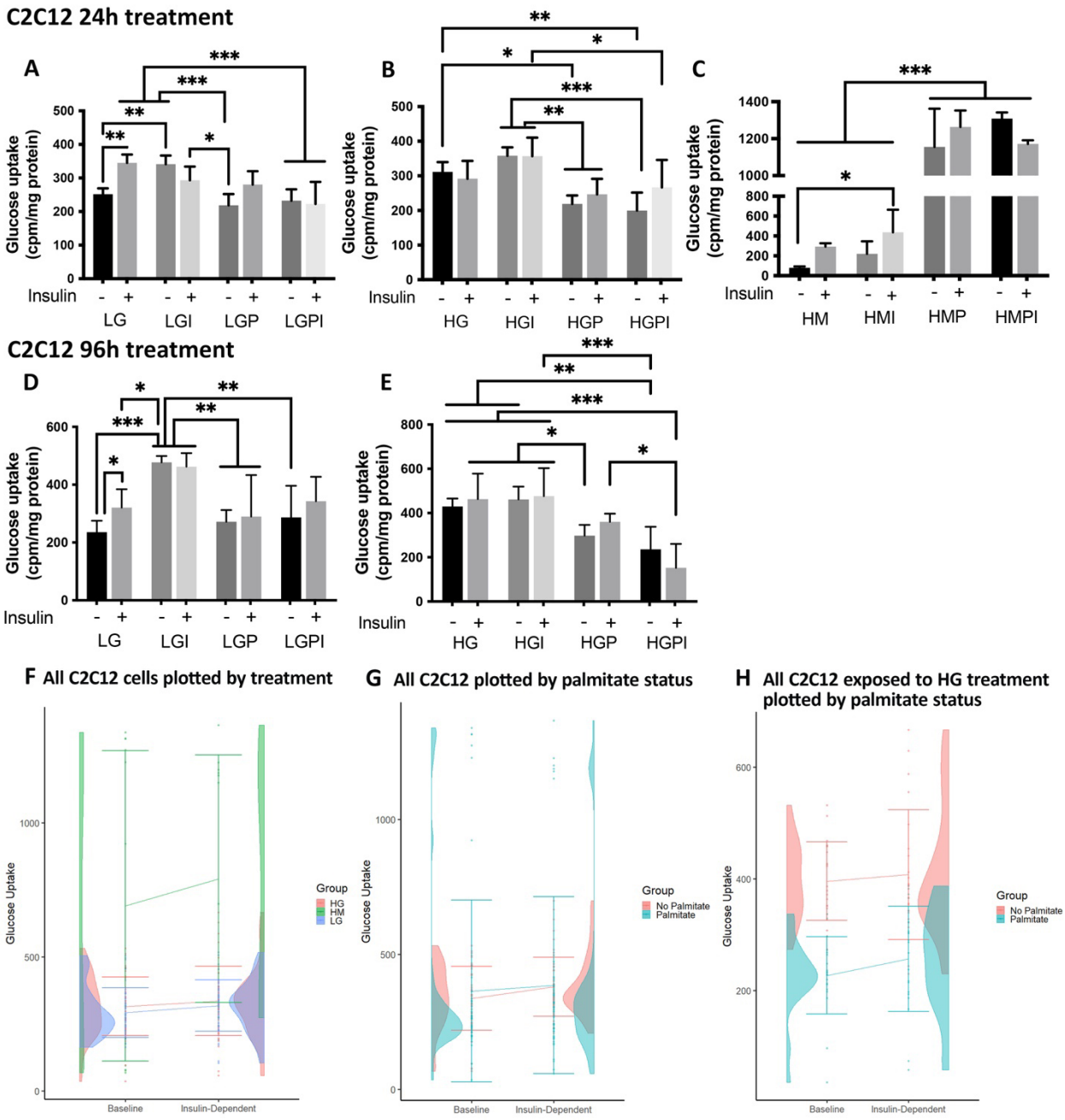

Fig. 7: Basal and insulin dependent ^{3}H-2-deoxy-glucose-uptake of C2C12 myotubes after 24h and 96h treatments. The effect upon an acute insulin stimulus (100nM) was compared between different T2D-mimicking conditions (HG, HGI, HGP, HGPI) and physiological (LG) and osmotic (HM) controls. A-C: Glucose uptake after 24h treatments. D + E: 96h treatments. F-H: Half-violin plots for combined 24h and 96h glucose uptake, with error bars for standard error and lines connecting mean glucose uptake between conditions, by group. F: All C2C12 cells by treatment G: All C2C12 cells by palmitate status. H: C2C12 cells receiving HG treatment by palmitate status. Due to a technical error in the scintillation counter 96h HM treatments could not be presented. Glucose uptake rates are

presented as cpm per mg protein. Values represent the means (SD); n=6 per treatment group for LG and HG treatments, n=3 per group for HM treatments. One-way ANOVA for A, B, C, D, E p<0.0001. Brackets indicate Tukey's multiple comparisons tests with *p<0.05, **p<0.01, ***p <0.001.

4.2.2 H9C2 myotubes

Insulin resistance occurs in all T2D-mimicking treatment groups. LG or LGI treated control cultures showed an increase in glucose uptake upon an acute insulin stimulus (100nM). After 24h treatment the increase just missed significance (LG p=0.6, LGI p=0.05), whereas after 96h treatment we observed a significant rise in insulin dependent glucose uptake compared to basal uptake (p<0.0001, **Fig. 8 A, D**). Basal glucose uptake rates in both LG and LGI treatment groups were similar, but insulin dependent rates were significantly higher in LGI compared to basal rates in LG **(Fig. 8 A)**. H9C2 myotubes treated short or long term with LG and palmitate (LGP and LGPI) showed significantly decreased glucose uptake rates compared to LG and LGI (24h LG vs LGP p<0.0001) **(Fig. 8 A, D)**. We observed similar effects on glucose uptake after short- or long-term treatments with HGP or HGPI **(Fig. 8 B, E)**, which is congruent with palmitate-induced inhibition of insulin sensitivity and glucose metabolism in these cells [59]. Groups treated short or long term with HG or HGI were insulin-resistant and showed a significantly higher basal and insulin dependent glucose uptake compared to groups treated with high glucose and palmitate (HG vs HGP p<0.0001, **Fig. 8 B, E**). In contrast, osmotic control cultures treated with HMP or HMPI showed a remarkable increase in both basal and insulin dependent glucose uptake compared to HM or HMI treatment (HM vs HMP p=0.0006, **Fig. 8 C**). We saw this effect similarly in glucose uptake assays with C2C12 myotubes **(Fig. 7 C)**. In summary HM treated groups showed lower glucose uptake rates compared to LG groups (LG basal rate mean = 207.33; HM basal rate mean = 45.95). Cultures treated with HM or HMI showed an increase in glucose uptake upon an acute insulin stimulus, however missing significance **(Fig. 8 C)**. Looking at the half-violin plots with combined data of 24h and 96h treatments, it appears that cells exposed to mannitol show the lowest glucose uptake rates of all treatments **(Fig. 8 F)**. Overall palmitate exerted a marked inhibitory effect on both basal and insulin dependent glucose uptake, particularly in the combination with HG treatment **(Fig. 8 G, H)**.

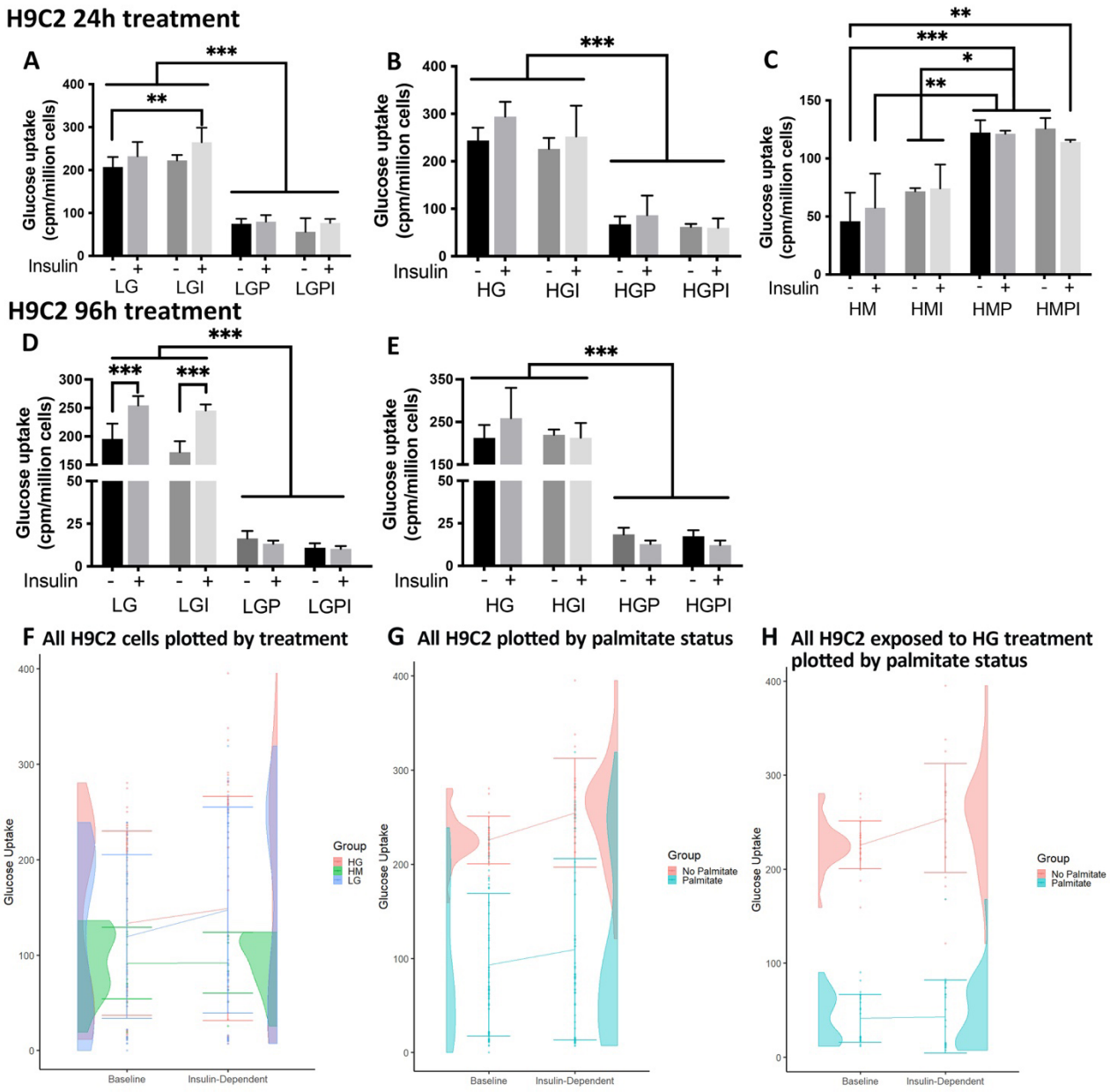

Fig. 8: Basal and insulin dependent ^{3}H-2-deoxy-glucose-uptake of H9C2 myotubes after 24h and 96h treatments. The effect upon an acute insulin stimulus (100nM) was compared between different T2D-mimicking conditions (HG, HGI, HGP, HGPI) and physiological (LG) and osmotic (HM) controls. A-C: Glucose uptake after 24h treatments. D + E: 96h treatments. F-H: Half-violin plots for combined 24h and 96h glucose uptake, with error bars for standard error and lines connecting mean glucose uptake between conditions, by group. F: All H9C2 cells by treatment. G: All H9C2 cells by palmitate status. H: H9C2 cells receiving HG treatment by palmitate status. Due to a technical error in the scintillation counter 96h HM treatments could not be presented. Glucose uptake rates are presented as cpm per million cells. Values represent the means (SD); n=6 per treatment

group for LG and HG treatments, n=3 per treatment group for HM treatments. One-way ANOVA for A, B, C, D, E $p<0.0001$. Brackets indicate Tukey's multiple comparisons tests with *$p<0.05$, **$p<0.01$, ***$p<0.001$.

4.3 Mitochondrial function measurements using the Agilent Seahorse XFe 96 Extracellular Flux Analyzer

To measure key parameters of mitochondrial function, we performed the Agilent Seahorse XF Cell Mito Stress Test. To get insights on glycolysis in our cultures we performed the Agilent Seahorse XF Glycolytic Rate Assay. We measured oxygen consumption rates (OCR) and extracellular acidification rate (ECAR) of H9C2 and C2C12 myotubes. With these rates, both glycolysis and oxidative phosphorylation can be calculated, as well as mitochondrial function.

4.3.1 Mitochondrial Stress Tests

Assays were performed after short term (24h) or long term (96h) treatments, as described in 3.2. We then determined the following parameters for analysis: basal respiration, ATP linked respiration (basal respiration minus oligomycin-inhibited respiration), maximal respiration (maximal uncoupled respiration minus non-mitochondrial respiration) and spare respiratory capacity. To get an overview on the metabolic phenotype of each treatment group we plotted Baseline OCR versus Baseline ECAR rates which shows us the XF Energy map (see introduction). In all Mito Stress Test assays with both C2C12 and H9C2 myotubes, relative oxygen consumption rate percentage of baseline did not differ statistically **(Fig. 9 D, I, Fig. 10 D, I)**. The results were expressed in pmol (O_2)/min.

4.3.1.1 C2C12 24h

Resting OCR was not significantly different between all treatment conditions (biological N = 3, technical replicates = 8-15 per assay). C2C12 myotubes treated 24h with non-physiological glucose levels (HG, HGI, HGP, HGPI) showed a significant decrease in ATP linked respiration compared to LG and LGI controls ($p<0.0001$). ATP linked respiration was significantly increased in LGI treated groups compared to LG control **(Fig. 9 A)**. Osmotic control cultures that were exposed to high concentrations of mannitol (HM, HMI) showed no difference to LG control groups in maximal respiration **(Fig. 9 B)** but a significant decrease in ATP-linked respiration **(Fig. 9 A)**. We observed no signficant differences in maximal respiration rates **(Fig. 9 B)**. Spare respiratory capacity rates were significantly increased in HGI, HGPI and HMI groups compared to LG control **(Fig. 9 C)**. In short term assays with

C2C12 myotubes we observed a shift towards glycolysis in all HG treated groups. Additionally, HM treated groups showed a metabolic shift towards glycolysis. LG groups showed a mainly aerobic metabolism and LGI groups were in between an aerobic and high energetic phenotype **(Fig. 9 E)**.

4.3.1.2 C2C12 96h

C2C12 myotubes treated 96h with high glucose (HG, HGI) or high mannitol (HM, HMI) showed a significant decrease in maximal respiration rates compared to LG and LGI (biological N = 3, technical replicates = 9-10 per assay) **(Fig. 9 G)**. A significant decrease in ATP-linked respiration of myotubes treated with high glucose or high mannitol, as seen before in 24h treatments, was observed (**Fig. 9 F**; LG vs HG $p<0.0001$; LG vs HGI $p=0.0003$; LGI vs HGI $p<0.0001$, LG vs HM, HMI $p<0.0001$). Spare respiratory capacity rates were significantly decreased in HG and HGI treated groups compared to LG control. HG, HGI, HM and HMI treated groups displayed a lower spare respiratory capacity compared to LGI **(Fig. 9 H)**. In the XF energy map HG and HGI treated groups showed a more glycolytic phenotype, while LG and LGI control groups were in between an aerobic (oxidative phosphorylation) and a high energetic phenotype. HM and HMI groups were less energetic compared to LG and less glycolytic compared to HG **(Fig. 9 J)**. All respiration rates were lower after 96h treatment compared to 24h treatment, with maximal respiration rates being remarkably lower in T2D-mimicking conditions after 96h compared to 24h treatment **(Table 5)**. After 96h treatment with HGP and HGPI we didn't observe significant difference to LG controls in one Mito Stress Test and therefore excluded these treatment groups in the following repetitions. Data is available in the attachments **(Fig. 16 B)**.

Table 5: ATP linked respiration and maximal respiration rates of C2C12 myotubes, 24h vs 96h. Data are representative for three independent biological replicates of each short- or long-term experiment.

	ATP linked respiration OCR (mean in pmol/min)		**Maximal respiration OCR (mean in pmol/min)**	
	24h	**96h**	**24h**	**96h**
LG	34,45 ± 1,765	21,6 ± 3,074	151,7 ± 8,830	115,63 ± 14,20
LGI	41,6 ± 3,141	24,45 ± 3,385	192,8 ± 17,39	148,96 ± 15,97
HG	8,071 ± 0,6310	1,81 ± 0,3371	147,8 ± 6,539	55,49 ± 8,181
HGI	8,601 ± 0,8590	5,36 ± 2,377	181,8 ± 10,56	50,82 ± 7,118
HM	6,855 ± 1,036	4,82 ± 1,018	142,9 ± 17,23	77,21 ± 10,54
HMI	8,331 ± 1,036	5,19 ± 0,7197	180 ± 22,52	59,21 ± 9,111

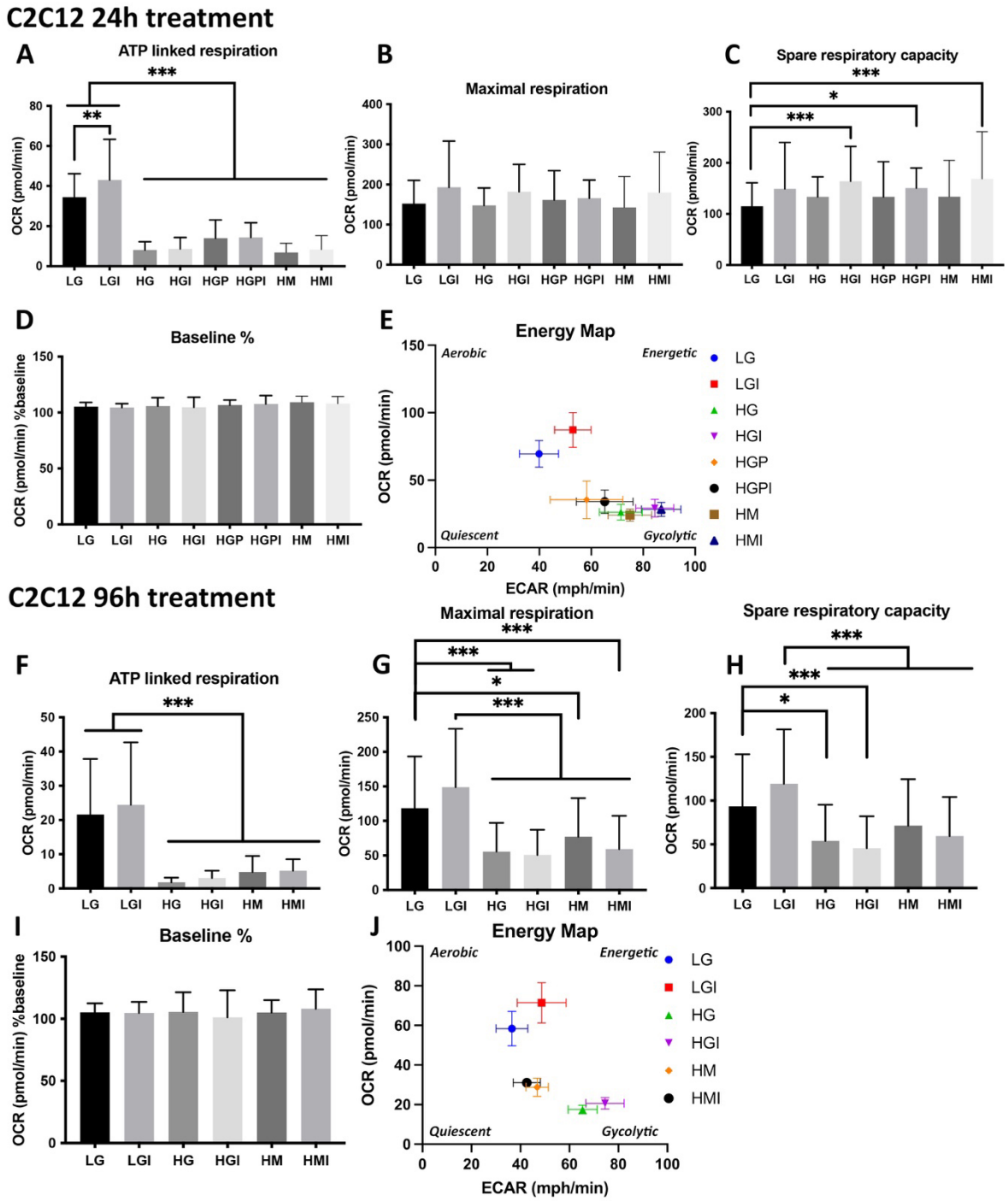

Fig. 9: Plate-based oxygen consumption measurements of C2C12 myotubes. The cells were plated at 1.2 x10^4 cells per well in XF96 microplates and differentiated for 5 days. Treatments were carried out for 24h (A – E) or 96h (F – J). A: ATP-linked respiration; two-way ANOVA treatment factor (Tf) F (7, 292) = 70.16, P<0.0001; Incubation factor (If) F (2, 292) = 9.807, P<0.0001 B: Maximal respiration; Tf F (7, 288) = 2.206, P=0.0338; If F (2, 288) = 9.502, P=0.0001. C: Spare respiratory capacity; F (7, 292) = 3.153, P=0.0031; If F (2, 292) = 15.72, P<0.0001. D, I: 24h (D: Tf F (7, 282) = 1.516, P=0.1614; If F (2, 282) = 5.305, P=0.0055) and 96h (I: Tf F (5, 168) = 0.7035, P=0.6216; If F (2, 168) = 2.439, P=0.0903)

relative oxygen consumption rate percentage (baseline of all groups). E, J: OCR plotted versus ECAR after 24h (E) and 96h (J) treatment. F: ATP-linked respiration, Tf F (5, 123) = 21.21, P<0.0001; If F (2, 123) = 28.60, P<0.0001. G: Maximal respiration, Tf F (5, 155) = 19.18, P<0.0001; If F (2, 155) = 38.29, P<0.0001. H: Spare respiratory capacity, Tf F (5, 154) = 12.12, P<0.0001; If F (2, 154) = 33.39, P<0.0001. Each graph represents data of minimum three independent biological replicates and is presented as means ± standard deviation, n per treatment group = 8-15 wells per assay. Tukey's multiple comparisons test between all treatment groups: *p<0.05, **p<0.01, ***p<0.001.

4.3.1.3 H9C2 24h

H9C2 myotubes treated 24h with high glucose in combination with insulin or palmitate (HGI, HGP, HGPI) showed a significant increase in ATP linked respiration and maximal respiration compared to LG and LGI control cultures, with HGPI groups displaying the significantly highest ATP linked respiration and respiration rates (biological N = 3, technical replicates = 9-10) **(Fig. 10 A, B)**. Spare respiratory capacity was significantly increased in treatment groups including palmitate (HGP and HGPI) compared to LG, LGI, HG and HGI **(Fig. 10 C)**. Plotting OCR vs ECAR respiration rates showed a trend towards more energetic phenotypes in T2D-mimicking conditions compared to LG controls **(Fig. 10 E)**. All treatment groups utilized both glycolysis and oxidative phosphorylation to generate energy. Osmotic control cultures that were exposed to high concentrations of mannitol showed no significant differences in all respiration rates compared to LG control groups in one Mito Stress Test assay and were therefore excluded in the following assay repetitions. Data is available in the attachments **(Fig. 16 C)**.

4.3.1.4 H9C2 96h

H9C2 myotubes treated 96h with high glucose in combination with insulin or palmitate (HGI, HGP, HGPI) showed a significant increase in ATP linked respiration and maximal respiration compared to LG and LGI control cultures (biological N = 3, technical replicates = 6-15) **(Fig 10 F, G)**. After 96h treatment no significant changes in spare respiratory capacity was detectable **(Fig. 10 H)**. Plotting OCR vs ECAR respiration rates after 96h treatment revealed LG control cultures to be more quiescent compared to 24h treatment and compared to T2D-mimicking conditions. HG, HGI, HGP and HGPI treated groups showed a phenotype in between glycolysis and oxidative phosphorylation, with HGPI being the most energetic **(Fig. 10 J)**.

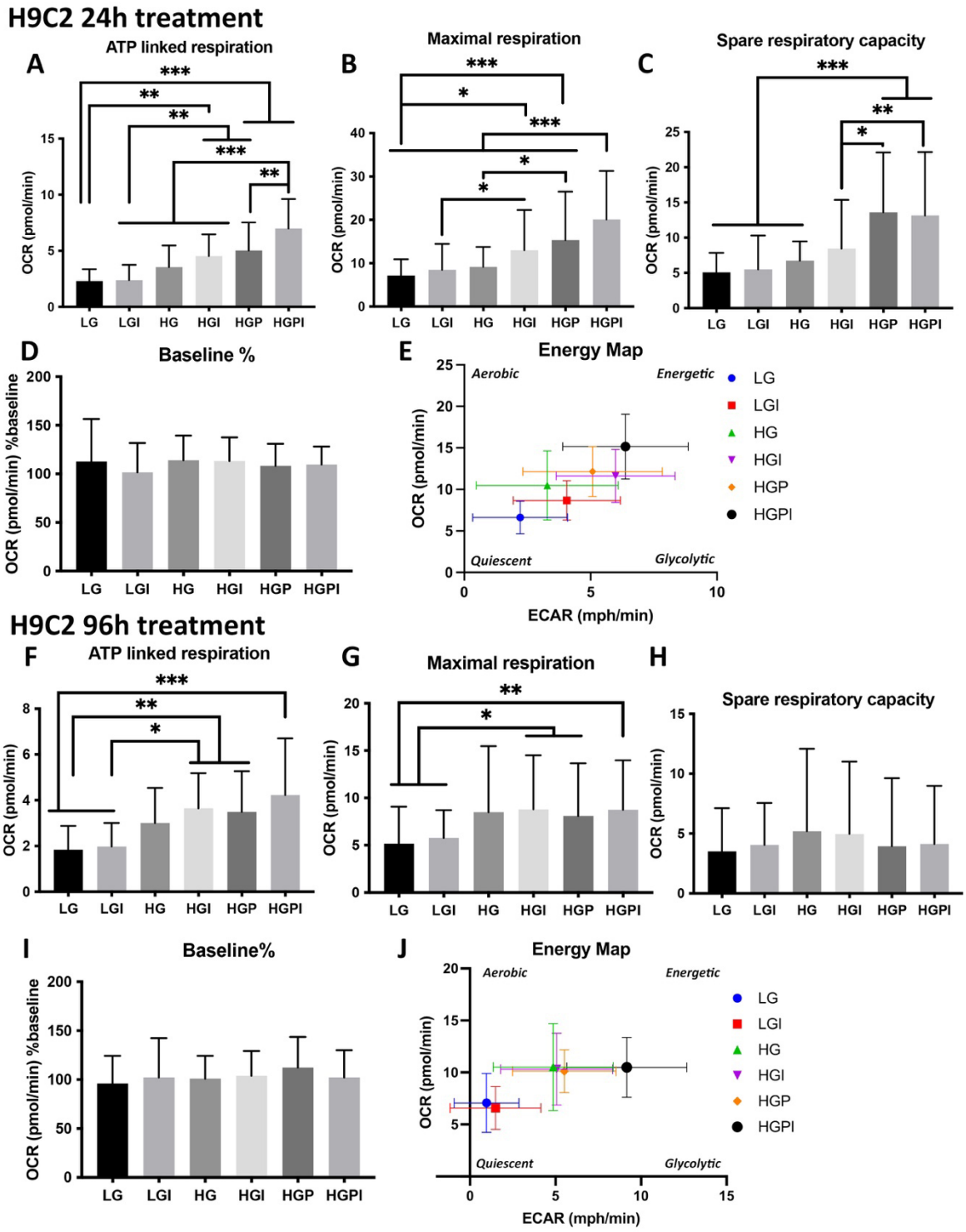

Fig. 10: Plate-based oxygen consumption measurements of H9C2 myotubes. The cells were plated at 1.2 x10^4 cells per well in XF96 microplates and differentiated for 7 days. Treatments were carried out for 24h (A – E) or 96h (F – J). A: ATP-linked respiration, two-way ANOVA treatment factor F (5, 139) = 23.58, P<0.0001; incubation factor F (2, 139) = 7.225, P=0.0010. B: Maximal respiration, Tf F (5, 144) = 20.55, P<0.0001; If F (2, 144) = 69.85, P<0.0001. C: Spare respiratory capacity, Tf F (5, 135) = 15.03, P<0.0001; If F (2, 135)

= 47.87, P<0.0001. D, I: 24h (D: Tf F (5, 146) = 0.6060, P=0.6955; If F (2, 146) = 1.126, P=0.3273) and 96h (I: Tf F (5, 131) = 0.8578, P=0.5115; If F (2, 131) = 0.7791, P=0.4609) relative oxygen consumption rate percentage (baseline of all groups). E, J: OCR plotted versus ECAR after 24h (E) and 96h (J) treatment. F: ATP-linked respiration, Tf F (5, 178) = 8.173, P<0.0001; If F (2, 178) = 0.2515, P=0.7779. G: Maximal respiration, Tf F (5, 185) = 5.086, P=0.0002; If F (2, 185) = 47.23, P<0.0001. H: Spare respiratory capacity, Tf F (5, 186) = 0.6408, P=0.6688; If F (2, 186) = 26.49, P<0.0001. Each graph represents data of minimum three independent biological replicates and is presented as means ± standard deviation of 6-15 wells per treatment group. Tukey's multiple comparisons tests: *p<0.05, **p<0.01, ***p <0.001.

4.3.2 Glycolytic Rate Assays

Assays were performed as described in 3.4.2. After 24h treatment of C2C12 myotubes with T2D-mimicking conditions, all treatment groups showed a switch towards glycolysis in the energy map compared to LG and LGI controls that showed a highly aerobic phenotype **(Fig. 11 C)**. An increased basal glycolysis was seen in all treatment groups including palmitate compared to LG control, and in HM and HMI groups. Also HGP treated groups showed a significantly higher basal glycolysis rate compared to HG. We observed decreased glycolysis rates in LGI compared to LG **(Fig. 11 A)**. Similar differences occurred in compensatory glycolysis rates after inhibition of mitochondrial respiration **(Fig. 11 B)**. After 96h treatment both basal and compensatory glycolysis was significantly increased in all groups treated with palmitate compared to treatments not including palmitate **(Fig. 11 E)**. In the energy map all treatments groups including palmitate showed a glycolytic phenotype whereas all other treatment groups were more quiescent **(Fig. 11 G)**.

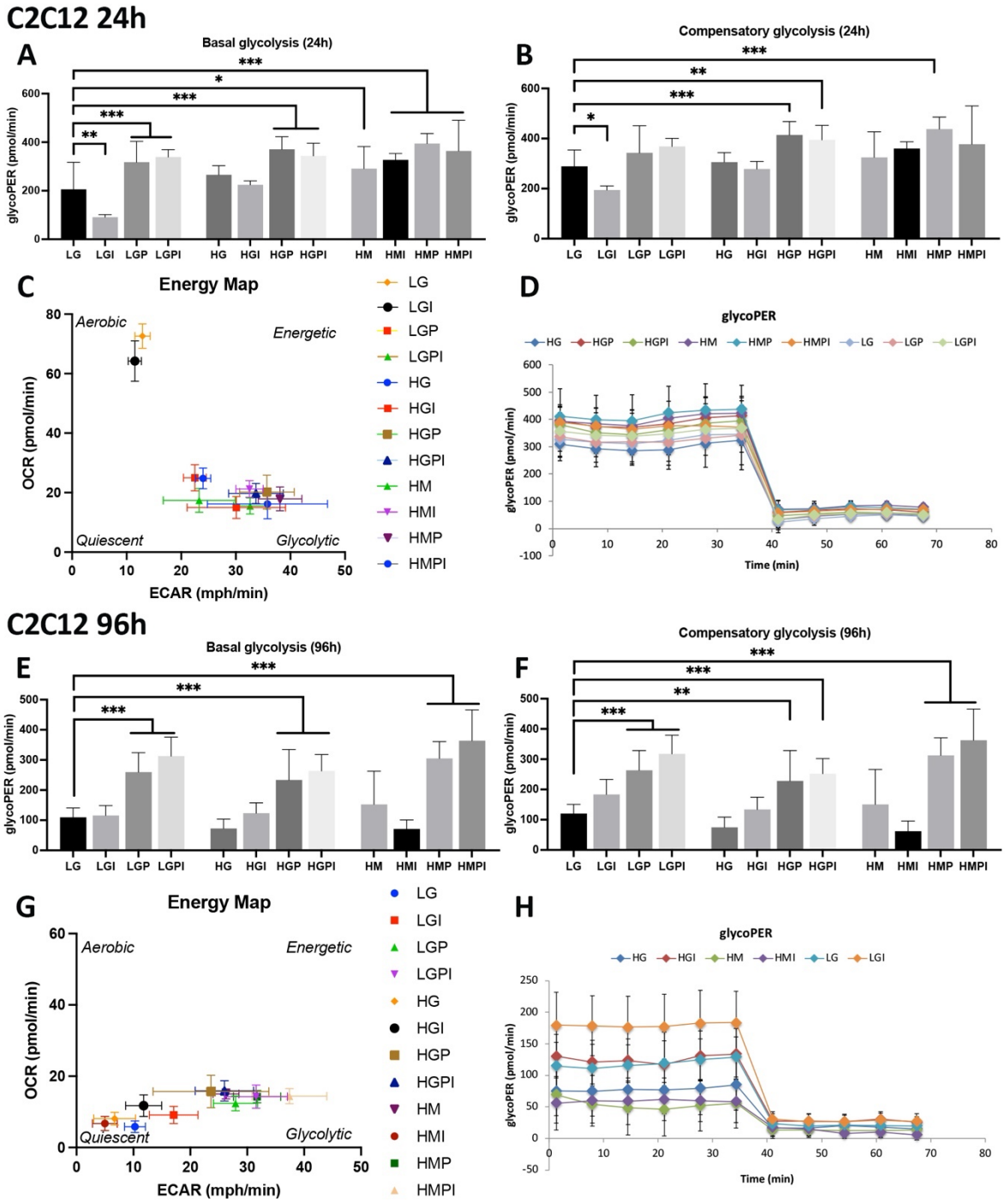

Fig. 11: Glycolytic rate assays of C2C12 myotubes treated with T2D-mimicking conditions (HG, HGP, HGPI) and control (LG, HM) for 24h (A-D) or 96h (E-H). A: Basal glycolysis treatment factor F (11, 138) = 18.63, P<0.0001; incubation factor F (1, 138) = 17.13, P<0.0001. B: Compensatory glycolysis Tf F (11, 138) = 10.24, P<0.0001; If F (1, 138) = 6.964, P=0.0093 E: Basal glycolysis Tf F (11, 135) = 30.30, P<0.0001; If F (1, 135) = 0.06125, P=0.8049 F: Compensatory glycolysis Tf F (11, 138) = 27.83, P<0.0001; If F (1, 138) = 0.004934, P=0.9441. C, G: OCR/ECAR plotted for energetic phenotyping. D, H: GlycoPER

as calculated by the Agilent seahorse assay generator. Data represents two assays with 6-10 wells per treatment per assay. Tukey's multiple comparisons tests were performed between all treatment groups, comparisons vs LG controls shown with brackets *p<0.05, **p<0.01, ***p<0.001.

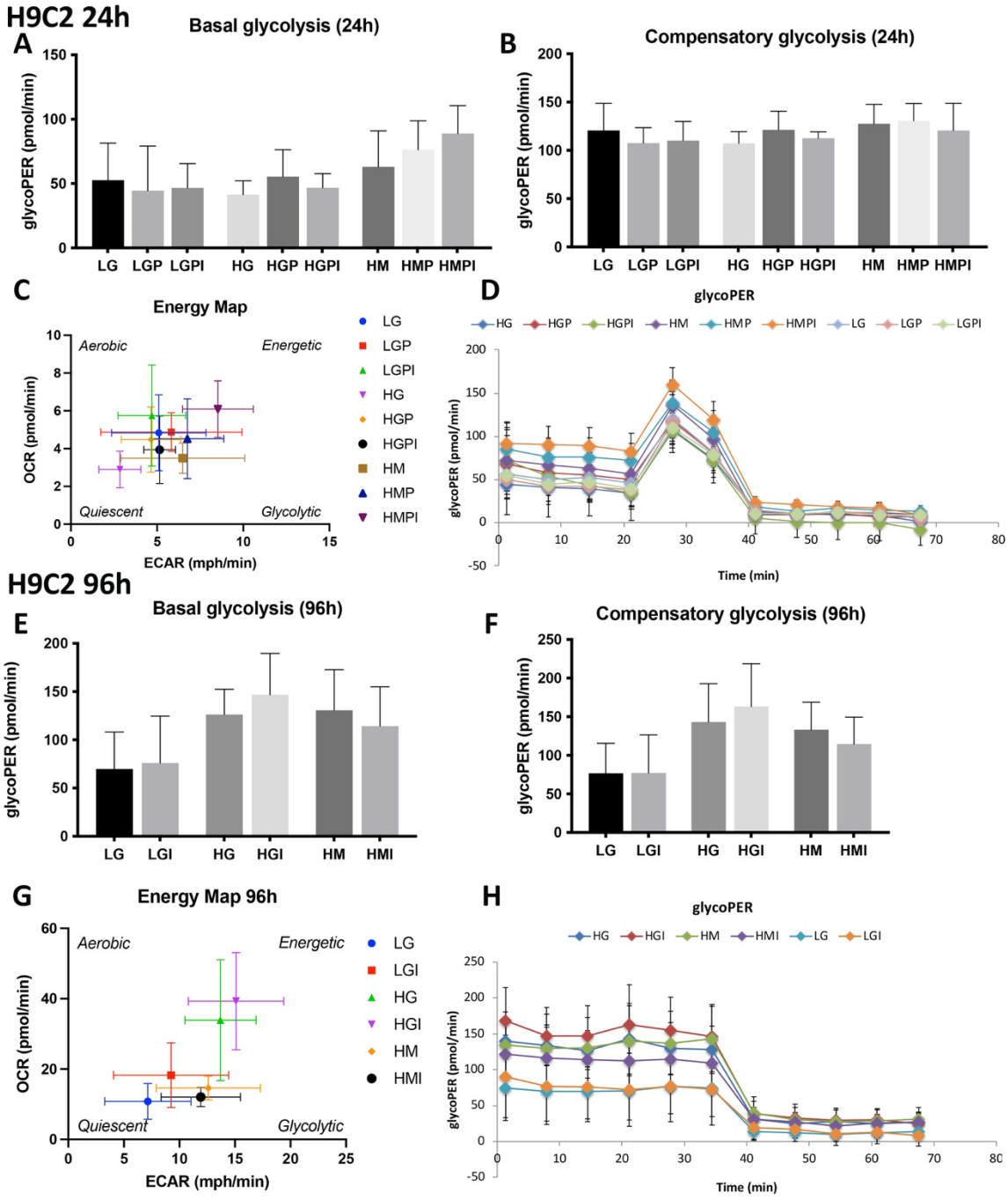

Fig. 12: Glycolytic rate assays of H9C2 myotubes treated with T2D-mimicking conditions and control for 24h (A-D) or 96h (E-H). A, E: Basal glycolysis. B, F: Compensatory glycolysis. C, G: OCR/ECAR plotted for energetic phenotyping. D, H: GlycoPER. 24h data represents one assay with n=6-11 wells per treatment group, 96h data represents one

assay with n=10 wells per treatment group. Data is presented as mean ± standard deviation.

After 24h treatment of H9C2 myotubes with T2D-mimicking conditions, compensatory glycolysis between groups appeared uniform **(Fig. 12 B)**. Basal glycolysis was increased in HMPI treated groups, compared to all LG and HG treated groups, corresponding to increased glucose uptake rates in Fig. 9 C **(Fig. 12 A)**. In the energy map HMPI seemed to have the most energetic phenotype but no remarkable differences were observed **(Fig. 12 C)**. After 96h treatment basal and compensatory glycolysis was increased in HG and HGI treated groups compared to LG and LGI **(Fig. 12 E, F)**. Basal glycolysis was increased in HM treated groups compared to LG and LGI **(Fig. 12 E)**. In the energy map HG and HGI treated groups displayed a more energetic phenotype compared to all other groups **(Fig. 12 G)**.

4.4 EM

4.4.1 Mitochondrial number and distribution

Perinuclear mitochondria of C2C12 and H9C2 myotubes were counted after 24h treatments and distribution were compared between a previously defined inner and outer perinuclear circle **(Fig. 13 A, B)**. C2C12 myotubes treated with HGPI showed a significantly lower total count of mitochondria compared to LG control. HGP treated groups also showed fewer mitochondria but not significant compared to LG **(Fig. 13 C)**. We could not detect any significant differences in the distribution of mitochondria in the inner vs outer perinuclear circle in C2C12 myotubes **(Fig. 13 D)**. Interestingly the mitochondrial size (area in square pixels) of C2C12 treated with HM was significantly decreased compared to HGP **(Fig. 13 E)**. H9C2 myotubes showed no significant difference between the different treatments in the total count of mitochondria **(Fig. 13 F)**. The distribution analysis showed a remarkably lower ratio of mitochondria in the outer circle compared to the inner circle of H9C2 treated with HG **(Fig. 13 G)**. The mitochondrial size (area in square pixels) of H9C2 treated with HGP or HGPI was significantly greater when compared to LG, HM or HG treatment **(Fig. 13 H)**. However, HGPI treated cells showed significantly smaller mitochondria compared to HGP **(Fig. 13 H)**.

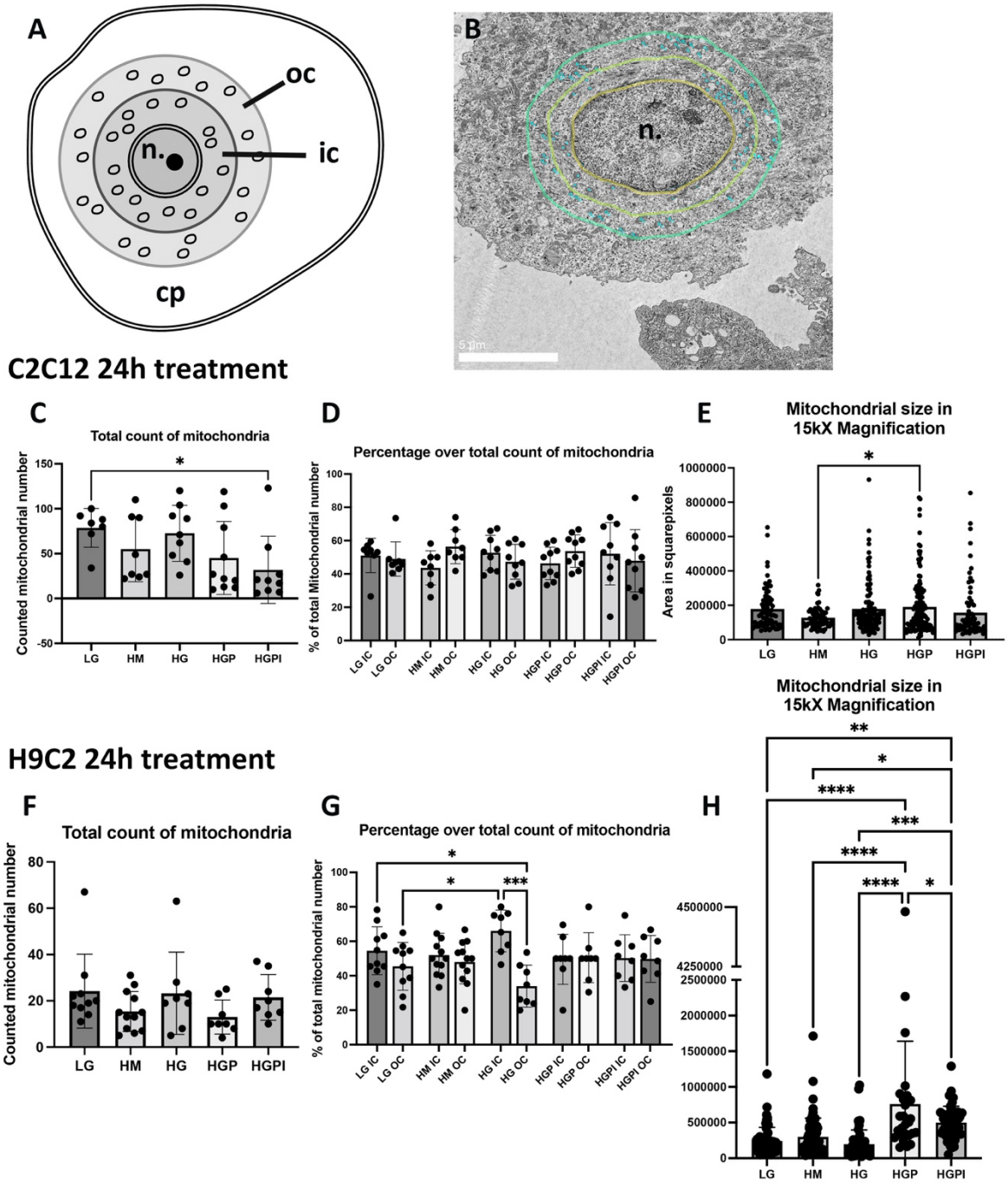

Fig. 13: Distribution, number and size of perinuclear mitochondria in C2C12 (C-E) and H9C2 (F-H) myotubes after 24h treatments with LG controls, HM osmotic controls and T2D mimicking conditions (HG, HGP, HGPI). A: Schematic comic of a cell used for counting of mitochondria. n. = nucleus, ic = inner circle (200px from nucleus), oc = outer circle (400px from nucleus), cp = cytoplasm. B: Example cell for mitochondria counting. C, F: Total count of mitochondria. D, G: Distribution of mitochondria in ic vs oc in % over the total count. E, H: Mitochondrial size in square pixels in 15kX magnification. Cell organelles were confirmed to be mitochondria before counting with pictures of the

same cells in 5000x and 15kx magnifications. For mitochondrial size analysis mitochondrial area was measured in square pixels in 15kx magnifications of randomly and blinded taken pictures of mitochondria. One-way ANOVA C p=0.053, D p=0.588, E p=0.0318, F p=0.235, G p=0.005, H p<0.0001. Tukey's multiple comparisons tests: *p<0.05, ***p<0.001, ****p<0.0001.

4.4.2 Mitochondrial morphology after 24h treatment

For mitochondrial morphology analysis the quantity of normal versus swollen mitochondria was compared after 24h treatment of C2C12 and H9C2 myotubes. Normal mitochondria were defined as indicated in **Fig. 14 A**, swollen mitochondria as indicated in **Fig. 14 B and C**. In C2C12 myotubes all treatment groups showed a significantly lower ratio of swollen mitochondria compared to normal mitochondria **(Fig. 14 I)**. HM, HGP and HGPI treated C2C12 showed a significantly higher fraction of swollen mitochondria compared to LG control groups. The fraction of swollen mitochondria in HG compared to HGP and HGPI treated groups was significantly lower **(Fig. 14 I)**. In H9C2 myotubes the fraction of normal mitochondria was significantly higher compared to swollen mitochondria in all treatment groups except for HGPI. When compared to LG control treatment, the percentage of swollen mitochondria was higher in HM, HG and HGPI treated H9C2 myotubes **(Fig. 15 F)**.

Swollen mitochondria are indicated as "sm" in **Fig. 14 and 15** in C2C12 HM, HGP and HGPI treatments **(Fig. 14 E, G, H)** and H9C2 HM, HG and HGPI treatments **(Fig. 15 B, C, E)**.

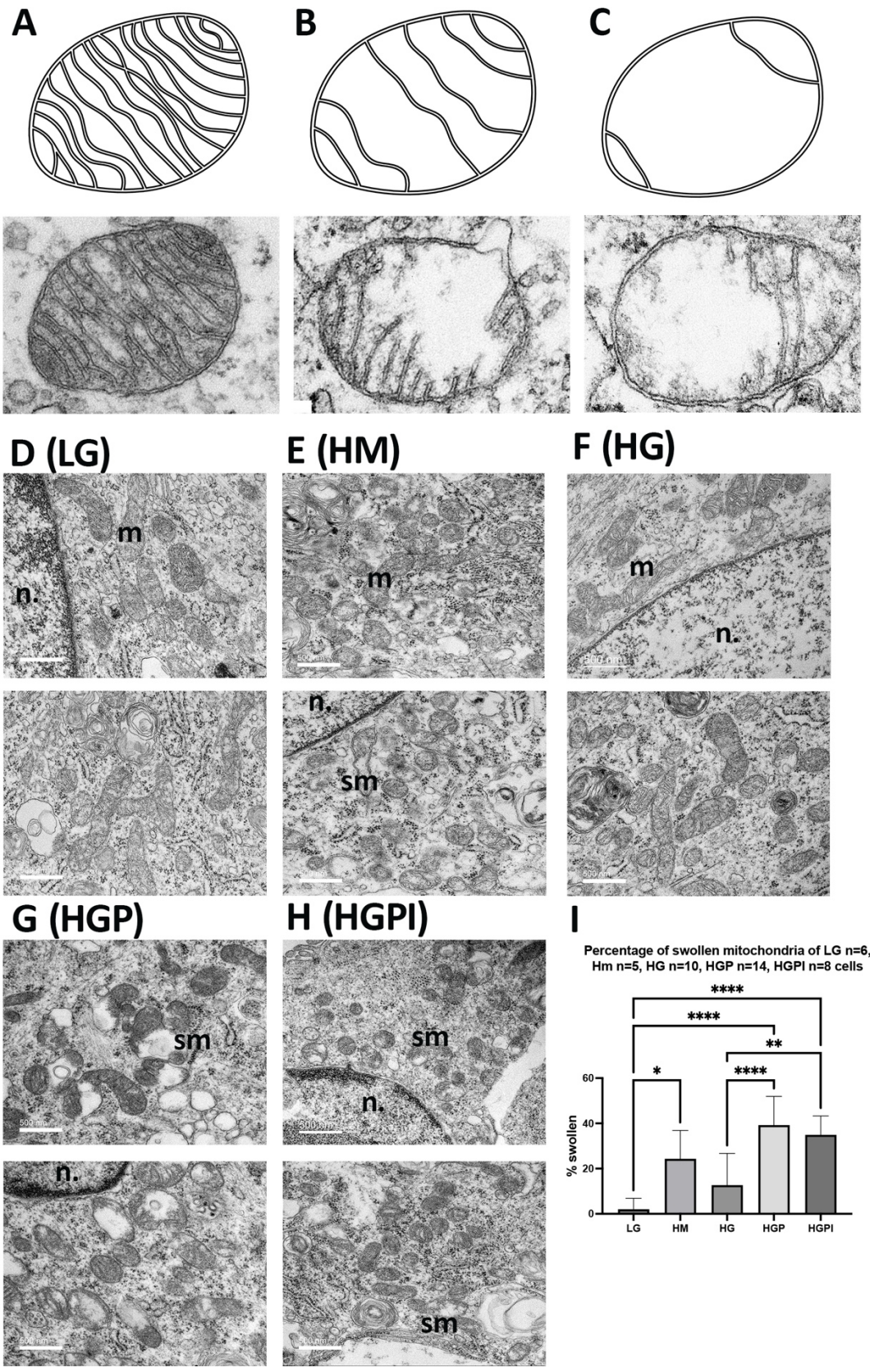

Fig. 14: Morphology and appearance of mitochondria in TEM. A: Normal mitochondria. B and C: Partially and completely swollen mitochondria. D-H: Mitochondria of C2C12 myotubes after 24h treatments with LG, HM, HG, HGP and HGPI (n. = nucleus, m =

mitochondrion, sm = swollen mitochondrion). I: Percentage of swollen mitochondria in C2C12 myotubes. Pictures were taken in 15kX magnifications. Comics by LA Kopp. One-way ANOVA of I p<0.0001. Tukey's multiple comparisons test *p<0.05, **p<0.01, ****p<0.0001.

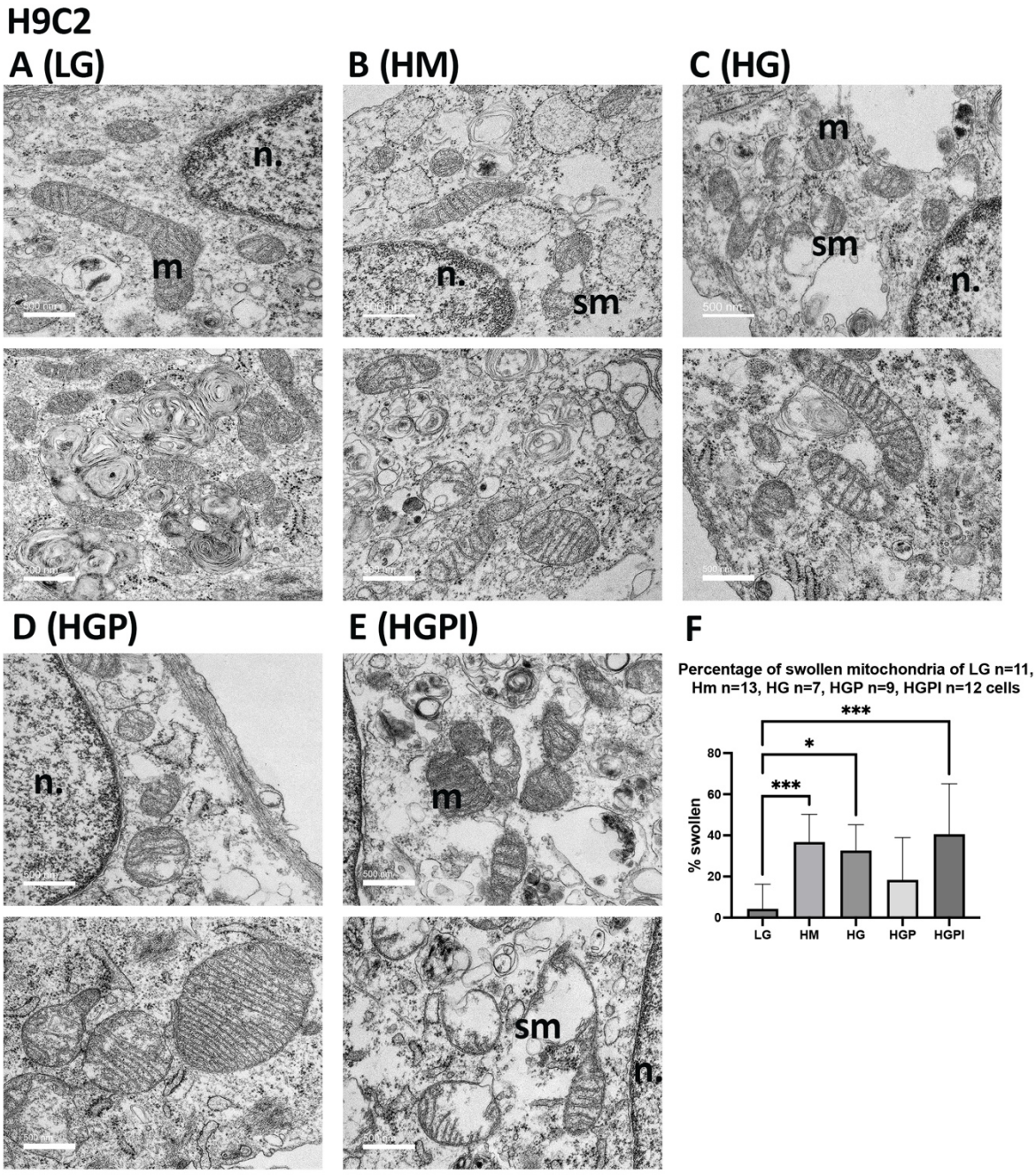

Fig. 15: A-E: Mitochondria of H9C2 myotubes after 24h treatment with LG, HM, HG, HGP and HGPI (n. = nucleus, m = mitochondrion, sm = swollen mitochondrion). F: Percentage of swollen mitochondria in H9C2 myotubes. For counting randomly and blinded taken pictures of mitochondria in 15kx magnifications were used. One-way ANOVA of F p<0.0001. Tukey's multiple comparisons test * p<0.05, ***p<0.001.

5. Discussion

5.1 Diabetes in a dish: Development of an *in vitro* model including the main aspects of type 2 diabetes

In our *in vitro* model of T2D we observed that the exposure to high glucose, palmitate and insulin has significant effects on the functionality of rodent skeletal and heart muscle cells: It leads to severe insulin resistance, changes in ATP linked respiration, shifts in energetic phenotypes and mitochondrial morphology changes, all consistent to what has been observed in muscle of patients suffering from T2D. Evolving and improving *in vitro* cell models will help researchers to save resources and facilitate the translation into animal or human studies. Pre-existing *in vitro* models of T2D often disregard many critical and complex aspects of the disease. The current study shows that by following some essential steps, a representative *in vitro* model of human T2D related changes in muscle cells can be created.

In our model of T2D, we focused on the chronic vicious circle of external and internal factors leading to T2D. Our model utilizes cells (both skeletal muscle and heart muscle) that rely on insulin dependent glucose uptake. Furthermore, the exposure of these cells to high glucose and palmitate allowed for an analogy of the Western diet which consists of high amounts of sugar and fatty acids [40 41 8]. Unlike in previous studies [57 58, 129], we grew and differentiated the cells in low glucose levels and were, therefore, able to create a model comparing physiological and diabetic glucose levels as they occur in humans [61 62 63 64]. To complete the *in vitro* simulation of T2D we combined high glucose, palmitate and insulin exposure.

Prior to assays, the growth and shape of myoblasts under all treatment conditions were examined by light microscopy in order to investigate if treatments cause cell death or abnormal changes in growth and differentiation. H9C2 and C2C12 myoblasts cultured in LG (5mM glucose) showed healthy growth. Adding mannitol (20mM) as osmotic control seemed to cause a slight change in cell shape after long term treatments. This effect has been poorly described yet in muscle cells and should be further investigated. However, it has been shown that higher mannitol exposure decreases the height of cerebral endothelial cells [183] and caused apoptosis in a dose dependent manner (100-300mM) in bovine aortic endothelial and smooth muscle cells [184]. Hyperosmolar treatment with glucose or mannitol (24h HG 30.5mM glucose; HM 25mM mannitol + 5.5 mM glucose) caused a reorganization of F-actin, induced cytoskeleton remodeling and promoted cell migration in human induced pluripotent stem cells [185]. On the contrary, cells treated with high glucose (25mM) appeared

to grow faster and exhibit healthy morphology, which might be the reason why various studies utilize high glucose concentrations to promote growth in cell culture [57] [129]. Under short- or long-term insulin (1nM glargine insulin) treatment we did not observe any significant changes in growth or morphology. Rossi *et al.* showed that 3T3-L1 pre-adipocytes did not decrease in cell number due to chronic insulin treatment (150nM for 5 days) [186]. In general, insulin is added to cell culture media to promote growth [187] [87] [188] [189]. For the treatment with FAs we started to use concentrations of 750 µM palmitate, which have been used previously and are in the physiological range (0.4-1.0mM) [86] [31]. After experiencing high cell loss due to lipotoxicity, we adjusted the palmitate concentrations to levels less toxic (150 or 75 µM) and still inducing IR, according to previous publications (50-500µM) [190] [191] [192]. For long term assays it is important to gradually increase palmitate concentrations to prevent rising toxicity.

In summary, we were able to calibrate our model to glucose, insulin and fatty acid concentrations closer to levels observed in T2D patients *in vivo* and lower than used in many previously published *in vitro* studies.

5.2 Effects of high glucose, palmitate and insulin on glucose uptake in C2C12 and H9C2 cells

Short- and long-term pre-treatment of C2C12 cells with LG showed the expected physiological elevation of glucose uptake upon an acute insulin stimulus (100nM). Individual insulin (1nM) pre-treatment (LGI) caused an increased baseline glucose uptake that could not further be stimulated by acute insulin (100nM). Starting from a lower baseline influx than C2C12 cells, H9C2 LG control groups showed a significant rise in insulin-dependent glucose uptake after 96h treatment, yet just missed significance after 24h treatment. In H9C2 cells pre-treated with LGI for 96h, baseline glucose uptake and its response to acute insulin stimulation were preserved similar to LG conditions. Taken together, these results validate our LG control groups as comparable to an insulin-sensitive subject.

Basal rates of glucose uptake were increased in both cell lines after HG treatment compared to LG, especially after long term exposure. This might have been facilitated by the gradient-driven glucose uptake via GLUT1 instead of insulin-dependent GLUT4. McMillin *et al.* showed that mGLUT4 knockout mice still showed increased basal glucose uptake after chronic exposure to high glucose. They also found that in mouse skeletal muscle cells GLUT1, 3, 6 or 10 almost exclusively mediate glucose uptake after chronic glucose overload [193]. Gosmanov *et al.* observed that, compared to 5mM glucose exposure, high glucose

treatment (30mM, up to 48h) of aortic endothelial cells increased GLUT1 expression and GLUT4 dependent glucose uptake, but didn't change baseline glucose uptake rates. Heilig *et al.* saw an 134% increase in GLUT1 mitochondrial RNA as well as a 50% increase in deoxy-glucose uptake in rat mesangial cells exposed to 20mM glucose for 3 days, when compared to cells adapted to physiological glucose levels (8mM). Both research groups could not find any effect of mannitol treatment on GLUT1 expression or glucose uptake [194] [195]. As HM control groups showed no increase, but in fact much lower basal glucose uptake rates compared to LG or HG, it can be assumed that the higher basal uptake rates in HG groups are not caused by osmotic pressure damage to the cell membrane integrity. Hwang *et al.* described an increase in glucose uptake and increase in GLUT1 expression in Clone 9 cells due to very high osmotic stress (treatment with 300mM Mannitol). This effect was not seen when cells were treated with only 50-100mM mannitol [196]. Taha *et al.* also observed increased GLUT 1 and 3 expression upon long term mannitol treatment (300mM) in L6 muscle cells and Farlinger *et al.* saw increased glucose uptake rates after 60 min mannitol (400mM) incubation of fast-twitch rat skeletal muscle [197] [198]. Under lower mannitol exposure (30 or 60mM) Fischereder *et al.* observed no increase in GLUT 1 or 3 in human peritoneal mesothelial cells [199]. However, a decrease in baseline glucose uptake with such low mannitol concentrations as used in our model has not been described before. A possible reason might be a direct hindrance by mannitol of glucose influx by one of the non-insulin-dependent glucose transporters, whereas an acute insulin stimulus still increased glucose influx in the presence of HM, yet fell just short of significance at n=3. Nonetheless, this postulation needs to be further explored.

In C2C12 myotubes, the treatment combinations of HG, HGI, HGP and HGPI all showed non-significant but diverging and more marked trends after 96h on basal glucose uptake, but all HG exposures caused complete resistance to subsequent insulin stimulation as it occurs in T2D. In HGPI glucose uptake even appeared to fall upon acute insulin stimulation.

In H9C2 cells HG and HGI, HGP and HGPI effects after 24h closely resembled those corresponding LG exposures, with LG, LGI, HG and HGI showing an increase in insulin-dependent glucose uptake, and LGP, LGPI, HGP and HGPI displaying marked reductions of glucose uptake. After 96h marked IR was present also in HG and HGI versus LG and LGI. These results fit well to the vicious cycle of intensified IR with chronic hyperglycemia and hyperlipidemia observed in T2D. HG alone resembles more closely uncontrolled T1D rather than T2D, however still caused a certain degree of IR in steady *in vitro* conditions in both cell lines. With increased insulin-independent baseline glucose uptake rates under HG

exposure, this IR might represent a protective mechanism against overwhelming glucose influx on insulin. However, IR alone does not define T2D, plus HG treatment alone is not sufficient to reflect T2D. Consequently, it is not sufficient to utilize glucose uptake assays alone to distinguish a model most likely mimicking T2D.

Interestingly, both C2C12 and -at a lower level- H9C2 myotubes exposed to HM and palmitate (HMP and HMPI) showed an increase in glucose uptake compared to HM and HMI exposures, but no further increase on insulin stimulation. This increase occurred from lowered glucose uptake levels in all cells exposed to HM and HMI, compared to LG, LGI, HG or HGI. Moreover, inclusion of palmitate (HMP and HMPI) not only reversed the obvious inhibitory effect of palmitate in LGP, LGPI, HGP and HGPI treated H9C2 cells, but also boosted glucose uptake in C2C12 cells severalfold above levels in LGP, LGPI, HGP and HGPI. This effect has not been described previously and possibly is a synergistic effect of the combination of mannitol with palmitate. As the effect is seen also in the absence of insulin, GLUT4 activation apparently is not needed for this massive increase in glucose uptake. Therefore, we suspect that under high osmolarity due to mannitol -but obviously not hyperosmolarity per se as seen in HGP or HGPI- GLUT1 might be activated by palmitate and allows for glucose entry into cells. Alternatively, inhibition of FA oxidation by mannitol could lead to higher glucose uptake to meet the energy demands of the cells via glycolysis. However, glucose uptake was decreased in all non-mannitol palmitate treatment groups, particularly in H9C2 myotubes which showed a substantial decrease in glucose uptake, compared to all non-palmitate treatment groups. This might be explained by a metabolic switch to more lipid oxidation and less glycolysis as well as the inhibition of glucose metabolism by palmitate. This hypothesis is explored in detail below.

5.3 Respiration and energetic dysfunction in type 2 diabetes

We examined mitochondrial function and metabolic phenotypes in rodent skeletal and heart muscle utilizing the Agilent Seahorse XF Analyzer, performing Mitochondrial Stress Tests and Glycolytic Rate Assays. The rate of maximal respiration mimics an energy demand, where the respiratory chain operates at maximum capacity. These respiration rates include ATP linked respiration as well as uncoupled respiration generating ROS. ROS production and impaired metabolic flexibility between lipid and glucose oxidation have been associated with IR and T2D (mainly in skeletal muscle) [200] [201] [202] [203] [204] [205]. Aguer *et al.* showed that skeletal myotubes from insulin sensitive subjects with a T2D family history have decreased ATP content, consistent to previous studies showing decreased ATP and impaired mitochondrial activity in myotubes from lean offspring of T2D patients [206] [162] [207]. Skeletal

muscle of subjects with overt T2D also showed a decreased mRNA expression of genes related to oxidative phosphorylation and a reduction of ATP synthase [208] [209].

Respectively to this knowledge, in our assays skeletal myotubes (C2C12) exposed to T2D-mimicking conditions showed similar maximal respiration rates compared to physiological controls, but significantly lower ATP linked respiration, indicating that more respiration is uncoupled and leads to ROS production. In contrary, cardiac myotubes (H9C2) showed elevated ATP linked respiration after 24 and 96h exposure to T2D-mimicking conditions that included insulin and/or palmitate, indicating a switch towards lipid oxidation and sustained resistance to a T2D environment.

C2C12 myotubes **(Fig. 10, 12)**: C2C12 myotubes that were exposed to high glucose and palmitate or insulin for 24h displayed a significant decrease in ATP linked respiration. Furthermore, groups exposed to HM and HMI showed the most marked decrease in ATP linked respiration, but similar maximal respiration rates as low glucose control groups. Treatment groups including insulin (LGI, HGI) displayed the highest maximal respiration rates. Spare respiratory capacity was increased in HGI and HMI treated groups. These findings indicate that after short term treatments insulin still partially prevents mitochondrial dysfunction and restores oxidation abilities and cellular fitness or flexibility. Groups treated with high glucose or high mannitol shifted towards glycolysis in the energy map, whereas LG control had an aerobic metabolism and LGI a high energetic phenotype. This could indicate that even when the cells are insulin resistant and show less glucose uptake via GLUT4, glycolysis is increased due to hyperosmolarity. After 96h exposure to high glucose or high mannitol, both ATP linked respiration, maximal respiration and spare respiratory capacity were substantially decreased compared to LG control, and HG treated groups still showed a more glycolytic phenotype. These findings suggest a chronically higher dependence on glycolysis in the diabetic phenotype and possibly decreased adaptions to stress, impaired cellular fitness, and mitochondrial dysfunction, partially caused by hyperosmolarity in a hyperglycemic environment.

In Glycolytic Rate Assays of C2C12 myotubes after 24h treatments **(Fig. 12)**, it was remarkable that all groups exposed to palmitate (LGP, LGPI, HGP, HGPI, HMP, HMPI), and also HM and HMI had increased basal glycolysis rates compared to LG and LGI. In the energy map LG and LGI control groups showed mainly oxidative phosphorylation, whereas all other treatment groups shifted towards glycolysis. After 96h, basal glycolysis was the same in LG, HG and HM treated groups, but in all groups treated with palmitate independently of the

glucose concentrations, glycolysis was increased. It is likely, that this increase in glycolysis is not connected to the insulin dependent glucose metabolism, as palmitate inhibits this pathway in muscle cells [59]. However, this shift towards glycolysis doesn't explain the observed decrease in ATP linked respiration. Even though oxidative phosphorylation generates more ATP per glucose than glycolysis, rapidly proliferating cells (i.e. cancer cells) prefer glycolysis as it generates ATP faster [210] [211] [212]. Therefore, this shift to glycolysis might indicate a stressed phenotype, possibly attempting to compensate the inhibition by palmitate.

Furthermore, Mailloux *et al.* also observed that C2C12 myotubes exposed to 24mM glucose for 24h showed a glycolytic phenotype and more ROS production compared to a low glucose control with an oxidative phenotype. However, ATP linked respiration was not altered, indicating that those myotubes still were metabolically flexible and achieved the demanded ATP supply via glycolysis [213]. Elkalaf *et al.* followed a similar approach and saw respiration differences in maximal respiration in hyperglycemic C2C12 myotube cultures and a switch in phenotypes. In both studies cells were differentiated for up to 7 days in media containing 5mM or 25mM glucose before any experiment [214]. Differentiating cells in high glucose might have caused an adaptation of the cells, leading to a restored cellular flexibility. In the current study, cells were differentiated in low glucose levels and only exposed to high glucose for 24-96h when already differentiated, which more accurately represents the changes of T2D *in vivo*, confirming our hypothesis 1 iii. Future experiments should include longer exposure to high glucose to investigate if following differentiation an adaptation to supraphysiological glucose and correspondingly non-altered ATP levels is possible.

It should be kept in mind that Tumova *et al.* had to increase palmitate concentrations up to 600µM for 24h exposure of C2C12 myotubes, to see a decrease in ATP production, which may result in the undesired side-effects of higher toxicity of palmitate [215]. Yuzefovych *et al.* observed a similar effect in L6 myotubes (skeletal muscle), exposing the cells to 100-1000µM palmitate for 6 and 24h, leading to a dose dependent decrease of ATP production. With higher palmitate doses they saw increased ROS production, mitochondrial DNA damage and increased apoptosis [216]. In our assays ATP linked respiration of C2C12 myotubes was significantly decreased in the combination of only 150µM palmitate and 25mM glucose for 24h. Using the combination of both palmitate and glucose in concentrations comparable to human plasma concentrations in a diabetic patient more likely represents T2D and has less toxic side effects of palmitate. Kitzmann *et al.* showed that skeletal myotubes of obese T2D patients were unable to increase palmitate beta-oxidation after 16h palmitate overload

(600µM), compared to healthy subjects [217]. Several prior studies measured mitochondrial function in blood cell types from diabetic patients: Hernandez-Mijares *et al.* reported lower oxygen consumption measured by Clark electrodes in neutrophiles and Avila *et al.* saw decreased oxygen consumption rates in platelets measured with the Agilent Seahorse Analyzer [218] [219]. However, knowledge about respiration of skeletal myotubes of diabetic patients is still limited.

H9C2 myotubes **(Fig. 11, 13)**: In our assays H9C2 myotubes showed significantly higher maximal respiration and ATP linked respiration rates after 24h exposure to all T2D-mimicking conditions (HGI, HGP, HGPI) except HG, when compared to low glucose control cultures. After 96h exposure ATP linked respiration rates were still significantly increased. These groups also showed a highly energetic phenotype compared to LG and LGI. In Glycolytic Rate Assays H9C2 myotubes did not show significant differences in compensatory glycolysis after 24h treatment. Basal glycolysis however was increased in HMP and HMPI, possibly connected to the effects on glucose uptake we observed after the same treatments. After 96h, glycolysis was significantly increased in HG and HGI treated groups. It appears that the cardiomyotubes either increased glycolysis after chronic exposure to HG due to the availability, or due to defects in other energy generating pathways. Unfortunately, long term data is missing due to shortage of materials, and it will be highly interesting to catch up on these experiments in the future.

Strongly increased respiration rates might be associated with elevated cellular stress, as it is known, that high glucose and palmitate levels lead to apoptosis in cardiomyocytes [220] [221] [222] [157]. On the other hand, it can also reflect a highly energetic phenotype with increased oxidation abilities [182]. The increase in ATP linked respiration might be associated with an increase of FA oxidation and decreased glucose utilization, which is assumed to be increased in the T2D heart in humans [223] [224]. Unlike glucose uptake, FA uptake into the heart is not hormonally controlled and mainly driven by the availability in the blood stream [225]. With an oversupply in fatty acids, not only FA oxidation is increased but also detrimental lipid metabolites (i.e., ceramides) accumulate in the myocytes [221] [226]. Chang *et al.* stated that under palmitate treatment of H9C2 cells, diacylglycerol (DAG) production is increased and activates protein kinase C (PKC), which then inhibits the insulin signaling cascade [59].

Various changes in molecular processes occur in the heart of patients with diabetic cardiomyopathy: due to IR it relies mainly on FA oxidation, shows signs of increased oxidative stress, cardiomyocyte apoptosis and low-grade inflammation [227] [228]. Carpentier *et*

al. stated that the reliance of the heart on FA oxidation to produce ATP might lead to oxidative stress and ischemic damage [94]. Glucose oxidation is advantageous when the oxygen supply is limited (stress/exercise/cardiomyopathy) as it requires less oxygen per ATP generated [229]. Therefore, losing the ability to switch to glycolysis combined to an increase in ROS due to the increased FA oxidation and increasing lipotoxicity contribute to both decreased ATP production and cardiac inefficiency. After short term treatments H9C2 cells exposed to HGP and HGPI showed a significant increase in spare respiratory capacity compared to all other treatment groups. This indicates the presence of an increased ability to respond to energetic demands and reflecting cellular fitness. Importantly, this effect was absent after long term treatments, which indicates that heart muscle is initially more resistant to a T2D environment compared to skeletal muscle. Consequently, our model might demonstrate the beginning of chronic metabolic changes in cardiomyocytes after 96h treatments, indicating a decreased cardiac efficiency complementing to what has been described about diabetic hearts previously [223] [224].

In conclusion, in our T2D model skeletal myotubes seem to be unable to sufficiently utilize substrates for ATP production, possibly leading to ROS production and lipid accumulation, and show a more glycolytic phenotype. Cardiac muscle cells on the contrary, increase respiration rates, ATP production and FA oxidation, showing a higher resistance and adaptability to T2D conditions, but possibly leading to exhaustion of the cells and metabolic inflexibility in a chronic state. However, to model what occurs in diabetic cardiomyopathy, treatments likely have to be applied for a longer time, whereas in skeletal myotubes diabetes related changes were already present after short term treatments.

5.4 Mitochondrial morphology in a type 2 diabetic environment

It has been reported that in patients with T2D, mitochondrial content is reduced, size and fusion are impaired and endoplasmic reticulum stress occurs in different cell types [89] [230] [231]. Chen *et al.* observed an increase in fission and impaired fusion in human renal glomerular endothelial cells treated with high glucose (30mM for 72h) [163]. A reduced number and fragmented mitochondria were found in skeletal muscle from Type 2 diabetic and obese subjects, as well as decreased electron transport chain activity [158] [126] [158].

In our study, we observed a significant decrease in mitochondrial number after HGPI treatment of C2C12 myotubes, consistent with decreased ATP linked respiration in these groups. We also observed significant changes in mitochondrial size, especially in H9C2 heart muscle myotubes. Cells treated with T2D mimicking conditions that included palmitate

showed a significant increase in mitochondrial size compared to control, which can be a sign of increased fusion, allowing an enhanced transport of metabolites and enzymes. This observation also is consistent to our Mito Stress Test results, where these cells were highly energetic and showed increased ATP linked respiration. This confirms the better adaptability to an *in vitro* T2D environment of heart muscle cells. In C2C12 myotubes treated with HM the size of the majority of mitochondria was significantly smaller compared to LG and HGP treated groups. This has not been described previously and it is likely that HM treated muscle cells are more quiescent and the osmotic water efflux from cells also affects the mitochondrial compartments.

Both C2C12 and H9C2 myotubes treated with HM and T2D mimicking conditions showed a higher fraction of swollen mitochondria compared to LG controls. Mitochondrial swelling can be caused by osmotic changes in cell culture media and FA treatments but is also a known sign of apoptosis and necrosis [175] [174] [168]. The question remains if whether the decreased ATP-linked respiration we observed in skeletal muscle cells in the T2D environment led to imminent apoptosis and then mitochondrial swelling, or if the T2D mimicking treatments directly caused mitochondrial swelling, subsequently leading to mitochondrial dysfunction and decreased ATP turnover.

5.5 Limitations

There are a number of limitations that must be considered in our studies. The differentiation of H9C2 myoblasts is time consuming and requires incubation and handling in the dark, as retinoic acid is light sensitive. However, it was reported that only after retinoic acid is added to the differentiation process, H9C2 cells show more characteristics of cardiomyotubes. Time is essential in research, which might be a reason why many groups work with undifferentiated myoblasts, thus accepting less specificity.

We chose to use the saturated FA palmitate for our investigations, as it has previously been used for studies addressing IR. Even when the western diet is dominated by saturated FAs, the use of only one saturated FA is not physiologically accurate since *in vivo* circulating FFAs are a mixture of various saturated and unsaturated FAs. For future experiments a mixture (i. e. palmitate and oleate) could be used.

High mannitol treatments served as osmotic controls for high glucose treatments in our study, as it has been widely applied in the literature. Yet we observed some hitherto undescribed effects especially after 96h high mannitol treatments, such as decreased ATP

linked respiration, a shift to glycolysis but decreased basal glucose uptake, and mitochondrial swelling. Lund *el al.*, who also performed Agilent Mitochondrial Stress Tests and Glycolytic Rate Assays, stated not having seen any effects of 15mM mannitol treatment on glucose uptake and oxidation in cultured human myotubes after 4 day treatments [232]. Lu *et al.* exposed H9C2 myoblasts to high levels of mannitol (22 mmol/l and 33 mmol/l) for 96h and didn't see increased numbers of apoptotic cells, but observed an increase in apoptosis by exposure to HG (22 and 33 mmol/l) [233]. They also didn't see elevated mitochondrial cytochrome *c* release in mannitol controls, which can be associated with the mitochondrial swelling that we observed by electron microscopy.

The increased glucose uptake after the combined treatment of palmitate and mannitol has also not been described before, as most groups only worked with high mannitol in the combination with low glucose but not with insulin or palmitate [234] [232]. The mechanistic background of the effects that we observed must still be explored but it can be stated that the impact of hyperosmolarity and hyperlipidemia in a hyperglycemic T2D environment appears more complex than expected.

To develop a well-founded cell model, we utilized numerous different treatment combinations (12 per cell line and duration). Therefore, it was not possible to fit all experimental conditions on a single assay plate for mitochondrial analysis. Numerous assays and biological replicates had to be run which inevitably leads to experimental noise from cell passage and differentiation. For future experiments, we suggest focusing on the HGPI treatment group, as it is most representative for T2D, and then more experimental conditions can be run in parallel on a single plate.

5.6 Conclusion

T2D is a complex disease still not fully understood. Animal and cell models of T2D play an important role in further exploring the pathophysiology of T2D and finding treatment options that could be translated into human studies. T2D is characterized by elevated blood glucose levels and IR. Skeletal muscle is the primary recipient of postprandial blood glucose. Heart muscle is also affected by IR and T2D leads to cardiac complications like diabetic cardiomyopathy, heart failure and cardiovascular disease.

Several existing *in vitro* models of T2D using muscle cells work with the easier to handle myoblasts, that express fewer specific characteristics than differentiated myotubes. This motivated our choice to work with myotubes which appear far more relevant. Additionally,

existing *in vitro* models usually work with either high glucose or high fatty acid treatment to induce IR as it is occurring in T2D, disregarding that the development of T2D is an interplay of western world lifestyle phenomena like physical inactivity and a dietary oversupply of both sugar and fat, compensated by elevated insulin in early disease states. There have been few approaches including the acclimatization to physiological glucose [66] prior to high glucose treatment, and using a similar cocktail to mimic T2D as was done in the current study [234].

For the first time we established a diabetes model where prior to any treatment skeletal and cardiac myoblasts were acclimatized to physiological glucose levels and further differentiated into myotubes using physiological glucose levels. Thereafter, the exposure to individual and combined diabetes mimicking conditions was initiated, and we were the first to compare effects of short-term (24h) vs. chronic (96h) exposure of the main aspects of T2D: hyperglycemia, hyperlipidemia and variably elevated insulin levels. This way we tried to accentuate in the model that T2D is a chronic, progressive and complex disease.

We were able to explore diabetes-related changes in a peripheral and cardiac myocyte model in glucose-uptake assays, mitochondrial respiration analysis and TEM pictures in a physiologically relevant manner. The main changes included IR, a switch in metabolic phenotypes, altered ATP linked respiration and morphologic changes of mitochondria, very similarly as it is reported in skeletal and cardiac muscle of patients suffering from T2D: C2C12 skeletal muscle myotubes showed IR, an impaired ATP linked respiration and switch to glycolysis, and an increase in mitochondrial swelling, indicating mitochondrial dysfunction and decreased oxidative abilities. H9C2 cardiac myotubes showed IR and an increase in FA oxidation, mitochondrial swelling, increased ATP linked respiration and spare respiratory capacity, but a loss of this reserve capacity after long term treatments, indicating a longer preserved resistance to diabetic conditions compared to skeletal muscle. This is consistent with more robust metabolic compensation mechanisms in the heart that may delay damage in a vital organ.

5.7 Outlook

Is it possible to model diabetes in a dish? We tried to use well differentiated cell models, compound concentrations close to *in vivo* levels, an acceptable time frame and complexity and that it potentially allows a broad spectrum of read-outs also in other cell types of interest. Furthermore, other important aspects of T2D could be added, especially the communication with other cell systems that play pivotal roles in disease development. Our

idea is it to create cell cultures where the communication and selected metabolite and signal exchange is possible with e.g., adipocytes, hepatocytes, and pancreatic beta cells. This way a model might ultimately be named “diabetes in a dish”.

In addition to our morphologic findings other aspects of mitochondrial dysfunction like metabolite handling and protein expression could be studied in our T2D model. Published evidence suggest that IR is related to low levels of mitochondrial fusion proteins such as mitofusin 2 [148]. Also it might be relevant to extend the observations we made in TEM to contact sites between the sarcoplasmatic reticulum and mitochondria, as they are critical for calcium signaling during muscle contraction and could give conclusions on contractile function in T2D [235] [236].

We used state of the art molecular biology techniques to collect important metabolic information and to validate this model as a basis for further research saving resources and the need of animal experiments.

Literature

1. Bommer C, Sagalova V, Heesemann E, et al. Global Economic Burden of Diabetes in Adults: Projections From 2015 to 2030. Diabetes care. 2018;41(5):963-970.
2. International Diabetes Federation. IDF Diabetes Atlas, 9th edn. Available at: https://www.diabetesatlas.org. Brussels, Belgium 2019.
3. World Health Organization. Global Report on Diabetes. Geneva, Switzerland 2016.
4. Mathers CD, Loncar D. Projections of global mortality and burden of disease from 2002 to 2030. PLoS medicine. 2006;3(11):e442.
5. Harreiter J, Roden M. [Diabetes mellitus-Definition, classification, diagnosis, screening and prevention (Update 2019)]. Wiener klinische Wochenschrift. 2019;131(Suppl 1):6-15.
6. Centers for Disease Control and Prevention. National Diabetes Statistics Report, 2020. 2020.
7. Website of the International Diabetes Federation. Metabolic Syndrome Available: www.idf.org/metabolic_syndrome. Accessed december 2020.
8. Hoffman EL, VonWald T, Hansen K. The metabolic syndrome. South Dakota medicine : the journal of the South Dakota State Medical Association. 2015;Spec No:24-28.
9. Lehtovirta M, Pietilainen KH, Levalahti E, et al. Evidence that BMI and type 2 diabetes share only a minor fraction of genetic variance: a follow-up study of 23,585 monozygotic and dizygotic twins from the Finnish Twin Cohort Study. Diabetologia. 2010;53(7):1314-1321.
10. Mozaffarian D, Benjamin EJ, Go AS, et al. Heart disease and stroke statistics--2015 update: a report from the American Heart Association. Circulation. 2015;131(4):e29-322.
11. Bhupathiraju SN, Hu FB. Epidemiology of Obesity and Diabetes and Their Cardiovascular Complications. Circulation research. 2016;118(11):1723-1735.
12. Ritchie RH, Abel ED. Basic Mechanisms of Diabetic Heart Disease. Circulation research. 2020;126(11):1501-1525.
13. Ohkuma T, Komorita Y, Peters SAE, et al. Diabetes as a risk factor for heart failure in women and men: a systematic review and meta-analysis of 47 cohorts including 12 million individuals. Diabetologia. 2019;62(9):1550-1560.
14. El Berri H, Gedik FG, Belkhadir J, et al. Tackling diabetes: how nurses can make the difference. Eastern Mediterranean health journal = La revue de sante de la Mediterranee orientale = al-Majallah al-sihhiyah li-sharq al-mutawassit. 2020;26(11):1318-1319.
15. World Health Organization. World Health Statistics 2020: Monitoring health for the SDGs. Geneva: World Health Organization; 2020 (https://www.who.int/gho/publications/world_health_statistics/2020/en/).
16. Pham T, Loiselle D, Power A, et al. Mitochondrial inefficiencies and anoxic ATP hydrolysis capacities in diabetic rat heart. American journal of physiology Cell physiology. 2014;307(6):C499-507.
17. Dufrane D, van Steenberghe M, Guiot Y, et al. Streptozotocin-induced diabetes in large animals (pigs/primates): role of GLUT2 transporter and beta-cell plasticity. Transplantation. 2006;81(1):36-45.
18. Hanafusa T, Miyagawa J, Nakajima H, et al. The NOD mouse. Diabetes Res Clin Pract. 1994;24 Suppl:S307-311.
19. King AJ. The use of animal models in diabetes research. British Journal of Pharmacology. 2012;166(3):877-894.
20. Lilao-Garzón J, Valverde-Tercedor C, Muñoz-Descalzo S, et al. In Vivo and In Vitro Models of Diabetes: A Focus on Pregnancy. In Islam MS, (Ed). Diabetes: from Research to Clinical Practice: Volume 4. Cham: Springer International Publishing 2021:553-576.

21. Reed MJ, Scribner KA. In-vivo and in-vitro models of type 2 diabetes in pharmaceutical drug discovery. Diabetes, Obesity and Metabolism. 1999;1(2):75-86.
22. Fuhlendorff J, Rorsman P, Kofod H, et al. Stimulation of insulin release by repaglinide and glibenclamide involves both common and distinct processes. Diabetes. 1998;47(3):345-351.
23. Hargrove DM, Nardone NA, Persson LM, et al. Comparison of the glucose dependency of glucagon-like peptide-1 (7-37) and glyburide in vitro and in vivo. Metabolism. 1996;45(3):404-409.
24. Chick WL, Warren S, Chute RN, et al. A transplantable insulinoma in the rat. Proc Natl Acad Sci U S A. 1977;74(2):628-632.
25. Asfari M, Janjic D, Meda P, et al. Establishment of 2-mercaptoethanol-dependent differentiated insulin-secreting cell lines. Endocrinology. 1992;130(1):167-178.
26. Tsonkova VG, Sand FW, Wolf XA, et al. The EndoC-βH1 cell line is a valid model of human beta cells and applicable for screenings to identify novel drug target candidates. Mol Metab. 2018;8:144-157.
27. Krause M, Keane K, Rodrigues-Krause J, et al. Elevated levels of extracellular heat-shock protein 72 (eHSP72) are positively correlated with insulin resistance in vivo and cause pancreatic β-cell dysfunction and death in vitro. Clinical Science. 2014;126(10):739-752.
28. Marchetti P, Schulte AM, Marselli L, et al. Fostering improved human islet research: a European perspective. Diabetologia. 2019;62(8):1514-1516.
29. Hart NJ, Powers AC. Use of human islets to understand islet biology and diabetes: progress, challenges and suggestions. Diabetologia. 2019;62(2):212-222.
30. Knutson VP, Yvonne B. 3T3-L1 Adipocytes as a Cell Culture Model of Insulin Resistance. In vitro cellular & developmental biology Animal. 1997;33(2):77-81.
31. Chavez JA, Summers SA. Characterizing the effects of saturated fatty acids on insulin signaling and ceramide and diacylglycerol accumulation in 3T3-L1 adipocytes and C2C12 myotubes. Archives of Biochemistry and Biophysics. 2003;419(2):101-109.
32. Sakoda H, Ogihara T, Anai M, et al. Dexamethasone-induced insulin resistance in 3T3-L1 adipocytes is due to inhibition of glucose transport rather than insulin signal transduction. Diabetes. 2000;49(10):1700-1708.
33. Jager J, Grémeaux T, Cormont M, et al. Interleukin-1β-Induced Insulin Resistance in Adipocytes through Down-Regulation of Insulin Receptor Substrate-1 Expression. Endocrinology. 2007;148(1):241-251.
34. Regazzetti C, Peraldi P, Grémeaux T, et al. Hypoxia Decreases Insulin Signaling Pathways in Adipocytes. Diabetes. 2009;58(1):95-103.
35. Martin WH, Hoover DJ, Armento SJ, et al. Discovery of a human liver glycogen phosphorylase inhibitor that lowers blood glucose in vivo. Proc Natl Acad Sci U S A. 1998;95(4):1776-1781.
36. Treadway JL, Mendys P, Hoover DJ. Glycogen phosphorylase inhibitors for treatment of type 2 diabetes mellitus. Expert Opin Investig Drugs. 2001;10(3):439-454.
37. Krako Jakovljevic N, Pavlovic K, Zujovic T, et al. In vitro models of insulin resistance: Mitochondrial coupling is differently affected in liver and muscle cells. Mitochondrion. 2021;61:165-173.
38. Chanon S, Durand C, Vieille-Marchiset A, et al. Glucose Uptake Measurement and Response to Insulin Stimulation in In Vitro Cultured Human Primary Myotubes. J Vis Exp. 2017(124):55743.
39. Carter S, Solomon TPJ. In vitro experimental models for examining the skeletal muscle cell biology of exercise: the possibilities, challenges and future developments. Pflügers Archiv - European Journal of Physiology. 2019;471(3):413-429.
40. Brown MA SL, Huang XF, et al. Dietary Fat and Carbohydrate Composition: Metabolic Disease. In Montmayeur JP le Coutre J, (Ed). Fat Detection: Taste, Texture, and Post Ingestive Effects: Boca Raton (FL): CRC Press/Taylor & Francis 2010.

41. Eckel RH, Grundy SM, Zimmet PZ. The metabolic syndrome. Lancet (London, England). 2005;365(9468):1415-1428.
42. Hotamisligil GS. Inflammation and endoplasmic reticulum stress in obesity and diabetes. International journal of obesity (2005). 2008;32 Suppl 7(Suppl 7):S52-54.
43. Laybutt DR, Preston AM, Akerfeldt MC, et al. Endoplasmic reticulum stress contributes to beta cell apoptosis in type 2 diabetes. Diabetologia. 2007;50(4):752-763.
44. Hotamisligil GS. Inflammation, metaflammation and immunometabolic disorders. Nature. 2017;542(7640):177-185.
45. Sethi JK, Vidal-Puig AJ. Targeting fat to prevent diabetes. Cell metabolism. 2007;5(5):323-325.
46. Griffin ME, Marcucci MJ, Cline GW, et al. Free fatty acid-induced insulin resistance is associated with activation of protein kinase C theta and alterations in the insulin signaling cascade. Diabetes. 1999;48(6):1270-1274.
47. Homko CJ, Cheung P, Boden G. Effects of free fatty acids on glucose uptake and utilization in healthy women. Diabetes. 2003;52(2):487-491.
48. Boden G, Chen X, Ruiz J, et al. Mechanisms of fatty acid-induced inhibition of glucose uptake. J Clin Invest. 1994;93(6):2438-2446.
49. Delarue J, Magnan C. Free fatty acids and insulin resistance. Current opinion in clinical nutrition and metabolic care. 2007;10(2):142-148.
50. Kraegen EW, Cooney GJ. Free fatty acids and skeletal muscle insulin resistance. Current opinion in lipidology. 2008;19(3):235-241.
51. Sears B, Perry M. The role of fatty acids in insulin resistance. Lipids in health and disease. 2015;14:121.
52. Lin N, Chen H, Zhang H, et al. Mitochondrial reactive oxygen species (ROS) inhibition ameliorates palmitate-induced INS-1 beta cell death. Endocrine. 2012;42(1):107-117.
53. Karaskov E, Scott C, Zhang L, et al. Chronic palmitate but not oleate exposure induces endoplasmic reticulum stress, which may contribute to INS-1 pancreatic beta-cell apoptosis. Endocrinology. 2006;147(7):3398-3407.
54. Oh YS, Bae GD, Baek DJ, et al. Fatty Acid-Induced Lipotoxicity in Pancreatic Beta-Cells During Development of Type 2 Diabetes. Frontiers in endocrinology. 2018;9:384.
55. I. S. Sobczak A, A. Blindauer C, J. Stewart A. Changes in Plasma Free Fatty Acids Associated with Type-2 Diabetes. Nutrients. 2019;11(9).
56. Katsarou A, Gudbjörnsdottir S, Rawshani A, et al. Type 1 diabetes mellitus. Nature Reviews Disease Primers. 2017;3(1):17016.
57. Ding W, Chang WG, Guo XC, et al. Exenatide Protects Against Cardiac Dysfunction by Attenuating Oxidative Stress in the Diabetic Mouse Heart. Frontiers in endocrinology. 2019;10:202.
58. Feng CC, Pandey S, Lin CY, et al. Cardiac apoptosis induced under high glucose condition involves activation of IGF2R signaling in H9c2 cardiomyoblasts and streptozotocin-induced diabetic rat hearts. Biomedicine & pharmacotherapy = Biomedecine & pharmacotherapie. 2018;97:880-885.
59. Chang W, Chen L, Hatch GM. Berberine treatment attenuates the palmitate-mediated inhibition of glucose uptake and consumption through increased 1,2,3-triacyl-sn-glycerol synthesis and accumulation in H9c2 cardiomyocytes. Biochimica et Biophysica Acta (BBA) - Molecular and Cell Biology of Lipids. 2016;1861(4):352-362.
60. Yang M, Wei D, Mo C, et al. Saturated fatty acid palmitate-induced insulin resistance is accompanied with myotube loss and the impaired expression of health benefit myokine genes in C2C12 myotubes. Lipids in health and disease. 2013;12:104.
61. American Diabetes Association. Diagnosis and classification of diabetes mellitus. Diabetes care. 2010;33 Suppl 1(Suppl 1):S62-S69.

62. World Health Organization. Mean fasting blood glucose Available: https://www.who.int/data/gho/indicator-metadata-registry/imr-details/2380. Accessed 16.02., 2021.
63. Brambilla P, La Valle E, Falbo R, et al. Normal fasting plasma glucose and risk of type 2 diabetes. Diabetes care. 2011;34(6):1372-1374.
64. Unwin N, Shaw J, Zimmet P, et al. Impaired glucose tolerance and impaired fasting glycaemia: the current status on definition and intervention. Diabetic medicine : a journal of the British Diabetic Association. 2002;19(9):708-723.
65. Zhou B, Lu Y, Hajifathalian K, et al. Worldwide trends in diabetes since 1980: a pooled analysis of 751 population-based studies with 4·4 million participants. The Lancet. 2016;387(10027):1513-1530.
66. Dohl J, Foldi J, Heller J, et al. Acclimation of C2C12 myoblasts to physiological glucose concentrations for in vitro diabetes research. Life sciences. 2018;211:238-244.
67. Fulco M, Cen Y, Zhao P, et al. Glucose restriction inhibits skeletal myoblast differentiation by activating SIRT1 through AMPK-mediated regulation of Nampt. Developmental cell. 2008;14(5):661-673.
68. Nelson BA, Robinson KA, Buse MG. High glucose and glucosamine induce insulin resistance via different mechanisms in 3T3-L1 adipocytes. Diabetes. 2000;49(6):981-991.
69. Ha H, Pak Y. Modulation of the caveolin-3 and Akt status in caveolae by insulin resistance in H9c2 cardiomyoblasts. Experimental & molecular medicine. 2005;37(3):169-178.
70. Henique C, Mansouri A, Fumey G, et al. Increased mitochondrial fatty acid oxidation is sufficient to protect skeletal muscle cells from palmitate-induced apoptosis. The Journal of biological chemistry. 2010;285(47):36818-36827.
71. Taheripak G, Bakhtiyari S, Rajabibazl M, et al. Protein tyrosine phosphatase 1B inhibition ameliorates palmitate-induced mitochondrial dysfunction and apoptosis in skeletal muscle cells. Free radical biology & medicine. 2013;65:1435-1446.
72. Coll T, Eyre E, Rodríguez-Calvo R, et al. Oleate reverses palmitate-induced insulin resistance and inflammation in skeletal muscle cells. The Journal of biological chemistry. 2008;283(17):11107-11116.
73. Hartmann T, Overhagen S, Ouwens DM, et al. Effect of the long-acting insulin analogues glargine and degludec on cardiomyocyte cell signalling and function. Cardiovascular diabetology. 2016;15:96.
74. Law BA, Liao X, Moore KS, et al. Lipotoxic very-long-chain ceramides cause mitochondrial dysfunction, oxidative stress, and cell death in cardiomyocytes. FASEB journal : official publication of the Federation of American Societies for Experimental Biology. 2018;32(3):1403-1416.
75. Xu K, Liu XF, Ke ZQ, et al. Resveratrol Modulates Apoptosis and Autophagy Induced by High Glucose and Palmitate in Cardiac Cells. Cellular physiology and biochemistry : international journal of experimental cellular physiology, biochemistry, and pharmacology. 2018;46(5):2031-2040.
76. Hsu HC, Chen CY, Lee BC, et al. High-fat diet induces cardiomyocyte apoptosis via the inhibition of autophagy. European journal of nutrition. 2016;55(7):2245-2254.
77. Zou L, Li X, Wu N, et al. Palmitate induces myocardial lipotoxic injury via the endoplasmic reticulum stress-mediated apoptosis pathway. Molecular medicine reports. 2017;16(5):6934-6939.
78. Abdelmagid SA, Clarke SE, Nielsen DE, et al. Comprehensive profiling of plasma fatty acid concentrations in young healthy Canadian adults. PloS one. 2015;10(2):e0116195.
79. Winder WW, Hardie DG. Inactivation of acetyl-CoA carboxylase and activation of AMP-activated protein kinase in muscle during exercise. American Journal of Physiology-Endocrinology and Metabolism. 1996;270(2):E299-E304.
80. Nawrocki A, Górski J. Effect of plasma free fatty acid concentration on the content and composition of the free fatty acid fraction in rat skeletal muscles. Hormone and metabolic research = Hormon- und Stoffwechselforschung = Hormones et metabolisme. 2004;36(9):601-606.

81. Park M, Kaddai V, Ching J, et al. A Role for Ceramides, but Not Sphingomyelins, as Antagonists of Insulin Signaling and Mitochondrial Metabolism in C2C12 Myotubes. Journal of Biological Chemistry. 2016;291(46):23978-23988.
82. Smith AG, Muscat GE. Skeletal muscle and nuclear hormone receptors: implications for cardiovascular and metabolic disease. The international journal of biochemistry & cell biology. 2005;37(10):2047-2063.
83. Tumova J, Andel M, Trnka J. Excess of free fatty acids as a cause of metabolic dysfunction in skeletal muscle. Physiological research. 2016;65(2):193-207.
84. Wong CY, Al-Salami H, Dass CR. C2C12 cell model: its role in understanding of insulin resistance at the molecular level and pharmaceutical development at the preclinical stage. Journal of Pharmacy and Pharmacology. 2020;72(12):1667-1693.
85. Mangnall D, Bruce C, Fraser RB. Insulin-stimulated glucose uptake in C2C12 myoblasts. Biochemical Society transactions. 1993;21(4):438s.
86. Ragheb R, Shanab GML, Medhat AM, et al. Free fatty acid-induced muscle insulin resistance and glucose uptake dysfunction: evidence for PKC activation and oxidative stress-activated signaling pathways. Biochemical and biophysical research communications. 2009;389(2):211-216.
87. Conejo R, Lorenzo M. Insulin signaling leading to proliferation, survival, and membrane ruffling in C2C12 myoblasts. Journal of Cellular Physiology. 2001;187(1):96-108.
88. Bryant NJ, Govers R, James DE. Regulated transport of the glucose transporter GLUT4. Nature reviews Molecular cell biology. 2002;3(4):267-277.
89. Abdelmoez AM, Sardón Puig L, Smith JAB, et al. Comparative profiling of skeletal muscle models reveals heterogeneity of transcriptome and metabolism. American journal of physiology Cell physiology. 2020;318(3):C615-c626.
90. Lawson MA, Purslow PP. Differentiation of Myoblasts in Serum-Free Media: Effects of Modified Media Are Cell Line-Specific. Cells Tissues Organs. 2000;167(2-3):130-137.
91. Opie LH, Knuuti J. The Adrenergic-Fatty Acid Load in Heart Failure. Journal of the American College of Cardiology. 2009;54(18):1637-1646.
92. Ashrafian H, Frenneaux MP, Opie LH. Metabolic Mechanisms in Heart Failure. Circulation. 2007;116(4):434-448.
93. Stanley WC, Recchia FA, Lopaschuk GD. Myocardial Substrate Metabolism in the Normal and Failing Heart. Physiological Reviews. 2005;85(3):1093-1129.
94. Carpentier AC. Abnormal Myocardial Dietary Fatty Acid Metabolism and Diabetic Cardiomyopathy. The Canadian journal of cardiology. 2018;34(5):605-614.
95. Westermeier F, Navarro-Marquez M, Lopez-Crisosto C, et al. Defective insulin signaling and mitochondrial dynamics in diabetic cardiomyopathy. Biochimica et biophysica acta. 2015;1853(5):1113-1118.
96. Young ME, Guthrie PH, Razeghi P, et al. Impaired long-chain fatty acid oxidation and contractile dysfunction in the obese Zucker rat heart. Diabetes. 2002;51(8):2587-2595.
97. Chiu HC, Kovacs A, Blanton RM, et al. Transgenic expression of fatty acid transport protein 1 in the heart causes lipotoxic cardiomyopathy. Circulation research. 2005;96(2):225-233.
98. Amaral N, Okonko DO. Metabolic abnormalities of the heart in type II diabetes. Diabetes & vascular disease research. 2015;12(4):239-248.
99. Kimes BW, Brandt BL. Properties of a clonal muscle cell line from rat heart. Experimental cell research. 1976;98(2):367-381.
100. Watkins SJ, Borthwick GM, Arthur HM. The H9C2 cell line and primary neonatal cardiomyocyte cells show similar hypertrophic responses in vitro. In vitro cellular & developmental biology Animal. 2011;47(2):125-131.
101. Ismael S, Nair RR. Reactivation of fatty acid oxidation by medium chain fatty acid prevents myocyte hypertrophy in H9c2 cell line. Molecular and cellular biochemistry. 2021;476(1):483-491.

102. Zordoky BN, El-Kadi AO. H9c2 cell line is a valuable in vitro model to study the drug metabolizing enzymes in the heart. Journal of pharmacological and toxicological methods. 2007;56(3):317-322.
103. Dillmann WH, Mestril R. Heat shock proteins in myocardial stress. Zeitschrift fur Kardiologie. 1995;84 Suppl 4:87-90.
104. Cai L, Li W, Wang G, et al. Hyperglycemia-induced apoptosis in mouse myocardium: mitochondrial cytochrome C-mediated caspase-3 activation pathway. Diabetes. 2002;51(6):1938-1948.
105. Joseph D, Kimar C, Symington B, et al. The detrimental effects of acute hyperglycemia on myocardial glucose uptake. Life sciences. 2014;105(1-2):31-42.
106. Patten V, Chabaesele I, Sishi B, et al. Cardiomyocyte differentiation: Experience and observations from 2 laboratories. Journal of the South African Heart Association (SA Heart). 2017;14:96-107.
107. Lopaschuk GD, Jaswal JS. Energy metabolic phenotype of the cardiomyocyte during development, differentiation, and postnatal maturation. Journal of cardiovascular pharmacology. 2010;56(2):130-140.
108. Nobuhara M, Saotome M, Watanabe T, et al. Mitochondrial dysfunction caused by saturated fatty acid loading induces myocardial insulin-resistance in differentiated H9c2 myocytes: a novel ex vivo myocardial insulin-resistance model. Experimental cell research. 2013;319(7):955-966.
109. Hudish LI, Reusch JE, Sussel L. β Cell dysfunction during progression of metabolic syndrome to type 2 diabetes. J Clin Invest. 2019;129(10):4001-4008.
110. Ha J, Sherman A. Type 2 diabetes: one disease, many pathways. American journal of physiology Endocrinology and metabolism. 2020;319(2):E410-e426.
111. Alam F, Islam MA, Khalil MI, et al. Metabolic Control of Type 2 Diabetes by Targeting the GLUT4 Glucose Transporter: Intervention Approaches. Current pharmaceutical design. 2016;22(20):3034-3049.
112. Yang Q, Graham TE, Mody N, et al. Serum retinol binding protein 4 contributes to insulin resistance in obesity and type 2 diabetes. Nature. 2005;436(7049):356-362.
113. Shepherd PR, Kahn BB. Glucose Transporters and Insulin Action — Implications for Insulin Resistance and Diabetes Mellitus. New England Journal of Medicine. 1999;341(4):248-257.
114. Valley MP, Karassina N, Aoyama N, et al. A bioluminescent assay for measuring glucose uptake. Analytical biochemistry. 2016;505:43-50.
115. Saito K, Lee S, Shiuchi T, et al. An enzymatic photometric assay for 2-deoxyglucose uptake in insulin-responsive tissues and 3T3-L1 adipocytes. Analytical biochemistry. 2011;412(1):9-17.
116. Yamamoto N, Ueda-Wakagi M, Sato T, et al. Measurement of Glucose Uptake in Cultured Cells. Current protocols in pharmacology. 2015;71:12.14.11-26.
117. Swerdlow RH, Koppel S, Weidling I, et al. Mitochondria, Cybrids, Aging, and Alzheimer's Disease. Progress in molecular biology and translational science. 2017;146:259-302.
118. Grimm A, Eckert A. Brain aging and neurodegeneration: from a mitochondrial point of view. Journal of neurochemistry. 2017;143(4):418-431.
119. Murphy E, Ardehali H, Balaban RS, et al. Mitochondrial Function, Biology, and Role in Disease: A Scientific Statement From the American Heart Association. Circulation research. 2016;118(12):1960-1991.
120. Gómez-Serrano M, Camafeita E, Loureiro M, et al. Mitoproteomics: Tackling Mitochondrial Dysfunction in Human Disease. Oxidative medicine and cellular longevity. 2018;2018:1435934-1435934.
121. Dai D-F, Rabinovitch PS, Ungvari Z. Mitochondria and cardiovascular aging. Circulation research. 2012;110(8):1109-1124.

122. Wallace DC. A mitochondrial bioenergetic etiology of disease. The Journal of clinical investigation. 2013;123(4):1405-1412.
123. Montgomery MK, Turner N. Mitochondrial dysfunction and insulin resistance: an update. Endocrine connections. 2015;4(1):R1-r15.
124. Di Meo S, Iossa S, Venditti P. Skeletal muscle insulin resistance: role of mitochondria and other ROS sources. The Journal of endocrinology. 2017;233(1):R15-r42.
125. Ding H, Heng B, He W, et al. Chronic reactive oxygen species exposure inhibits glucose uptake and causes insulin resistance in C2C12 myotubes. Biochemical and biophysical research communications. 2016;478(2):798-803.
126. Kelley DE, He J, Menshikova EV, et al. Dysfunction of mitochondria in human skeletal muscle in type 2 diabetes. Diabetes. 2002;51(10):2944-2950.
127. Kim JY, Hickner RC, Cortright RL, et al. Lipid oxidation is reduced in obese human skeletal muscle. American journal of physiology Endocrinology and metabolism. 2000;279(5):E1039-1044.
128. Rabol R, Larsen S, Hojberg PM, et al. Regional anatomic differences in skeletal muscle mitochondrial respiration in type 2 diabetes and obesity. The Journal of clinical endocrinology and metabolism. 2010;95(2):857-863.
129. Hong Y, Lee JH, Jeong KW, et al. Amelioration of muscle wasting by glucagon-like peptide-1 receptor agonist in muscle atrophy. Journal of cachexia, sarcopenia and muscle. 2019.
130. Chen L, Knowlton AA. Mitochondria and heart failure: new insights into an energetic problem. Minerva cardioangiologica. 2010;58(2):213-229.
131. Dean RT, Fu S, Stocker R, et al. Biochemistry and pathology of radical-mediated protein oxidation. The Biochemical journal. 1997;324 (Pt 1)(Pt 1):1-18.
132. Schieber M, Chandel Navdeep S. ROS Function in Redox Signaling and Oxidative Stress. Current Biology. 2014;24(10):R453-R462.
133. Jackson JH, Schraufstatter IU, Hyslop PA, et al. Role of oxidants in DNA damage. Hydroxyl radical mediates the synergistic DNA damaging effects of asbestos and cigarette smoke. J Clin Invest. 1987;80(4):1090-1095.
134. Cabiscol E, Levine RL. Carbonic anhydrase III. Oxidative modification in vivo and loss of phosphatase activity during aging. The Journal of biological chemistry. 1995;270(24):14742-14747.
135. Agilent Technologies. How Agilent Seahorse XF Analyzers Work Available: https://www.agilent.com/en/products/cell-analysis/how-seahorse-xf-analyzers-work. Accessed 20.12., 2020.
136. Nicholls DG, Darley-Usmar VM, Wu M, et al. Bioenergetic profile experiment using C2C12 myoblast cells. J Vis Exp. 2010(46).
137. Hong S, Pedersen PL. ATP synthase and the actions of inhibitors utilized to study its roles in human health, disease, and other scientific areas. Microbiol Mol Biol Rev. 2008;72(4):590-641, Table of Contents.
138. Votyakova TV, Reynolds IJ. ΔΨm-Dependent and -independent production of reactive oxygen species by rat brain mitochondria. Journal of Neurochemistry. 2001;79(2):266-277.
139. Mookerjee SA, Nicholls DG, Brand MD. Determining Maximum Glycolytic Capacity Using Extracellular Flux Measurements. PloS one. 2016;11(3):e0152016.
140. Campioni G, Pasquale V, Busti S, et al. An Optimized Workflow for the Analysis of Metabolic Fluxes in Cancer Spheroids Using Seahorse Technology. Cells 2022.
141. Pasquale V, Ducci G, Campioni G, et al. Profiling and Targeting of Energy and Redox Metabolism in Grade 2 Bladder Cancer Cells with Different Invasiveness Properties. Cells. 2020;9(12).
142. Wu L, Zhao J, Cao K, et al. Oxidative phosphorylation activation is an important characteristic of DOX resistance in hepatocellular carcinoma cells. Cell Commun Signal. 2018;16(1):6.

143. Alhourani AH, Tidwell TR, Bokil AA, et al. Metformin treatment response is dependent on glucose growth conditions and metabolic phenotype in colorectal cancer cells. Scientific Reports. 2021;11(1):10487.
144. Kuffner K, Triebelhorn J, Meindl K, et al. Major Depressive Disorder is Associated with Impaired Mitochondrial Function in Skin Fibroblasts. Cells. 2020;9(4):884.
145. Costa CF, Pinho SA, Pinho SLC, et al. Mitochondrial and metabolic remodeling in human skin fibroblasts in response to glucose availability. bioRxiv. 2021:2021.2002.2024.432508.
146. Mookerjee SA, Gerencser AA, Nicholls DG, et al. Quantifying intracellular rates of glycolytic and oxidative ATP production and consumption using extracellular flux measurements. Journal of Biological Chemistry. 2017;292(17):7189-7207.
147. Li R, Steyn FJ, Stout MB, et al. Development of a high-throughput method for real-time assessment of cellular metabolism in intact long skeletal muscle fibre bundles. J Physiol. 2016;594(24):7197-7213.
148. Picard M, White K, Turnbull DM. Mitochondrial morphology, topology, and membrane interactions in skeletal muscle: a quantitative three-dimensional electron microscopy study. Journal of Applied Physiology. 2013;114(2):161-171.
149. Holloszy JO. Biochemical adaptations in muscle: effects of exercise on mitochondrial oxygen uptake and respiratory enzyme activity in skeletal muscle. Journal of biological chemistry. 1967;242(9):2278-2282.
150. Schwerzmann K, Hoppeler H, Kayar SR, et al. Oxidative capacity of muscle and mitochondria: correlation of physiological, biochemical, and morphometric characteristics. Proc Natl Acad Sci U S A. 1989;86(5):1583-1587.
151. Ørtenblad N, Nielsen J, Boushel R, et al. The Muscle Fiber Profiles, Mitochondrial Content, and Enzyme Activities of the Exceptionally Well-Trained Arm and Leg Muscles of Elite Cross-Country Skiers. Front Physiol. 2018;9:1031.
152. Willingham TB, Ajayi PT, Glancy B. Subcellular Specialization of Mitochondrial Form and Function in Skeletal Muscle Cells. Frontiers in Cell and Developmental Biology. 2021;9.
153. McCarron JG, Wilson C, Sandison ME, et al. From Structure to Function: Mitochondrial Morphology, Motion and Shaping in Vascular Smooth Muscle. Journal of Vascular Research. 2013;50(5):357-371.
154. Westermann B. Bioenergetic role of mitochondrial fusion and fission. Biochimica et biophysica acta. 2012;1817(10):1833-1838.
155. Benard G, Bellance N, James D, et al. Mitochondrial bioenergetics and structural network organization. J Cell Sci. 2007;120(Pt 5):838-848.
156. Shenouda SM, Widlansky ME, Chen K, et al. Altered Mitochondrial Dynamics Contributes to Endothelial Dysfunction in Diabetes Mellitus. Circulation. 2011;124(4):444-453.
157. Fetterman JL, Holbrook M, Westbrook DG, et al. Mitochondrial DNA damage and vascular function in patients with diabetes mellitus and atherosclerotic cardiovascular disease. Cardiovascular diabetology. 2016;15:53.
158. Ritov VB, Menshikova EV, He J, et al. Deficiency of Subsarcolemmal Mitochondria in Obesity and Type 2 Diabetes. Diabetes. 2005;54(1):8-14.
159. Yu T, Robotham JL, Yoon Y. Increased production of reactive oxygen species in hyperglycemic conditions requires dynamic change of mitochondrial morphology. Proceedings of the National Academy of Sciences of the United States of America. 2006;103(8):2653-2658.
160. Bonnard C, Durand A, Peyrol S, et al. Mitochondrial dysfunction results from oxidative stress in the skeletal muscle of diet-induced insulin-resistant mice. J Clin Invest. 2008;118(2):789-800.
161. Williams M, Caino MC. Mitochondrial Dynamics in Type 2 Diabetes and Cancer. Frontiers in endocrinology. 2018;9:211-211.

162. Morino K, Petersen KF, Dufour S, et al. Reduced mitochondrial density and increased IRS-1 serine phosphorylation in muscle of insulin-resistant offspring of type 2 diabetic parents. The Journal of clinical investigation. 2005;115(12):3587-3593.
163. Chen W, Xiang H, Chen R, et al. S1PR2 antagonist ameliorate high glucose-induced fission and dysfunction of mitochondria in HRGECs via regulating ROCK1. BMC Nephrology. 2019;20(1):135.
164. Glancy B, Balaban RS. Energy metabolism design of the striated muscle cell. Physiol Rev. 2021;101(4):1561-1607.
165. Takahashi M, Hood DA. Protein Import into Subsarcolemmal and Intermyofibrillar Skeletal Muscle Mitochondria: DIFFERENTIAL IMPORT REGULATION IN DISTINCT SUBCELLULAR REGIONS *. Journal of Biological Chemistry. 1996;271(44):27285-27291.
166. Sivitz WI, Yorek MA. Mitochondrial dysfunction in diabetes: from molecular mechanisms to functional significance and therapeutic opportunities. Antioxidants & redox signaling. 2010;12(4):537-577.
167. Lu X, Thai PN, Lu S, et al. Intrafibrillar and perinuclear mitochondrial heterogeneity in adult cardiac myocytes. Journal of Molecular and Cellular Cardiology. 2019;136:72-84.
168. Ghadially FN. 3 - Mitochondria. In Ghadially FN, (Ed). Ultrastructural Pathology of the Cell and Matrix (Third Edition): Butterworth-Heinemann 1988:191-328.
169. Lehninger AL. Reversal of thyroxine-induced swelling of rat liver mitochondria by adenosine triphosphate. The Journal of biological chemistry. 1959;234(8):2187-2195.
170. Chappell JB, Crofts AR. CALCIUM ION ACCUMULATION AND VOLUME CHANGES OF ISOLATED LIVER MITOCHONDRIA. CALCIUM ION-INDUCED SWELLING. Biochemical Journal. 1965;95(2):378-386.
171. Raaflaub J. [Swelling of isolated mitochondria of the liver and their susceptibility to physicochemical influences]. Helv Physiol Pharmacol Acta. 1953;11(2):142-156.
172. Lemasters JJ, Nieminen AL, Qian T, et al. The mitochondrial permeability transition in cell death: a common mechanism in necrosis, apoptosis and autophagy. Biochimica et biophysica acta. 1998;1366(1-2):177-196.
173. Scorrano L, Ashiya M, Buttle K, et al. A Distinct Pathway Remodels Mitochondrial Cristae and Mobilizes Cytochrome c during Apoptosis. Developmental cell. 2002;2(1):55-67.
174. Lemasters JJ. Chapter 5 - Hepatotoxicity Due to Mitochondrial Injury. In Kaplowitz N, DeLeve LD, (Eds). Drug-Induced Liver Disease (Third Edition). Boston: Academic Press 2013:85-100.
175. Davis MA, Jeffery EH. 4 - Organelle Biochemistry and Regulation of Cell Death. In Haschek WM, Rousseaux CG, Wallig MA, (Eds). Handbook of Toxicologic Pathology (Second Edition). San Diego: Academic Press 2002:67-81.
176. Sun MG, Williams J, Munoz-Pinedo C, et al. Correlated three-dimensional light and electron microscopy reveals transformation of mitochondria during apoptosis. Nat Cell Biol. 2007;9(9):1057-1065.
177. Bleck CKE, Kim Y, Willingham TB, et al. Subcellular connectomic analyses of energy networks in striated muscle. Nature Communications. 2018;9(1):5111.
178. Berdichevsky A, Guarente L, Bose A. Acute Oxidative Stress Can Reverse Insulin Resistance by Inactivation of Cytoplasmic JNK*. Journal of Biological Chemistry. 2010;285(28):21581-21589.
179. Pereira SL, Ramalho-Santos J, Branco AF, et al. Metabolic remodeling during H9c2 myoblast differentiation: relevance for in vitro toxicity studies. Cardiovascular toxicology. 2011;11(2):180-190.
180. Romero N, Swain P, Dranka B. Characterization of Glycolysis with a Panel of Common Cellular Models Using Agilent Seahorse XF Technology. Agilent Technologies, Inc. 2018 Printed in the USA, 5991-9411EN https://www.agilent.com/cs/library/applications/application-characterization-of-glycolysis-cell-analysis-5991-9411en-us-agilent.pdf.

181. Bugge A, Dib L, Collins S. Chapter Thirteen - Measuring Respiratory Activity of Adipocytes and Adipose Tissues in Real Time. In MacDougald OA, (Ed). Methods in Enzymology: Academic Press 2014:233-247.
182. Divakaruni AS, Paradyse A, Ferrick DA, et al. Chapter Sixteen - Analysis and Interpretation of Microplate-Based Oxygen Consumption and pH Data. In Murphy AN, Chan DC, (Eds). Methods in Enzymology: Academic Press 2014:309-354.
183. Bálint Z, Krizbai IA, Wilhelm I, et al. Changes induced by hyperosmotic mannitol in cerebral endothelial cells: an atomic force microscopic study. European biophysics journal : EBJ. 2007;36(2):113-120.
184. Malek AM, Goss GG, Jiang L, et al. Mannitol at clinical concentrations activates multiple signaling pathways and induces apoptosis in endothelial cells. Stroke. 1998;29(12):2631-2640.
185. Madonna R, Geng Y-J, Shelat H, et al. High glucose-induced hyperosmolarity impacts proliferation, cytoskeleton remodeling and migration of human induced pluripotent stem cells via aquaporin-1. Biochimica et Biophysica Acta (BBA) - Molecular Basis of Disease. 2014;1842(11):2266-2275.
186. Rossi A, Eid M, Dodgson J, et al. In vitro characterization of the effects of chronic insulin stimulation in mouse 3T3-L1 and human SGBS adipocytes. Adipocyte. 2020;9(1):415-426.
187. Hill DJ, Milner RDG. Insulin as a Growth Factor. Pediatric Research. 1985;19(9):879-886.
188. Beith JL, Alejandro EU, Johnson JD. Insulin Stimulates Primary β-Cell Proliferation via Raf-1 Kinase. Endocrinology. 2008;149(5):2251-2260.
189. Straus DS. Growth-Stimulatory Actions of Insulin in Vitro and in Vivo*. Endocrine Reviews. 1984;5(2):356-369.
190. Jeon JY, Choi SE, Ha ES, et al. GLP-1 improves palmitate-induced insulin resistance in human skeletal muscle via SIRT1 activity. International journal of molecular medicine. 2019;44(3):1161-1171.
191. Okatan EN, Olgar Y, Tuncay E, et al. Azoramide improves mitochondrial dysfunction in palmitate-induced insulin resistant H9c2 cells. Molecular and cellular biochemistry. 2019;461(1-2):65-72.
192. Song R, Zhao X, Cao R, et al. Irisin improves insulin resistance by inhibiting autophagy through the PI3K/Akt pathway in H9c2 cells. Gene. 2021;769:145209.
193. McMillin SL, Schmidt DL, Kahn BB, et al. GLUT4 Is Not Necessary for Overload-Induced Glucose Uptake or Hypertrophic Growth in Mouse Skeletal Muscle. Diabetes. 2017;66(6):1491-1500.
194. Gosmanov AR, Stentz FB, Kitabchi AE. De novo emergence of insulin-stimulated glucose uptake in human aortic endothelial cells incubated with high glucose. American Journal of Physiology-Endocrinology and Metabolism. 2006;290(3):E516-E522.
195. Heilig CW, Liu Y, England RL, et al. D-Glucose Stimulates Mesangial Cell GLUT1 Expression and Basal and IGF-I–Sensitive Glucose Uptake in Rat Mesangial Cells: Implications for Diabetic Nephropathy. Diabetes. 1997;46(6):1030-1039.
196. Hwang D-Y, Ismail-Beigi F. Stimulation of GLUT-1 glucose transporter expression in response to hyperosmolarity. American Journal of Physiology-Cell Physiology. 2001;281(4):C1365-C1372.
197. Taha C, Tsakiridis T, McCall A, et al. Glucose transporter expression in L6 muscle cells: regulation through insulin- and stress-activated pathways. American Journal of Physiology-Endocrinology and Metabolism. 1997;273(1):E68-E76.
198. Farlinger CM, Lui AJ, Harrison RC, et al. Extracellular hyperosmotic stress stimulates glucose uptake in incubated fast-twitch rat skeletal muscle. Appl Physiol Nutr Metab. 2013;38(6):605-612.
199. Fischereder M, Schröppel B, Wiese P, et al. Regulation of glucose transporters in human peritoneal mesothelial cells. J Nephrol. 2003;16(1):103-109.

200. Kelley DE, Goodpaster B, Wing RR, et al. Skeletal muscle fatty acid metabolism in association with insulin resistance, obesity, and weight loss. The American journal of physiology. 1999;277(6):E1130-1141.
201. Corpeleijn E, Mensink M, Kooi ME, et al. Impaired Skeletal Muscle Substrate Oxidation in Glucose-intolerant Men Improves After Weight Loss. Obesity. 2008;16(5):1025-1032.
202. Aas V, Hessvik NP, Wettergreen M, et al. Chronic hyperglycemia reduces substrate oxidation and impairs metabolic switching of human myotubes. Biochimica et biophysica acta. 2011;1812(1):94-105.
203. Dey D, Mukherjee M, Basu D, et al. Inhibition of Insulin Receptor Gene Expression and Insulin Signaling by Fatty Acid: Interplay of PKC Isoforms Therein. Cellular Physiology and Biochemistry. 2005;16(4-6):217-228.
204. Pimenta AS, Gaidhu MP, Habib S, et al. Prolonged exposure to palmitate impairs fatty acid oxidation despite activation of AMP-activated protein kinase in skeletal muscle cells. Journal of Cellular Physiology. 2008;217(2):478-485.
205. Martins AR, Nachbar RT, Gorjao R, et al. Mechanisms underlying skeletal muscle insulin resistance induced by fatty acids: importance of the mitochondrial function. Lipids in health and disease. 2012;11:30.
206. Petersen KF, Dufour S, Befroy D, et al. Impaired mitochondrial activity in the insulin-resistant offspring of patients with type 2 diabetes. The New England journal of medicine. 2004;350(7):664-671.
207. Befroy DE, Petersen KF, Dufour S, et al. Impaired Mitochondrial Substrate Oxidation in Muscle of Insulin-Resistant Offspring of Type 2 Diabetic Patients. Diabetes. 2007;56(5):1376-1381.
208. Mootha VK, Lindgren CM, Eriksson KF, et al. PGC-1alpha-responsive genes involved in oxidative phosphorylation are coordinately downregulated in human diabetes. Nat Genet. 2003;34(3):267-273.
209. Højlund K, Wrzesinski K, Larsen PM, et al. Proteome analysis reveals phosphorylation of ATP synthase beta -subunit in human skeletal muscle and proteins with potential roles in type 2 diabetes. J Biol Chem. 2003;278(12):10436-10442.
210. Pfeiffer T, Schuster S, Bonhoeffer S. Cooperation and Competition in the Evolution of ATP-Producing Pathways. Science. 2001;292(5516):504-507.
211. Vander Heiden MG, Cantley LC, Thompson CB. Understanding the Warburg Effect: The Metabolic Requirements of Cell Proliferation. Science. 2009;324(5930):1029-1033.
212. Zheng J. Energy metabolism of cancer: Glycolysis versus oxidative phosphorylation (Review). Oncol Lett. 2012;4(6):1151-1157.
213. Mailloux RJ, Harper M-E. Glucose regulates enzymatic sources of mitochondrial NADPH in skeletal muscle cells; a novel role for glucose-6-phosphate dehydrogenase. The FASEB Journal. 2010;24(7):2495-2506.
214. Elkalaf M, Anděl M, Trnka J. Low glucose but not galactose enhances oxidative mitochondrial metabolism in C2C12 myoblasts and myotubes. PloS one. 2013;8(8):e70772-e70772.
215. Tumova J, Malisova L, Andel M, et al. Protective Effect of Unsaturated Fatty Acids on Palmitic Acid-Induced Toxicity in Skeletal Muscle Cells is not Mediated by PPARδ Activation. Lipids. 2015;50(10):955-964.
216. Yuzefovych L, Wilson G, Rachek L. Different effects of oleate vs. palmitate on mitochondrial function, apoptosis, and insulin signaling in L6 skeletal muscle cells: role of oxidative stress. American journal of physiology Endocrinology and metabolism. 2010;299(6):E1096-1105.
217. Kitzmann M, Lantier L, Hébrard S, et al. Abnormal metabolism flexibility in response to high palmitate concentrations in myotubes derived from obese type 2 diabetic patients. Biochimica et Biophysica Acta (BBA) - Molecular Basis of Disease. 2011;1812(4):423-430.

218. Hernandez-Mijares A, Rocha M, Apostolova N, et al. Mitochondrial complex I impairment in leukocytes from type 2 diabetic patients. Free radical biology & medicine. 2011;50(10):1215-1221.
219. Avila C, Huang RJ, Stevens MV, et al. Platelet mitochondrial dysfunction is evident in type 2 diabetes in association with modifications of mitochondrial anti-oxidant stress proteins. Exp Clin Endocrinol Diabetes. 2012;120(4):248-251.
220. Wang X, McLennan SV, Allen TJ, et al. Adverse effects of high glucose and free fatty acid on cardiomyocytes are mediated by connective tissue growth factor. American Journal of Physiology-Cell Physiology. 2009;297(6):C1490-C1500.
221. Hickson-Bick DL, Buja LM, McMillin JB. Palmitate-mediated alterations in the fatty acid metabolism of rat neonatal cardiac myocytes. J Mol Cell Cardiol. 2000;32(3):511-519.
222. Nishi H, Higashihara T, Inagi R. Lipotoxicity in Kidney, Heart, and Skeletal Muscle Dysfunction. Nutrients. 2019;11(7).
223. Lisa CH, Kieran C. Metabolism, hypoxia and the diabetic heart. Journal of Molecular and Cellular Cardiology. 2011;50(4):598-605.
224. Barsotti A, Giannoni A, Di Napoli P, et al. Energy metabolism in the normal and in the diabetic heart. Current pharmaceutical design. 2009;15(8):836-840.
225. An D, Rodrigues B. Role of changes in cardiac metabolism in development of diabetic cardiomyopathy. American Journal of Physiology-Heart and Circulatory Physiology. 2006;291(4):H1489-H1506.
226. Sharma S, Adrogue JV, Golfman L, et al. Intramyocardial lipid accumulation in the failing human heart resembles the lipotoxic rat heart. The FASEB Journal. 2004;18(14):1692-1700.
227. Bayeva M, Sawicki KT, Ardehali H. Taking Diabetes to Heart—Deregulation of Myocardial Lipid Metabolism in Diabetic Cardiomyopathy. Journal of the American Heart Association. 2013;2(6):e000433.
228. Herrero P, McGill J, Lesniak DS, et al. PET detection of the impact of dobutamine on myocardial glucose metabolism in women with type 1 diabetes mellitus. Journal of Nuclear Cardiology. 2008;15(6):791-799.
229. Boudina S, Abel ED. Diabetic cardiomyopathy revisited. Circulation. 2007;115(25):3213-3223.
230. Zorzano A, Liesa M, Palacín M. Role of mitochondrial dynamics proteins in the pathophysiology of obesity and type 2 diabetes. The international journal of biochemistry & cell biology. 2009;41(10):1846-1854.
231. Peter A, Weigert C, Staiger H, et al. Individual stearoyl-coa desaturase 1 expression modulates endoplasmic reticulum stress and inflammation in human myotubes and is associated with skeletal muscle lipid storage and insulin sensitivity in vivo. Diabetes. 2009;58(8):1757-1765.
232. Lund J, Ouwens DM, Wettergreen M, et al. Increased Glycolysis and Higher Lactate Production in Hyperglycemic Myotubes. Cells. 2019;8(9):1101.
233. Cai L, Li W, Wang G, et al. Hyperglycemia-Induced Apoptosis in Mouse Myocardium: Mitochondrial Cytochrome c–Mediated Caspase-3 Activation Pathway. Diabetes. 2002;51(6):1938-1948.
234. Russell JS, Griffith TA, Peart JN, et al. Cardiomyoblast caveolin expression: Effects of simulated diabetes, α-linolenic acid and cell signaling pathways. American journal of physiology Cell physiology. 2020.
235. Eisner V, Csordás G, Hajnóczky G. Interactions between sarco-endoplasmic reticulum and mitochondria in cardiac and skeletal muscle - pivotal roles in Ca^{2+} and reactive oxygen species signaling. J Cell Sci. 2013;126(Pt 14):2965-2978.
236. Tubbs E, Chanon S, Robert M, et al. Disruption of Mitochondria-Associated Endoplasmic Reticulum Membrane (MAM) Integrity Contributes to Muscle Insulin Resistance in Mice and Humans. Diabetes. 2018;67(4):636-650.

Attachment

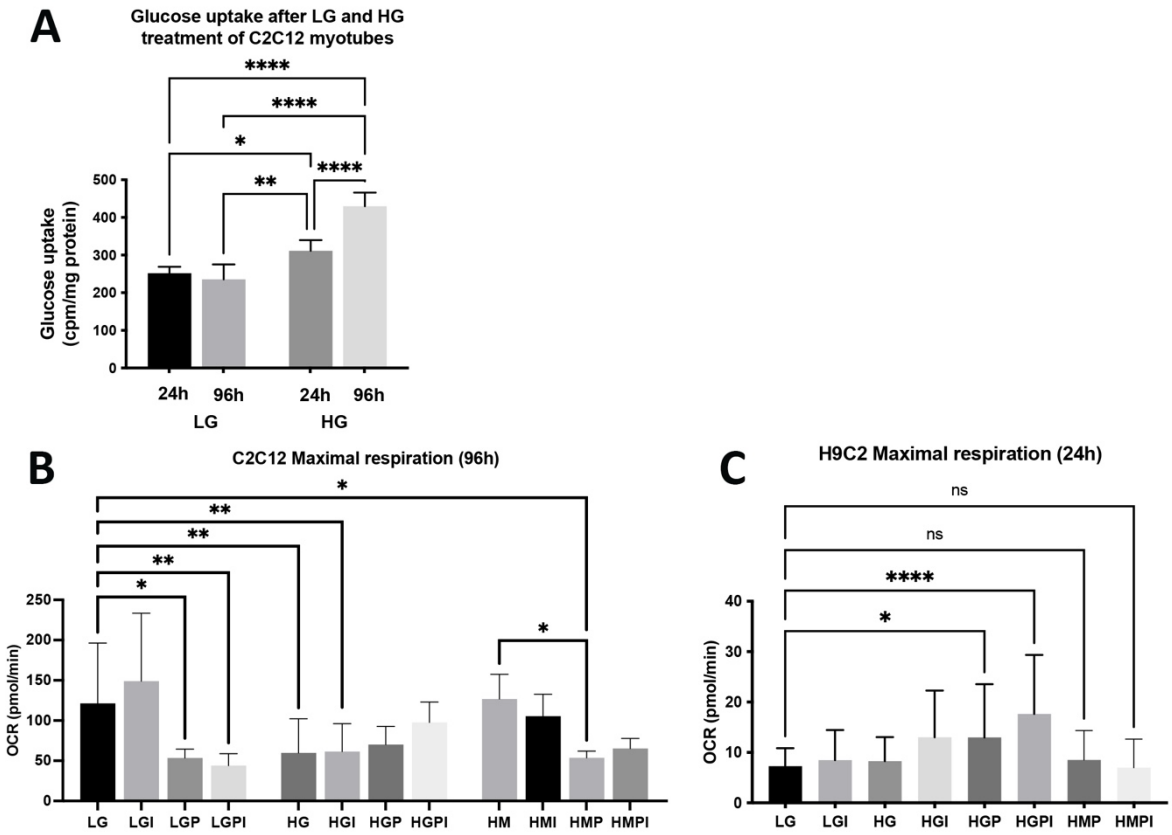

Fig. 16: A: Basal glucose uptake rates of C2C12 myotubes treated with LG or HG, 24 vs 96h, n=6. B: Maximal respiration rates of C2C12 myotubes after 96h treatments. C: Maximal respiration rates of H9C2 myotubes after 24h treatments. B + C represent data from each one Mito Stress Test assay with n=6-11 wells per Treatment group. Brackets represent Tukey's multiple comparisons tests *p<0.05, **p<0.01, ****p<0.0001.

Danksagungen

An dieser Stelle möchte ich mich bei allen bedanken, die mir mein Studium und die Promotionsarbeit ermöglicht haben.

Zunächst möchte ich mich bei Prof. Hemal Patel bedanken, für den kreativen Anstoß zum Thema meiner Dissertation, die Unterstützung und die vielen motivierenden Gespräche. Hier möchte ich mich auch besonders bei allen Mitarbeitern in den Cardiac And Neuro Protection Laboratories der University of California San Diego bedanken, allen voran bei Alice Zemljic-Harpf, Mehul Dhanani, Jan Schilling, Raphael Cuomo, Jake Russel und Ying Jones, die mir alle stets zur Seite standen und von denen ich alle angewandten Techniken erlernen durfte. Vielen Dank auch an die Kollaboration und Bereitstellung des radioaktiven Glucose-uptake assays von Prof. Sushil Mahata und der Hilfe von Gautam Bandyopadhyay an Wochenenden und jeder erdenklichen Uhrzeit. Außerdem bei Ingrid Niesman, die mit Analyse-Ideen zu den TEM Bildern beisteuerte.

Weiterer Dank gilt Prof. Reinhard Lorenz, für die unermüdliche Geduld, Hilfe und alle kritischen Anregungen.

Ganz besonderer Dank gilt auch Dr. Daniel Deußen, für seine Motivation, Korrekturen, Bestätigung und Geduld und meiner Familie für deren grenzenlose Unterstützung.

Auch bei Prof. Jochen Seißler und PD Cornelia Then von der Diabetesambulanz des Klinikums der Ludwig-Maximilians-Universität München möchte ich mich für thematische Anregungen, Hilfen und Korrekturen bedanken und bei Dr. Crispin für Statistik-Tipps.

Jaqueline Bonds und Elizabeth Jones danke ich für die grammatikalischen und sprachlichen Hilfen.

Außerdem bedanke ich mich bei der Bayer Foundation und dem Carl-Duisberg-Stipendium für die finanzielle Unterstützung, wodurch mir der Forschungsaufenthalt an der UCSD ermöglicht wurde.

Affidavit

LMU LUDWIG-MAXIMILIANS-UNIVERSITÄT MÜNCHEN | Promotionsbüro Medizinische Fakultät | MMRS

Eidesstattliche Versicherung

Kopp, Elena

Name, Vorname

Ich erkläre hiermit an Eides statt,

dass ich die vorliegende Dissertation mit dem Titel:

Diabetes in a dish: Modeling and phenotyping acute and chronic type 2 diabetes mellitus *in vitro* in rodent heart and skeletal muscle cells

selbständig verfasst, mich außer der angegebenen keiner weiteren Hilfsmittel bedient und alle Erkenntnisse, die aus dem Schrifttum ganz oder annähernd übernommen sind, als solche kenntlich gemacht und nach ihrer Herkunft unter Bezeichnung der Fundstelle einzeln nachgewiesen habe.

Ich erkläre des Weiteren, dass die hier vorgelegte Dissertation nicht in gleicher oder in ähnlicher Form bei einer anderen Stelle zur Erlangung eines akademischen Grades eingereicht wurde.

München, 22.08.2023 — Elena Kopp

Ort, Datum — Unterschrift Doktorandin bzw. Doktorand